LATVIAN JOURNAL of PHYSICS and TECHNICAL SCIENCES

ISSN 0868 - 8257

5

(Vol. 60)

2023

CONTENTS

K. Carjova, M. Banov, A. Unbedahts,
G. Strautmanis, L. Vinogradov, I. Kurjanovics
Characteristics of Mathematical Modeling of Acoustic Emission Method for Diagnosis of Fatigue Cracks in the Elements of Marine Power Plants 3

U. Rogulis, A. Fedotovs, P. Rodionovs, M. Kemere,
A. Antuzevics, A. Sarakovskis, K. Alps, V. Kiseleva
Application of Calcium Aluminate Doped with Mn And Cr in Optical Thermometry 15

L. Smelkovs, V. Viksna, J. Teterovskis, J. Grube
Synthesis of $NaYF_4$:Yb^{3+}, Tm^{3+} Nanocrystals via the Thermal Decomposition Method Using Refined Sunflower Oil 22

K. Gicevskis, O. Linkevics
The Role of Decentralized Electrode Boiler in Ancillary Services and District Heating: A Feasibility Assessment 32

L. Zemite, L. Jansons, N. Zeltins, S. Lappuke, I. Bode
Blending Hydrogen with Natural Gas/Biomethane and Transportation in Existing Gas Networks 43

A. Cimbale, I. Amolina, I. Geipele, N. Zeltins
Analysis and Implementation of Energy Efficiency Measures in Multi-apartment Buildings in Latvia 56

A. Korenkovs, E. Gerins, A. Kromanis
The Design and Performance of Internally Cooled Cutting Tools for Turning: A Literature Review 73

LATVIAN JOURNAL of PHYSICS and TECHNICAL SCIENCES

LATVIJAS FIZIKAS un TEHNISKO ZINĀTŅU ŽURNĀLS

ЛАТВИЙСКИЙ ФИЗИКО-ТЕХНИЧЕСКИЙ ЖУРНАЛ

Published six times a year since February 1964
Iznāk sešas reizes gadā kopš 1964. gada februāra
Выходит шесть раз в год с февраля 1964 года

5 (Vol. 60) • 2023

RĪGA

Language Editor: O. Ivanova
Computer Designer: I. Begicevs

INDEXED (PUBLISHED) IN

www.scopus.com
www.sciendo.com
EBSCO (Academic Search Complete, www.epnet.com), INSPEC (www.iee.org.com).
VINITI (www.viniti.ru), Begell House Inc/ (EDC, www.edata-center.com).

Issuers: Institute of Physical Energetics,
Institute of Solid State Physics, University of Latvia
Registration Certificate Number: 000700221

Editorial Contacts:
14 Dzerbenes Street, Riga, LV-1006
LATVIA
tel: +371 26245896
M: +371 29363105
leo@lza.lv

sciendo

LATVIAN JOURNAL OF PHYSICS
AND TECHNICAL SCIENCES
2023, N 5

DOI: 10.2478/lpts-2023-0026

CHARACTERISTICS OF MATHEMATICAL MODELING OF ACOUSTIC EMISSION METHOD FOR DIAGNOSIS OF FATIGUE CRACKS IN THE ELEMENTS OF MARINE POWER PLANTS

K. Carjova*, M. Banov, A. Unbedahts, G. Strautmanis,
L. Vinogradov, I. Kurjanovics

Riga Technical University, Latvian Maritime Academy,
12 Flotes Str., LV – 1016, Riga, LATVIA
*e-mail: kristine.carjova@rtu.lv

This article analyses the main characteristics of marine power plants, which include internal combustion engines (ICE) and gas turbine engines (GTE). At the same time, gas turbines are considered in comparison with aircraft engines. The study considers the possibility of using the acoustic emission (AE) method to evaluate the fatigue resistance of critical elements of ICE and GTE, based on the valve block in the ICE and turbine rotor blades. AE criteria for determining the growth of fatigue cracks are analysed, a method for evaluating individual durability and a method for calculating crack length are proposed.

Keywords*: Acoustic emission, cyclic loading, fatigue destruction, gas turbine engine, internal combustion engine, turbine rotor blade.*

1. INTRODUCTION

The power plants of modern ships, especially diesel engines and gas turbine engines (GTE), operate at high pressures (up to 21 MPa) and temperatures. Power plant failure is associated with high financial costs and can lead to environmental damage and pollution. Timely detection of hidden defects and switching to technical maintenance based on the actual technical condition of the power plant makes it possible to increase the uptime and thus the profitability of the ship operation.

Diagnosis of the technical condition of a power plant is the control of its technical condition by processing the obtained measurement data without dismantling or partial dismantling of the object, which allows making decisions about the technical condi-

tion of the power plant and determining its future performance [1], [2]. In recent years, the number of electronic components (engine control units) (ECU), such as sensors and transducers, has increased. However, most condition monitoring programmes are not designed for the detection and unambiguous definition of power plant defects and prediction of their occurrence, which is particularly important for the prediction and planning of intervals of technical maintenance.

Gas turbine engines (GTE) have high specific characteristics and for this reason have been used in aviation since the 1940s. To this day, this is the main type of engine used in aircraft for military and commercial purposes. Since the 1960s, GTEs have also been used as marine engines – first as acceleration engines for torpedo boats, then as propulsion engines for submarines and other warships [3]. GTUs are also the main propulsion type for amphibious assault ships and hydrofoils.

The capacity of GTU transport ships is currently 0.07 ... 14.5 MW, specific effective fuel consumption is 285–330 g / (kWh), turbine speed is 5000–8000 rpm. It is considered that the prospects of gas turbines with their use as the main engines with a capacity of 5 ... 40 MW for large ships with horizontal loading, ferries, ice ships, etc. correlate. The main manufacturers of marine GTU are currently General Electric and Pratt & Whitney (both the USA), Rolls-Royce (the UK), Saturn NGO (Russia).

Modern marine gas turbines are gas turbine engines (GTE) 1 with a free power turbine 2 rotating the screw propeller 3 via a reduction gear 4 (Fig. 1). Marine GTEs are structurally similar to aircraft engines; they are often developed based on proven aerospace structures. For example, the LM2500 GTE (General Electric) is a modification of the TF39 aircraft engine; the M75РУ marine engine (Saturn NGO) was developed on the basis of gas turbine engines (GTE) for aviation, designed by the design bureau named after A. Lulka, etc.

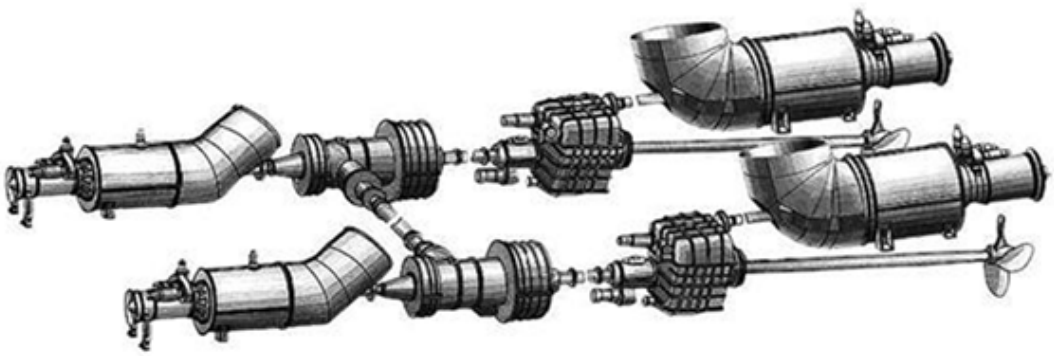

Fig.1. Configuration of a multi-engine marine GTE.
1 – gas turbine engines; 2 – free power turbine; 3 – propeller; 4 – reduction gearbox.

The gas turbine engine consists of a gas generator with a compressor 1, a combustion chamber 2 and a compressor turbine 3 (Fig. 2). The most stressed parts of the GTE, which determine its resources and reliability, are the elements of the combustion chamber 2 and gas turbines such as flame tubes 4, nozzles 5, rotor blades 6 and the like.

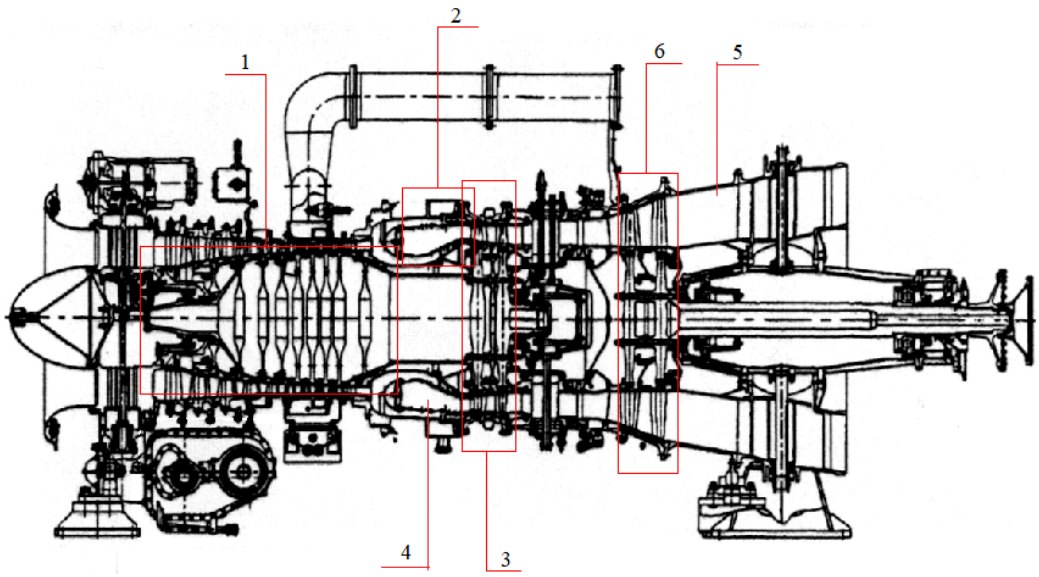

Fig. 2. Gas generator of a marine GTE. 1 – compressor; 2 – combustion chamber; 3 – turbine compressor; 4 – flame tubes; 5 – nozzles; 6 – working blades.

Compared to aircraft gas turbine engines (GTE), marine power plants operate under more difficult conditions because the sea air contains salty components. As a result, corrosion damage increases. In this case, the most dangerous is high-temperature salt corrosion on the turbine blades, which is caused by a mixture of salt vapours and combustion products. Reliability assessment is associated with the use of methods of non-destructive testing of parts that determine the service life of the engine.

2. ACOUSTIC EMISSION METHOD

Currently, traditional methods of non-destructive testing used to evaluate the technical condition of various machines and structures include visual-optical, ultrasonic, eddy current, magnetic particle, and liquid penetrant (coloured and luminescent) methods. However, their capabilities are limited when it comes to detecting defects such as fatigue cracks, which in most cases are hidden (internal) defects. Thus, visual-optical methods and fluid penetration methods are only effective when the formation of cracks on the surface is visible in certain places. Ultrasonic, eddy current and magnetic particle methods make it possible to detect hidden defects such as subsurface cracks. Ultrasonic methods can also be used to find cracks deep within the material. However, all these methods have limitations related to the construction of the inspected parts. For example, they are ineffective in detecting a defect in the engine at the very beginning of its occurrence or checking cooled working blades of the gas turbine system (GTS). Thus, conventional methods are effective when disassembly of the structure is possible, and they have limited efficiency when disassembly is limited or impossible.

It is therefore advisable to consider the possibility of using other, non-standard methods of non-destructive testing and diagnosis. One such method could be the method of acoustic emission (AE). Its main advantage is the fact that with its help it is possible to detect only developing defects, thus allowing a more accurate assessment of the degree of their threat to the inspected object. By analysing acoustic signals, it is possible to assess the technical condition of parts such as injectors, intake / exhaust valves, crankshafts, cylinder-piston groups, etc. It is particularly important to detect defects in the intake / exhaust valves, crankshaft, internal combustion engine shaft and cooled rotor blades of the GTS, as these are the most expensive parts of the power equipment.

The methods of acoustic control of metals have been known for a long time [4]. The acoustic method uses the radiation of mechanical waves from the material due to dynamic changes in the internal structure of the material caused by any kind of loading. AE can be caused by plastic deformation, crack formation and growth, fluid / gas flow in pipelines, corrosion, loss of oil layer between rubbing parts (increased friction), gas / fluid flow in defects and other deformations of solids. It can be assumed that AE signals in materials are caused by a change in pressure, stress or temperature.

The stress acts on the material and causes local plastic deformations. These deformations in the material create an AE: an elastic wave that propagates in all directions from the source and is detected by a sensor installed at some distance. As a result, the sensor generates an electrical signal that is transmitted to electronic devices for further processing. The basic principle of the method AE is shown in Fig. 3.

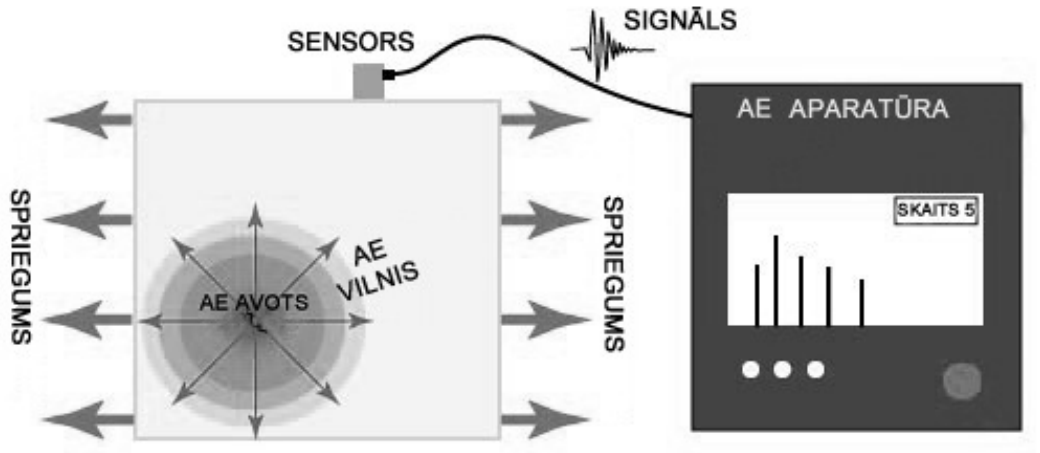

Fig. 3. The principles of AE method.

Components of marine power plants are subjected to various loads that can cause fatigue cracks in the material, and it is important to determine not only the existence of a defect, but also its location. The main defect detection circuit is shown in Fig. 4.

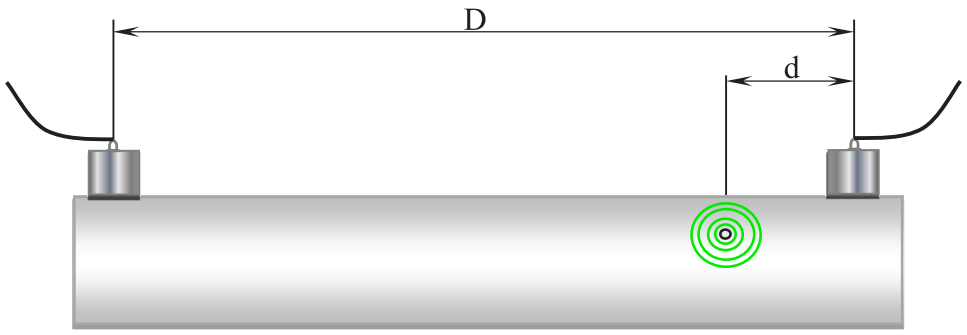

Fig. 4. AE method for identifying and determining the defect location [5].

The distance from the sensor to the defect is determined by Eq. (1).

$$d = \frac{1}{2}(D - \Delta T \cdot V), \tag{1}$$

where d signifies the distance from the first sensor to the defect;
D – is the distance between the sensors;
V – velocity of wave propagation;
$\Delta T = t_1 - t_2$ – time difference of the acoustic emission signal processing circuit from the defect to the second and first sensors.

The method AE does not respond to non-developing (static) defects, which are usually detected by most other methods of non-destructive testing and from which the degree of their threat to the object is inferred. The application of the method AE naturally raises issues related to the identification of fracture criteria and prediction of fatigue life of structures [6], [7].

Let us consider these issues using the example of the operation of the inlet and exhaust valves of an internal combustion engine, as shown in Fig. 5, and the rotor blade of the turbine GTE, as shown in Fig. 6.

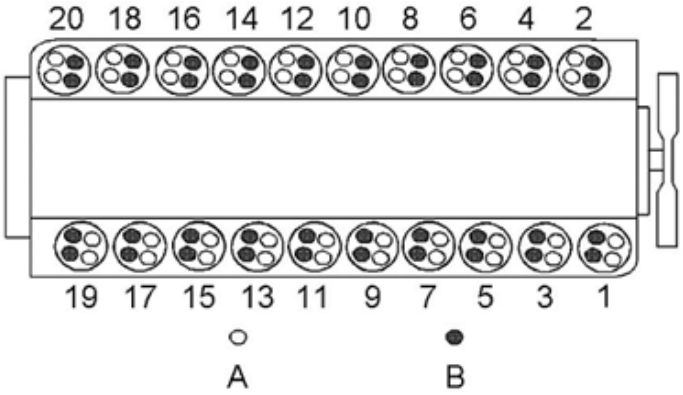

Fig. 5. The arrangement of cylinders and valves of the internal combustion engine (ICE);
A – exhaust valves, B – exhaust valves.

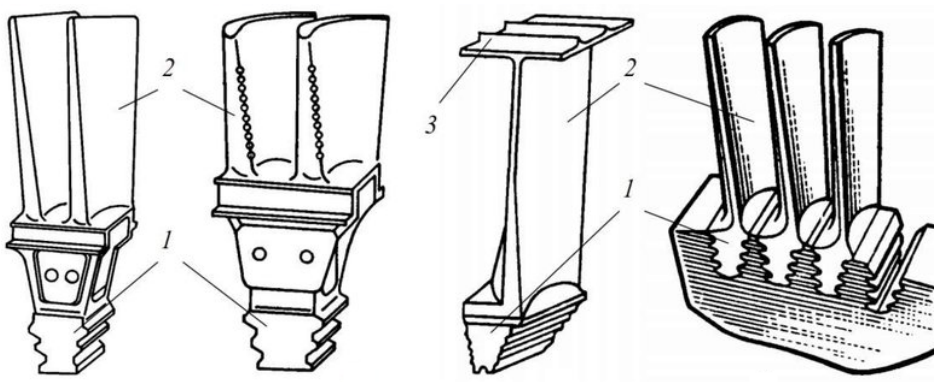

Fig. 6. GTE turbine blades.
1 – blade lock; 2 – spring; 3 – cover plate.

Static tests were performed to determine the most stressed areas and the maximum permissible stresses in the blades. The stresses were determined using strain gauges, whose installation scheme can be seen in Fig. 7.

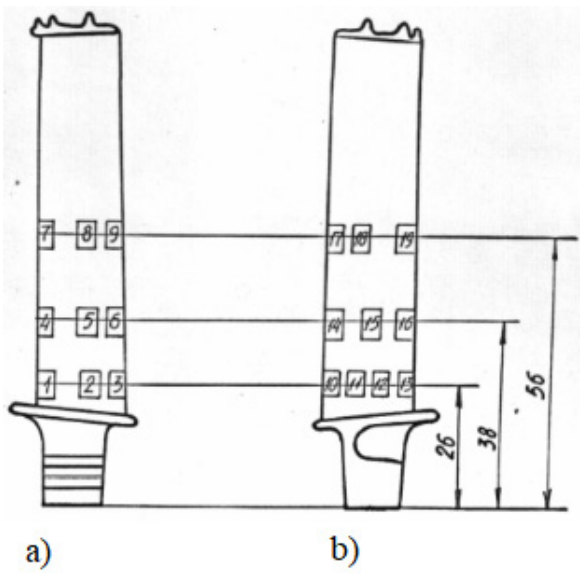

Fig. 7. GTE blades with strain gauges.
a) view from the side of the back, b) view from the bucket side.

A cyclically alternating load was applied to the blade on a vibration test rig, while the stress value in the dangerous section varied according to the vibration amplitude, which changed the blade curvature. Figure 8 illustrates a schematic diagram of a vibration test rig with a fixed blade and the installation location of the AE sensor.

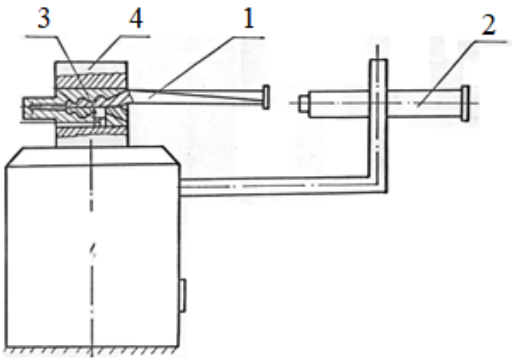

Fig.8. Vibration diagram.
1 – blade; 2 – microscope; 3 – AE sensor; 4 – hydraulic lock.

AE Criteria

Testing ICE Valves. This article deals with malfunctions of the valves and their nozzles in a gas-fuelled marine engine [8]. In this case, the AE signals from sensors installed in the area of the malfunctioning valve create a turbulent gas flow in the channel, which occurs as a result of a defect and causes a leak. Leakage can be caused, for example, by the most common malfunctions in the operation of valves and their nozzles, such as increased abrasion and stratification of the surface, which cause gas to escape from the cylinder even when the valves are closed. The most common defect is an irregularly shaped channel and configurations in the valve disc and / or valve seat.

It is assumed that AE signals occur only during turbulent motion of the gas, when the occurrence of unstable vortices causes pressure pulsations (stress waves) on the channel walls of the controlled object and the AE signals are recorded as turbulence noise in the ultrasonic range.

To simplify the theoretical analysis of the acoustic signals, it is assumed that the duct is straight, has smooth walls, has a constriction r (the size of the gap between the valve and its seat) and a length L (the thickness of the valve), and is perpendicularly connected to the main duct (which is connected to the cylinder) (Fig. 9). The relative length (length) of the channel characterises the parameter $\lambda=L/r$.

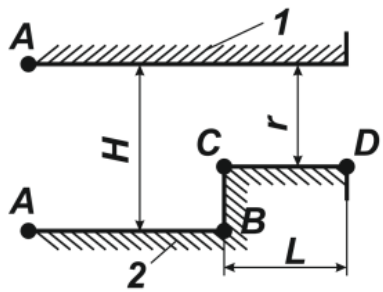

Fig. 9. Defect model.

In addition, the assumptions were made that the parameter r is sufficiently small compared to the cylinder size and the duct height H, the gas flow in the duct and in the constriction is isothermal, and the flow continuity condition is satisfied.

In the presence of a defect in the valve, there is a turbulent mode of gas movement in the channel determined by the AE method. The mathematical model of gas outflow through a defect in the valve consists of the following equations, which express the critical ratio of the pressure

upstream of the valve to the atmospheric pressure (2) and the limit value of the valve clearance (3), at which the gas flows out at the speed of sound:

$$\left(\frac{p_A}{p_{at}}\right)_{kr} = \sqrt{1+\xi\lambda}, \quad (2)$$

$$r_{lim} = \frac{\mu \cdot Re_{kr}}{2 \cdot \rho_D \cdot c} = \frac{\mu \cdot Re_{kr}}{2 \cdot \sqrt{\rho_D \cdot p_D}}, \quad (3)$$

where $\xi = \xi(Re)$ is the coefficient of hydraulic resistance in the valve;
μ – the coefficient of dynamic viscosity of the gas;
Re_{kr} – Reynold's number at the speed of sound;
ρ_D, p_D – density and pressure of the gas upstream of the valve (at point D, Fig. 9);
c – speed of sound.

When analysing the test results of ICE valves using the AE method, the most important factors were filtered out:

- The maximum amplitude of the AE signal;
- Rise speed of the AE signal;
- Decay speed of the signal.

GTE Blade Investigation. In the study of a gas turbine engine using the AE method, the turbine blades were selected as the most critical and expensive installation elements. Several blades were selected from the total number of rotor blades. The maximum value of external cyclic load applied to the working blades did not exceed the permissible values.

Tests of rotor blades under cyclic loading showed that the acoustic emission signal reflected the main stages of damage accumulation and destruction, which were the subject of control. Figure 10 shows the change of energy ***E*** of the ***AE*** signal as a function of the number of loading cycles ***N***. The character of the energy change described above is characteristic of all types of blades.

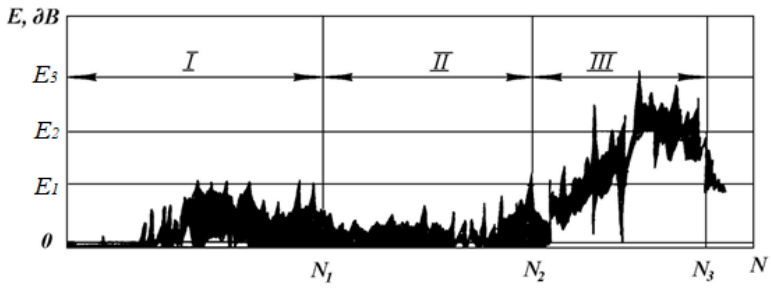

Fig.10. **AE E** energy change based on the number of **N** loading cycles.

Three main stages of the damage accumulation process can be identified here: Hardening (***I***); Stabilization (***II***) and Destruction (***III***). In the initial phase of loading (phase I), microplastic deformations occur, generating AE signals. Then, the level of AE signals decreases (phase ***II***), indicating the stabilization of the damage of the accumulation process. In the last loading phase (phase ***III***), there is a sharp increase in the AE signal, which is connected with the process of fatigue crack growth and fracture of the control object. A similar picture is obtained when registering a total balance: AE N_{AE}: dependent $lgN_{AE} = f(N)$ is shown in Fig. 11.

Thus, the analysis of these dependencies makes it possible to determine the criteria for

fatigue failure. They can be used as:

- ***E***-criterion, i.e., exceeding of the AE signal level above a certain threshold after the stabilization phase;
- ***α***-criterion, which indicates the break angle of the dependent $lgN_{AE} = f(N)$ after the stabilization phase.

Further studies have shown that the α-criterion is a simpler and more reliable criterion for fatigue crack detection. Thus, fractographic analysis confirmed that this criterion could detect micro-cracks with a size of 0.02 ... 0.05 mm and less [9]. An increase in the reliability of using the α-criterion can be achieved by analysing the AE signal in each loading cycle [10].

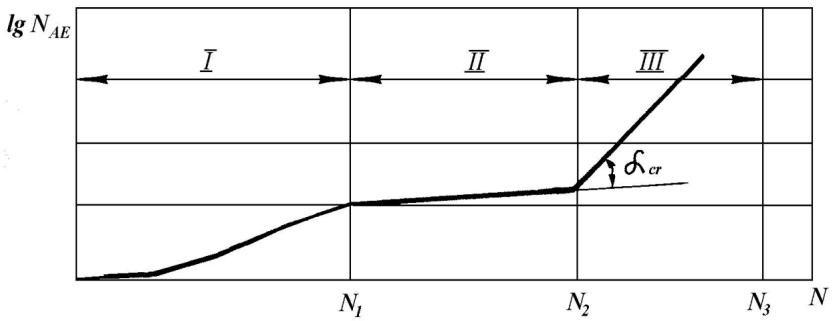

Fig. 11. Dependence of the total number of AE on the number of loading cycles.

Individual Durability

The same features can be used to predict the individual durability of rotor blades. For this purpose, it is necessary to determine the total number N_{AEII} during the loading cycle in the stabilization phase (phase ***II)***. The individual N_{LT} durability can be determined by using the following equation:

$$lg(N_{LT}) = a - b \cdot lg(N_{AEII}), \qquad (4)$$

where ***a*** and ***b*** – are constant coefficients determined by the geometric properties of the blades and the magnitude of the cyclic loads in the stabilization phase.

In the experimental verification of this formula, the correlation coefficient between the N_{LT} durability and the total N_{AEII} emission value was 0.85 ... 0.97, indicating the potential of using this approach.

Crack Length

Test Results for ICE Valves – Crack Length

Experimental measurements on internal combustion engine valves (ICE) have resulted in the following conclusions:

1. When the valves have reduced thermal clearance, the gas exchange cycle changes, and both the amplitude and duration of the signal are slightly reduced.
2. If there are precipitates on the exhaust valve, the amplitude and duration of the sound are reduced.
3. If the inlet valve has a crack, the amplitude decreases and the duration of the sound increases.
4. If the exhaust valve has increased precipitation and outburning, the amplitude decreases and the duration of the sound increases.

Since valve cracks are the most dangerous defects that can lead to an engine damage, the following intake valve crack locations are examined for a more detailed analysis:

- Six valve closures with no defect;
- Six valve closures with an early-stage crack;
- Six valve closures with a crack in the final stage (before the planned repair).

The following diagrams show only two of the six AE signals (Fig. 12):

1. AE signals when the valve closes without failure;
2. AE signals when a cracked valve closes at the initial stage;
3. AE signals at the end of the crack (before detection).

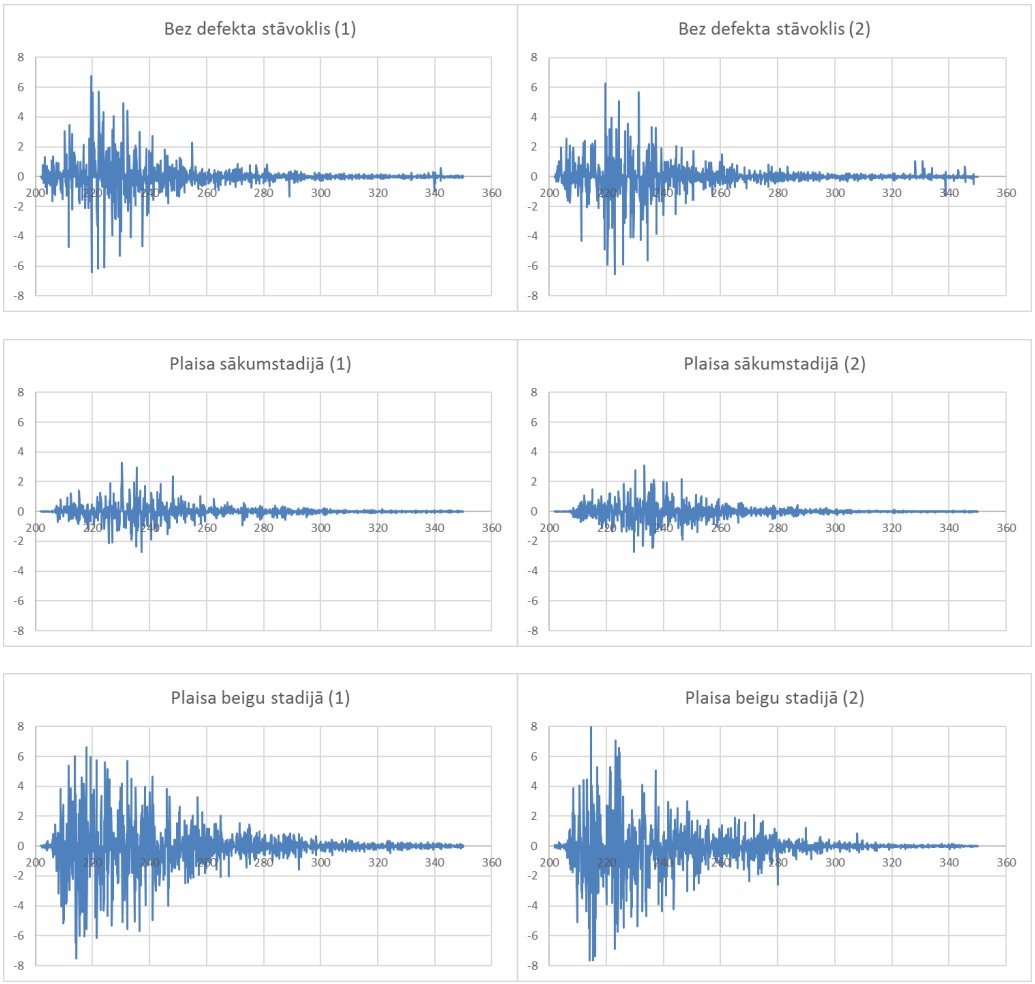

Fig. 12. Graphical representation of the measurements for a valve without a defect and with a defect.

Results of Testing GTE Blades. When examining a gas turbine, in order to assess the technical condition of the blade, it is important to determine the length ***l*** of the fatigue crack and the rate of its growth ***dl/dN***. For this purpose, it is proposed to additionally register the velocity accounts AE N. The tests showed that in the process of destruction (phase *III*) after crack initiation, there was initially an accelerated growth, which was then followed by a fragment in which crack growth occurred only in single cycles. As the process continued, accelerated and decelerated growth repeated, with stages of acceleration and, in principle, there might be several decelerations of

growth. In the transformation of fatigued microcracks into macrocracks, the cracks begean to grow steadily with each loading cycle. Only in this case, the crack can be detected by conventional non-destructive testing methods.

At the stage of stable crack growth, the dependent can be used to determine its parameters, from which the crack length is determined: l_{stab}:

$$N_{stab} = A\left(\frac{dl}{dN}\right)^{B}_{stab}, \quad (5)$$

where ***A*** and ***B*** are constant coefficients for a given blade type.

In the phases of unstable growth, which are composed of phases of accelerated and slow growth, the length of the crack in the phase of accelerated growth $\boldsymbol{l_{istab}}$ can be determined by an equation similar to (5), proposed for the process of stable growth:

$$N_{istab} = A_i\left(\frac{dl}{dN}\right)^{B}_{istab}. \quad (6)$$

The extent of crack growth in the slow growth phase $\Delta\, l_i$ can be determined by the dependent:

$$\Delta l_i = \xi \cdot \left(\frac{dl}{dN}\right)_{iaver} \cdot \Delta t_i \cdot f, \quad (7)$$

where $^{dl}/_{dN}$ is the average speed of crack growth;
Δt_i – ongoing phase;
f – loading frequency;
ξ – loading coefficient.

The total length of the crack is obtained from the equation:

$$l = l_{stab} + \sum_i (l_{istab} + \Delta l_i), \quad (8)$$

where *i* is the number of fragments of unstable growth.

3. CONCLUSION

As a result of the research, a mathematical justification for the application of the AE method for the search and detection of fatigue microcracks in the components of marine power plants has been determined. The potential of the AE method has been given for:

- the detection of defects in the valves of ICE;
- the identification of turbine rotor blades with internal cracks (including cracks in the channels of the cooled blades);
- the assessment of the development degree of fatigue cracks in critical parts of marine power plants;
- the determination of the residual strength of blades during repair.

ACKNOWLEDGEMENTS

The research has been supported by the Latvian Science Council, project "Development of Smart Technologies for Efficient and Well-Thought-Out Water Operations (STEEWO)" (No. Lzp-2019 / 1-0478).

REFERENCES

1. Jones, N.B., & Li, Y-H.. (2000). A Review of Condition Monitoring and Fault Diagnosis for Diesel Engines. *Tribotest, 6* (3), 267–291.
2. Kruger, U., McCullough, G., McDowell, N., & Wang, X. (2006). Fault Diagnosis for Internal Combustion Engines. *Automation Technology in Practice, 3*, 19–26.
3. Inozemcev, A., Nihamkin, M., & Sandrackiy, V. (2008). *Fundamentals of Aircraft Engines and Power Plants Design, Gas Turbine Engines Series*. Moscow: Mechanical Engineering, 174–188. (in Russian).
4. Aleshin, I.P., & Beliy, V.E. (1989). *Methods for acoustic control of metals*. Moscow: Mechanical Engineering. (in Russian).
5. NTC NefteGazDiagnostika (n.d.). *Acoustic Emission Control.* Available at https://ntcngd.com/uslugi/article_post/tehnicheskoe-diagnostirovanie-i-ekspertiza-promyshlennoy-bez
6. Kurjanovičs, I., Feščuks, J., & Banovs, M. (2013). Diesel engine common rail injector acoustic emission pattern obtaining. In *Transport Means 2013: Proceedings of the 17th International Conference*, (pp. 145–148). Lietuva, Kaunas/Klaipeda, 2013.
7. Evseev, D., Medvedev, B., Medvedev, P., Strautmanis, G., & Samoshkin, S. (2018). Acoustic emission approach to determining survivability in fatigue tests. In *ICTE in Transportation and Logistics 2018 (ICTE 2018)*, (pp. 282–287). 1 January, 2019, Lithuania, Klaipeda.
8. Urbahs, A., & Unbedahts, A. (2015). Acoustic Emission Method Evaluation for High Speed Ship Engines Condition Monitoring. *Transport Means*, 587–590. ISSN 1822-296x.
9. Banov, M., Konjaev, E., & Troenkin, D. (1981). Method for Determining the Fatigue Strength of Gas Turbine Blades by the Acoustic Emission Method. *Flaw Detection, 2,* 26–28. (in Russian).
10. Urbahs, A., Banov, M., Doroshko, S., & Nasibullin, A. (2008). Acoustic Emission Monitoring of Landing Gear Fatigue Testing. *Transport Means 2008*, 33–36.

sciendo

LATVIAN JOURNAL OF PHYSICS
AND TECHNICAL SCIENCES
2023, N 5

DOI: 10.2478/lpts-2023-0027

APPLICATION OF CALCIUM ALUMINATE DOPED WITH Mn AND Cr IN OPTICAL THERMOMETRY

U. Rogulis[1]*, A. Fedotovs[1], P. Rodionovs[1], M. Kemere[1],
A. Antuzevics[1], A. Sarakovskis[1], K. Alps[2], V. Kiseleva[2]

[1]Institute of Solid State Physics, University of Latvia,
8 Kengaraga Str., Riga, LV-1063, LATVIA
[2]Light Guide Optics International Ltd,
8 Celtniecības Str., Livani, LV-5316, LATVIA
*e-mail: uldis.rogulis@cfi.lu.lv

Optical thermometers are advantageous for temperature measurement in electromagnetic fields and aggressive environments; however, their composition mostly relies on materials doped with expensive and resource-limited rare earth ions.

In this article, we describe the application of calcium aluminate doped with transition metal ions (Mn^{2+} and Cr^{3+}) in optical thermometry, employing optical fibres for signal transmission. Upon excitation with 450 nm laser diode radiation, changes in the luminescence of Mn^{2+} ions in the 500– 550 nm band are followed along with changes in the Cr^{3+} band at 750–800 nm.

The application has been tested in the temperature range from 20 °C to 800 °C. The temperature dependence of Cr^{3+} luminescence encompasses the high-temperature range, whereas the luminescence band of Mn^{2+} ions gives an increase in the total intensity and provides a more consistent change in the range from 400 °C to 550 °C.

Keywords*: Calcium aluminate, electron paramagnetic resonance (EPR), Mn^{2+} and Cr^{3+} ions, luminescence, optical thermometry.*

1. INTRODUCTION

Temperature sensors (thermometers) are widely used in science, industry and everyday life [1]. Physical phenomena used in thermometers are related to thermal expansion, thermoelectric effects (thermocouples) and changes in optical signals due to temperature [1], [2]. Thermal expansion thermometers often have difficulty with electrical readings of temperature. Thermocouples have a broad range of applications, but face limitations in aggressive environments and electromagnetic fields. In con-

trast, optical temperature sensors are the most suitable for operation in electromagnetic fields and aggressive environments.

Optical temperature sensors process the optical signal of absorption, reflection, Rayleigh or Raman scattering, or luminescence [2]. Luminescent temperature sensors can use luminescence intensity or band parameters, decay time, or luminescence polarization [3]. Among these, sensors using changes in the luminescence signal and decay times are the most popular. There is a widespread method of determining the relative intensity ratio of luminescence (fluorescence) bands (fluorescence intensity ratio – FIR, also luminescence intensity ratio – LIR) depending on temperature [4]-[6]. So far, the applicability of rare earth elements for optical temperature detection has been widely studied [4], [5], [7], [8]. The luminescence spectra of rare earth ions are characterised by a wide distribution of bands in the ranges of ultraviolet radiation, visible light, and infrared radiation.

Transition metal ions are less used in optical temperature sensors, and the range of their application temperatures discussed in the literature is not so wide, especially for applications in the highest temperature range from 400 up to 800 °C [4], [7], [8]. The most suitable transition metals in optical temperature sensor materials are Mn and Cr [4], [7], [8], constituting approximately 96 % of all proposed transition metal activators [3]. The use of transition metal activators in the sensor makes it possible to abandon the use of expensive and resource-limited rare earth ions. The use of Mn^{2+} ions in luminescence thermometry has been described for temperatures up to 400 °C, and Cr^{3+} ions – for temperatures up to 500 °C [4], [7].

In this study, we present a combination of Mn^{2+} and Cr^{3+} in calcium aluminate, which enables us to achieve changes in the total intensity of luminescence of the material in the temperature range of 20–800 °C.

2. EXPERIMENTAL

A. Samples. Polycrystalline hexaaluminate $CaA_{l12}O_{19}$ samples doped with 5 mol% of Mn^{2+} (CA_6:Mn) and 2 mol% of Cr^{3+} (CA_6:Cr) were produced using the high temperature solid state synthesis method. Stoichiometric amounts of $CaCO_3$, Al_2O_3, MnO_2, and Cr_2O_3 were mixed in agate mortar. Obtained homogeneous mixtures were heat treated at high temperature: 1500 ºC in air for the Cr^{3+} doped sample and 1300 ºC in reducing atmosphere for the Mn^{2+} doped sample until the reaction was completed. A mixture of polycrystalline CA_6:Mn and CA_6:Cr was pelletized with the 2:1 ratio to obtain the material for optical temperature sensing.

B. EPR measurements. The Bruker ELEXSYS-II E500 CW-EPR spectrometer was used for EPR spectra measurements at room temperature. Powdered CA_6:Mn and/or CA_6:Cr samples were filled into EPR tubes with an outer diameter of 5 mm. Magnetic field modulation parameters were 100 kHz and 0.2 mT, while microwaves were generated at 9.835 GHz frequency and 10 mW power. Normalisation of signal intensities to sample mass was performed for a relative comparison of the paramagnetic ion concentration.

B. Luminescence measurements. The emission and excitation spectra of polycrystalline samples at room temperature were obtained using an FLS1000 spectrometer manufactured by Edinburgh Instruments

(model: FLS1000-DD-stm). The spectrometer was equipped with a CW 450 W Xenon lamp (model: Xe2) and a red photomultiplier tube (model: R928P, cooled for better detection). The spectra were corrected to the instrumental response.

D. Optical fibres and temperature dependence. The temperature dependence measurements were carried out using an Andor SR-303i-B spectrometer with DU401-BV CCD camera to measure spectra in the range from 430 to 1000 nm. Excitation was performed using a 450 nm laser diode with a power of 1.0 W. To filter out the excitation light, a 500 nm long-pass filter from Thorlabs was employed. Temperature was stabilized using the LUMEL RE19 PID controller. The temperature dependence was investigated in 50 °C increments, starting from room temperature up to 850 °C. Both excitation and luminescence light were transmitted through an appropriate light guide bundle manufactured by Light Guide Optics International Ltd in Latvia. To obtain integral intensities, 50 nm wide ranges were selected, centred at 525 nm for the green band and 775 nm for the red band.

3. RESULTS AND DISCUSSION

The incorporation of Mn^{2+} and Cr^{3+} activators in the CA_6 lattice is confirmed by the EPR spectra presented in Fig. 1. Due to the differences in electronic configurations, each transition metal ion exhibits a distinct EPR signal. Cr^{3+} is a d^3 electronic configuration ion with three unpaired electrons, which gives rise to the zero-field splitting of the ground state and the emergence of EPR spectra fine structure. In CA_6:Cr^{3+}, we observe a signal at 355 mT, low field structure in the range of 100–230 mT and several resonances in the high field region, which is in line with the previous investigation of the host [9]. As a result, multi-site incorporation of Cr^{3+} ions in the CA_6 lattice can be implied. Analysis of the Mn-doped samples is more challenging as the activators can have both Mn^{2+} and Mn^{4+} oxidation states each with unique magnetic and optical characteristics [10]. Moreover, hyperfine structure due to electronic spin interaction with the 100 % abundant nuclear spin of ^{55}Mn nucleus typically complicates and broadens EPR spectra. However, considering the number of fine structure components in the EPR spectrum and the reducing synthesis conditions of the Mn-doped sample, the dominant contribution can be attributed to Mn^{2+} centres. It is noteworthy to highlight that the EPR spectrum of CA_6:Mn^{2+} notably differs from that of CA_6: Mn^{2+} [11], implying variations in the local structure of Mn^{2+} ions in the two materials, which are also reflected in the luminescence spectra. Finally, the determined relative weights of Mn^{2+} and Cr^{3+} EPR signals of 1.94:1.00 in the mixed CA_6 material are consistent with the intended 2:1 ratio.

For use in an optical temperature sensor, we investigated the luminescence properties of CA_6 poly-crystals doped by Mn^{2+} and Cr^{3+} ions. Figure 2 shows the luminescence spectra of CA_6 polycrystalline samples doped by Mn^{2+} and Cr^{3+} ions, excited by 450 nm Xe lamp excitation. A luminescence band of Mn^{2+} ions is observed in the 500–550 nm spectral range, with the maximal intensity at 518 nm (Fig. 2(a-b)). The observed green luminescence band occurs due to the transition $^4T_1(^4G) \rightarrow {}^6A_1(^6S)$ of Mn^{2+} ions in the CA_6 structure [12], [13]. The valence of manganese ions in the CA_6 can be controlled with the preparation con-

ditions. The reduction of Mn^{4+} to Mn^{2+} ions in CA_6 is promoted by using a reducing atmosphere during the sample synthesis [12]. In the red and near-infrared spectral range, luminescence bands of Cr^{3+} ions have been observed (Fig. 2(a-b)). The narrow luminescence band at 689 nm with the phonon side-bands in the 660–730 nm range is attributed to the $^2E \rightarrow {}^4A_2$ transition of Cr^{3+} ions (spin-forbidden transition), and the broad luminescence band in the 750-850 nm range is assigned to the $^4T_2 \rightarrow {}^4A_2$ transition (spin-allowed transition) [14]. The two Cr^{3+} luminescence bands arise from the incorporation of Cr^{3+} ions in several non-equivalent sites in the CA_6 structure, possessing different coordination environments and crystal field strengths affecting the luminescence properties of Cr^{3+} ions [14].

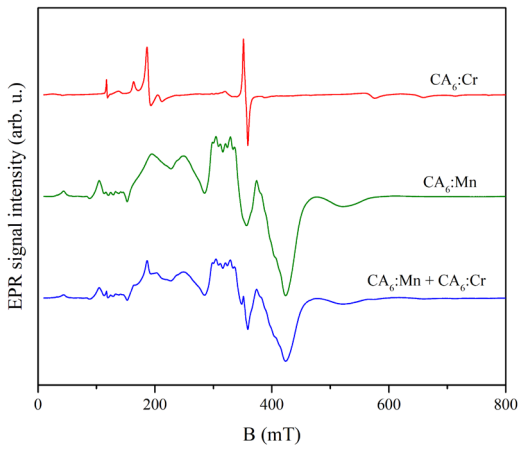

Fig. 1. EPR spectra of the investigated CA_6 samples.

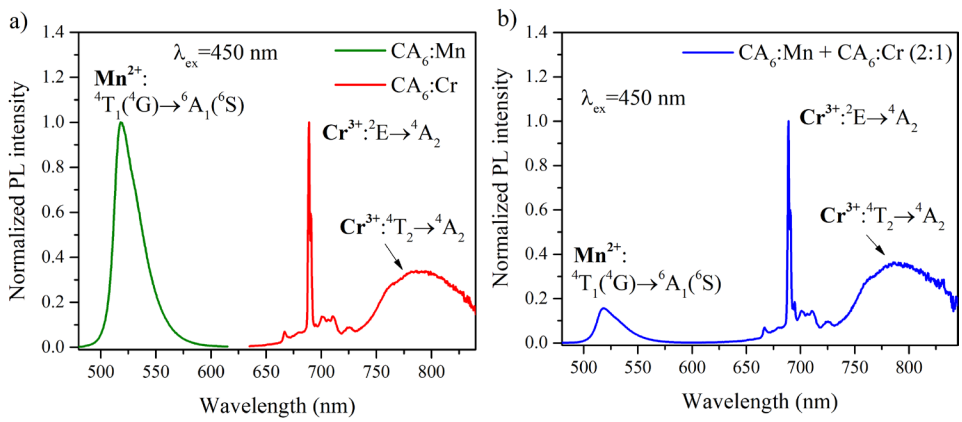

Fig. 2. The luminescence spectra of Mn^{2+}- and Cr^{3+}-doped CA_6 powders with 450 nm excitation. a) Mn^{2+} and Cr^{3+} singly-doped samples, b) Mn^{2+} and Cr^{3+} doubly-doped sample.

The luminescence excitation spectra of Mn^{2+} (at 518 nm) and Cr^{3+} (at 760 nm) ions depicted in Fig. 3 show that 450 nm is suitable for the excitation of both Mn^{2+} and Cr^{3+} ions. The Cr^{3+} excitation bands of 760 nm emission are assigned to $^4A_2 \rightarrow {}^4T_1(^4P)$ (225-300 nm), $^4A_2 \rightarrow {}^4T_1(^4F)$ (330-490 nm), and $^4A_2 \rightarrow {}^4T_2(^4F)$ (490-650 nm) with the maximal excitation intensity around 390 nm ($^4A_2 \rightarrow {}^4T_1(^4F)$) [14]. The excitation spectrum of Mn^{2+} ions (λ_{em}=518 nm) consists of relatively narrower bands

at 358 nm ($^6A_1(^6S)\rightarrow{}^4E_g(^4D)$), 386 nm ($^6A_1(^6S)\rightarrow{}^4T_{2g}(^4D)$), 426 nm ($^6A_1(^6S)\rightarrow{}^4A_{1g}$, $^4E_g(^4G)$), and 450 nm ($^6A_1(^6S)\rightarrow{}^4T_2(^4G)$) [13]. Thus, Fig. 3 shows that 450 nm radiation overlaps with the most intense excitation bands of Cr^{3+} and Mn^{2+} ions in CA_6.

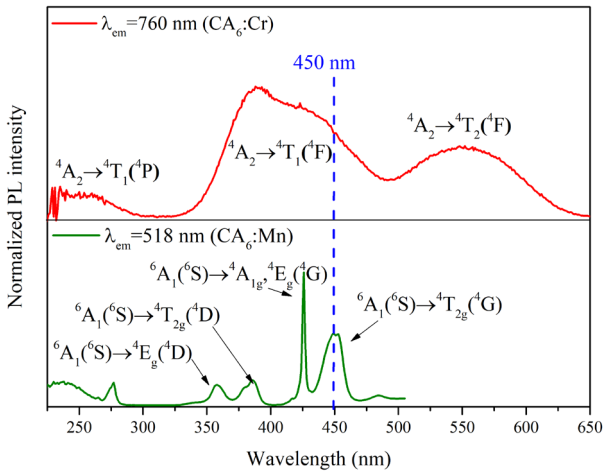

Fig. 3. Luminescence excitation spectra of Cr^{3+} (λ_{em}=760 nm) and Mn^{2+} (λ_{em}=518 nm) ions in CA_6 powders.

To obtain temperature dependences of luminescence, we chose 450 nm as the optimal excitation wavelength, using which luminescence of both Mn^{2+} and Cr^{3+} centres is excited at comparable intensities. As a result of the experiments, it was determined that 450 nm excitation provides the most monotonous temperature dependence of the total Mn^{2+} (500 – 550 nm) and Cr^{3+} (750–800 nm) luminescence in the entire studied temperature range from 20 °C to 800 °C (see Fig. 4). The temperature dependence of the Cr^{3+} ion covers the high temperature range, while the Mn^{2+} ion luminescence band gives an increase in the total intensity and provides a more uniform change in the range from 400 °C to 550 °C.

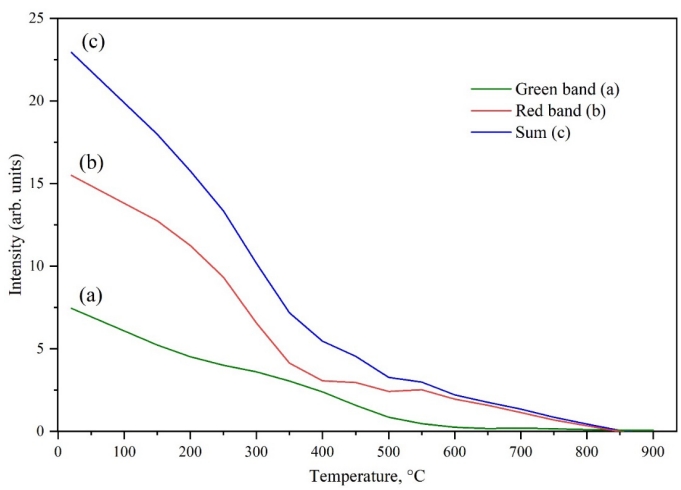

Fig. 4. Temperature dependence of the luminescence intensities of CA_6:Mn + Cr sample: a) Mn^{2+} luminescence (Green band, 500–550 nm), b) Cr^{3+} luminescence (Red band, 750–800 nm), c) Mn^{2+} luminescence + Cr^{3+} luminescence (Sum).

For optimal input and transmission of luminescence excitation radiation (450 nm) and emission bands of Mn^{2+} (green) and Cr^{3+} (red), we suggest using the scheme shown in Fig. 5. The optical bundle is made of 100 μm fused silica fibres with fluorine doped fused silica cladding. Polyimide coating withstand temperatures up to 385 °C, but since the optical bundle end is not in a direct contact with hot surface, it can be used to measure temperatures up to 800 °C. The sample holding probe (Fig. 5, part No. 5) is made of stainless steel with calcium aluminate phosphor containing capsule.

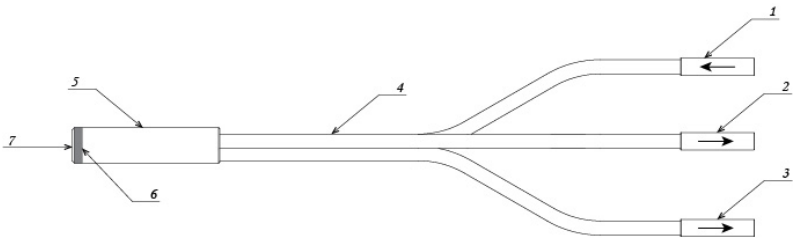

Fig. 5. The operating principle of the optical temperature sensor, using optical fibres to transmit light: 1) exciting light input – 450 nm laser diode, 2) filtered green light (500-550 nm) output, 3) filtered red light (750–800 nm) output, 4) optical fibre bundle, 5) temperature measuring probe body, 6) phosphor in the form of a tablet made from with Mn^{2+} and Cr^{3+} of doped calcium aluminate material, 7) temperature measurement point.

The thermal resistance of the active end of the temperature sensor design must also reach the mentioned 800 °C. In the temperature range above 600 °C, light modulation and a lock-in detector can be used to separate the thermal radiation background.

4. CONCLUSIONS

The application of CA_6 material doped with Mn and Cr in optical thermometry was investigated. The incorporation of Mn^{2+} and Cr^{3+} ions in CA_6 was confirmed by EPR and luminescence spectroscopy techniques. In the Mn-doped material, a single luminescence band at 518 nm was detected, whereas the luminescence spectrum of the Cr-doped sample comprised of overlapping Cr^{3+} signals in the 660–850 nm range. An excitation wavelength of 450 nm provided optimal results for simultaneous luminescence excitation in the mixed Mn- and Cr-doped CA_6 material. Using a specially designed optical fibre bundle and filtering Mn^{2+} (500–550 nm) and Cr^{3+} (750–800 nm) luminescence signals, a proof-of-concept optical temperature sensor was successfully demonstrated, operating within a temperature range of 20–800 °C.

ACKNOWLEDGEMENTS

We greatly acknowledge the financial support via the ERDF project No.1.1.1.1/19/A/020.

Institute of Solid State Physics, University of Latvia as the Centre of Excellence has received funding from the European Union's Horizon 2020 Framework Programme H2020-WIDESPREAD-01-2016-2017-TeamingPhase2 under grant agreement No. 739508, project CAMART².

REFERENCES

1. Childs, P.R.N., Greenwood, J.R., & Long, C.A. (2000). Review of Temperature Measurement. *Rev. Sci. Instrum*., *71*, 2959–2978. doi:10.1063/1.1305516
2. Wang, X.D., Wolfbeis, O.S., & Meier, R.J. (2013). Luminescent Probes and Sensors for Temperature. *Chem. Soc. Rev*., *42*, 7834e7869. https://doi.org/10.1039/C3CS60102A.
3. Dramićanin, M.D. (2020). Trends in Luminescence Thermometry. *Journal of Applied Physics, 128* (4), 40902. https://doi.org/10.1063/5.0014825
4. Wang, Q., Liao, M., Lin, Q., Xiong, M., Zhongfei, M., & Wu, F. (2021). A Review on Fluorescence Intensity Ratio Thermometer Based on Rare-Earth and Transition Metal Ions Doped Inorganic Luminescent Materials. *Journal of Alloys and Compounds, 850*. 156744. https://doi.org/10.1016/j.jallcom.2020.156744.
5. Wang, X., Liu, Q., Bu, Y., Liu, C.-S., Liu, T., & Yan, X. (2015). Optical Temperature Sensing of Rare-Earth Ion Doped Phosphors. *RSC Advances, 5* (105), 86219–86236. https://doi.org/10.1039/c5ra16986k.
6. Zhou, Y., Qin, F., Zheng, Y., Zhang, Z., & Cao, W. (2015). Fluorescence Intensity Ratio Method for Temperature Sensing. *Optics letters, 40* (19), 4544–4547. https://doi.org/10.1364/OL.40.004544
7. Marciniak, L., Kniec, K., Elzbieciak-Piecka, K., Trejgis, K., Stefanska, J., & Dramićanin, M. (2022). Luminescence Thermometry with Transition Metal Ions. A Review. *Coordination Chemistry Reviews, 469*, 214671. https://doi.org/10.1016/j.ccr.2022.214671.
8. Abbas, M.T., Khan, N.Z., Mao, J., Qiu, L., Wei, X., Chen, Y., & Khan, S.A. (2022). Lanthanide and Transition Metals Doped Materials for Non-contact Optical Thermometry with Promising Approaches. *Materials Today Chemistry, 24*, 100903. https://doi.org/10.1016/j.matchem.2022.100903.
9. Singh, V., Chakradhar, R.P.S. Rao, J.L., & Kim, D.K. (2008). Photoluminescence and EPR Studies of Cr-doped Hibonite ($CaAl_{12}O_{19}$) Phosphors. *Solid State Sci., 10*, 1525–1532. https://doi.org/10.1016/j.solidstatesciences.2008.03.006.
10. Singh, V., Natarajan, V., & Zhu, J.J., (2007). Luminescence and EPR Investigations of Mn Activated Calcium Aluminate Prepared via Combustion Method. *Opt Mater (Amst)*., *30*, 468–472. https://doi.org/10.1016/j.optmat.2007.01.003.
11. Kemere, M., Antuzevics, A., Rodionovs, P., Rogulis, U., & Sarakovskis, A., (2022). Photoluminescence and Electron Paramagnetic Resonance Studies of Mn^{2+} Doped $CaAl_4O_7$. *Opt Mater (Amst)*., *127*, 112352. https://doi.org/10.1016/j.optmat.2022.112352.
12. Lu, J., Pan, Y., Wang, J., Chen, X., Huang, S., & Liu, G. (2013). Reduction of Mn^{4+} to Mn^{2+} in $CaAl_{12}O_{19}$ by Co-doping Charge Compensators to Obtain Tunable Photoluminescence. *RSC Advances, 3* (14), 4510–4513. https://doi.org/10.1039/c3ra22938f.
13. Hu, J., Song, E., Zhou, Y., Zhang, S., Ye, S., Xia, Z., & Zhang, Q. (2019). Non-stoichiometric Defect-Controlled Reduction toward Mixed-Valence Mn-doped Hexaaluminates and their Optical Applications. *Journal of Materials Chemistry C*, *7* (19), 5716–5723. https://doi.org/10.1039/C9TC01026B
14. Yang, H., Zhao, W., Song, E., Yun, R., Huang, H., Song, J., … & Li, Y. (2020). Highly Flexible Dual-Mode Anti-counterfeiting Designs Based on Tunable Multi-band Emissions and Afterglow from Chromium-Doped Aluminates. *Journal of Materials Chemistry, C 8* (46), 16533–16541. https://doi.org/10.1039/d0tc04469e.

sciendo

LATVIAN JOURNAL OF PHYSICS
AND TECHNICAL SCIENCES
2023, N 5

DOI: 10.2478/lpts-2023-0028

SYNTHESIS OF $NaYF_4:Yb^{3+}$, Tm^{3+} NANOCRYSTALS VIA THE THERMAL DECOMPOSITION METHOD USING REFINED SUNFLOWER OIL

L. Smelkovs*, V. Viksna, J. Teterovskis, J. Grube

Institute of Solid State Physics, University of Latvia,
8 Kengaraga Str., Riga, LV-1063, LATVIA
*e-mail: lukass.smelkovs@cfi.lu.lv

In recent years, up-conversion luminescence nanoparticles have attracted significant attention from researchers in fields such as analytical chemistry (for example qualitative and quantitative analysis of metal and non-metal ions) and biomedicine (cancer imaging, drug delivery, treatment, etc.) due to their high rate of emission efficiency, easy surface functionalization, great chemical and thermal and photostability and other favorable properties. $NaYF_4$ in particular has attracted interest of researchers as a host material due to its low phonon energy, thus increasing the efficiency of emission. In this study, the synthesis of $NaYF_4:Yb^{3+},Tm^{3+}$ nanocrystals using the hydrothermal method was successfully carried out. Refined sunflower oil containing oleic acid was used as a solvent instead of analytical grade oleic acid and octadecene-1, reducing the cost of the synthesis. Using semi-quantitative XRD measurement analysis, it was determined that 25.3 % hexagonal β-$NaYF_4:Yb^{3+},Tm^{3+}$ as well as 23.8 % cubic α-$NaYF_4$ nanocrystal crystalline phases were found in the synthesized sample. The sample showed mainly luminescent characteristics typical of hexagonal $NaYF_4:Yb^{3+},Tm^{3+}$ lattice nanoparticles.

Keywords: *$NaYF_4:Yb^{3+}$, Tm^{3+}, refined sunflower oil, thermal decomposition, up-conversion luminescence.*

1. INTRODUCTION

Nanoparticles emitting up-conversion luminescence (UCNPs) are a type of nanoparticles that are able to emit visible and even ultraviolet (UV) light upon excitation by near infrared (NIR) radiation via the anti-Stokes process, where multiple IR photons absorbed by a material are converted into photons with higher energy [1]. $NaYF_4$ nanoparticles in particular have attracted the interest of researchers due to low phonon

energy, resulting in enhanced emission characteristics [2]. Like other UCNPs, they have shown to exhibit properties such as relatively high rate of emission efficiency, great chemical and thermal photostability, low toxicity, easy surface functionalization, and excellent biocompatibility (e.g., with human cells, blood serum). Due to these abilities, the research so far has been primarily focused on biosensing and cancer imaging, drug delivery, virus detection and treatment [3]–[6], as well as quantitative analysis of metal and non-metal ions, inorganic compounds, organic compounds in water, food, saliva and human blood/serum [7]–[12].

In particular, the hexagonal crystalline phase of $NaYF_4$:Yb^{3+},Tm^{3+} several nanoparticle synthesis methods can be found in academic literature. Hexagonal crystalline phase nanocrystals and their synthesis methods are of particular interest, since the hexagonal crystalline phase of $NaYF_4$:Yb^{3+},Tm^{3+} exhibits better up-conversion (UC) luminescence properties as opposed to the cubic crystalline phase [13]–[14].

There are several methods that can be used to synthesize hexagonal $NaYF_4$:Yb^{3+},Tm^{3+} nanoparticles, including co-precipitation, microemulsion, thermal decomposition, combustion synthesis, sol-gel method, and hydro/solvothermal synthesis. Co-precipitation method is useful for creating small nanocrystals. The method is cheap and time-efficient. It is economical, eco-friendly, and needs low (ambient) temperature, which allows for its application in large-scale production to afford nanocrystals with high aqueous solubility.

Moreover, the reaction conditions for precipitation are mild and can be easily adjusted to achieve the desired outcome. The downsides of this method are the synthesized UCNPs need for high temperature calcination and post-annealing, as well as the tendency towards poor/undesired morphology and uneven size distribution. Additional drawback of this method is the formation of hard aggregates, mainly due to the bridging of adjacent particles with H_2O through hydrogen bonds and the corresponding broad capillary forces created during drying. Another synthesis method is thermal decomposition. Its advantages include monodispersed crystals with good morphology and strong up-conversion emission. The disadvantages of this method are fairly difficult synthesis conditions, use of expensive and sensitive metal precursors, as well as generation of toxic byproducts. Sol-gel processing uses cheap precursors, produces nanoparticles with high UC luminescence intensity and may be scaled to industrial levels due to the high crystallinity formed at high annealing temperature. The drawbacks include the necessity of post-heating treatment.

Other issues are considerable particle aggregation, broad particle size distribution, irregular morphology, and insolubility in water. The advantages of microemulsion method are relatively easy operation, the small size of the UCNPs, and the ability for the control of morphology of products by adjusting the dosage of the surfactant, solvent, as well as the aging time. This method, however, usually produces low yield, the scope of analysis is narrow, and sample separation is difficult. A hydro/solvothermal method can also be conducted, in which core-shell-structured nanoparticles are synthesized. The advantages of this method lie in the method ability to produce nanocrystals of desired lattice (cubic, hexagonal) and size fairly consistently, to ensure high purity grade of nanoparticles, which several other methods lack, as well as mild reaction conditions and high reaction activity. Furthermore, it does not require a very exacting operation of the synthesis process. A significant disadvantage is that this method usually requires an autoclave, which means that the growth

of nanocrystals cannot be monitored in real time, and the reaction time is generally long [15]–[20].

The synthesis method employed in this paper is thermal decomposition, where core-shell nanoparticle structure is synthesized. Advantages of the method include monodispersed crystals with good, uniform morphology, high crystal transition strength, easily adjustable and monitorable parameters during crystal growth, as well as strong up-conversion emission. The disadvantages of this method are fairly difficult synthesis conditions, use of expensive and sensitive metal precursors, need for further surface modification for biomedical application, as well as generation of toxic byproducts. [15]–[18], [20], [21]. An outstanding benefit of the core-shell technology is that different rare-earth ions can be confined in different layers to achieve a controllable interaction between the doped ions and their environment, and an additional benefit is improved UC emission [21].

Typically, this synthesis method is done utilizing ocatdecene-1 and oleic acid. Oleic acid is used both as a solvent and a reactant, the polar part of which reacts with nanocrystals when forming the core-shell structure, while octadene-1, being non-polar, is used only as a solvent. In this synthesis, both of these solvents were swapped out for refined sunflower oil (RSO), reducing the cost of the synthesis, since RSO is much cheaper than analytical grade oleic-acid and octadecene-1, reducing the overall cost of the synthesis method, as well as using a much more common and readily available solvent, thus making the industrial production of nanocrystals more feasible, plausible and appealing. Although there has been considerable amount of research in nanoparticle synthesis using sunflower oil [22], to our knowledge, there have been no prior accounts in literature of synthesizing $NaYF_4:Yb^{3+},Tm^{3+}$ using RSO as a solvent via the thermal decomposition method.

2. EXPERIMENTAL

2.1. Synthesis Process

Materials used in the synthesis: 74.7 % Y_2O_3, 25% Yb_2O_3 and 0.3 % Tm_2O_3 for core part of nanoparticles, and 100 % Y_2O_3 for shell up-conversion nanoparticles. Other materials used for synthesis are 37 % hydrochloric acid (HCl), deionized water, refined sunflower oil (RSO), petroleum, cyclohexane, chloroform, methanol, sodium hydroxide (NaOH), and ammonium fluoride (NH_4F).

2.1.1. Shell Synthesis

In the three-necked flask 0.113 g of Y_2O_3 is added and 36 ml of diluted HCl solution (30 ml of deionized water and 6 ml HCl). The flask is then placed in magnetic heated stirrer, and the solution is heated up till it becomes clear. It is then transferred to an oven that is heated to 110 °C, and kept for 24 hours. The following day, the flask is taken out of the oven, and 21 ml of RSO is added. The flask is then placed back in magnetic heated stirrer and is connected to argon gas cylinder, thermometer and water jet pump. Three aeration cycles are done (making vacuum and adding argon 3 times) to get rid of all the oxygen. The solution is heated up to 240 °C and then cooled down to room temperature. In the meantime, methanol solution is prepared. In two

separate containers, methanol solution is made. One contains 0.1 g of NaOH and 10 ml methanol, while the other contains 0.2 g of NH_4F and 10 ml of methanol. Both containers are then placed in ultrasonic bath to mix for approximately 1 hour until everything is dissolved. After that, both methanol solutions are combined and poured in flask, which is at room temperature. Solution is then mixed for 30 minutes, and then three aeration cycles are done. Once all the methanol has evaporated, the solution is heated up to 300 °C, so that nanoparticles can start to form and grow. For 5 minutes, the solution is held at 300 °C, and then cooled down to room temperature. 50 ml of petroleum is added and mixed for 30 minutes. The solution is then poured in centrifuge tubes and placed in a centrifuge at 6000 revolutions per minute (rpm) for 10 minutes. After centrifugation, petroleum with other liquids is poured out and is left with sediments. 20 ml of petroleum is added to each centrifuge tube, and all sediments are dissolved. The solution is then poured back into three-necked flask, mixed for 24 hours more to get more organic byproducts out of the solution. The solution is then added into centrifuge and centrifuged at 6000 rpm for 10 minutes. The petroleum is then poured out and 10 ml of cyclohexane is added to each centrifuge tube. 5 ml of RSO is then added into a beaker and heated up until all of the cyclohexane evaporates. The solution is left to cool down and shell nanoparticles are ready to be injected into synthesized core nanocrystals.

2.1.2. Core Synthesis

Core synthesis is similar to shell synthesis as the only difference is the concentrations of additives. In the three-necked flask 0.201 g of R_2O_3 (R: Y_2O_3, Yb_2O_3, Tm_2O_3) is added with 54 ml of diluted HCl solution (45 ml of deionized water and 9 ml HCl). Solution is heated till it becomes clear and is transferred to the oven that is heated to 110 °C and kept for 24 hours. The next day 31.5 ml of RSO is added to the flask. Methanol solution is made with 0.15 g of NaOH and 12.5 ml of methanol and 0.3 g of NH_4F and 12.5 ml of methanol. The next few steps are done exactly as in shell synthesis. Once the solution has reached 300 °C it is held at that temperature for 2 hours and then shell particles are injected into core structure. The solution cools down to approximately 280 °C once the shell is injected. It is then heated back up to 300 °C and held for an additional hour. Once the solution has cooled down to room temperature, 50 ml of petroleum is added, it is then mixed for 30 minutes. The solution is then centrifuged at 6000 rpm for 10 minutes. Petroleum is then poured out so that the tubes contain only the sediments. 20 ml of chloroform is then added to each centrifuge to dissolve the sediments containing the nanocrystals.

2. RESULTS AND DISCUSSION

3.1. Synthesized Sample Morphology and Fluorescent Property Characterisation

Synthesized sample morphology was studied using Scanning Electron Microscope (SEM) Thermo Scientific Helios UX 5 in scanning transmission electron microscope (STEM) mode. UCNP size analysis was performed using ImageJ soft-

ware. Sample structure was studied using RIGAKU X-Ray diffractometer MiniFlex 600. The measurements were taken at 40 kV and 15 mA with copper X-ray tube.

UC luminescence spectra of synthesized nanoparticles was measured using standard luminescence measurements setup. UC luminescence was excited using Thorlabs L975P1WJ CW laser diode on TCLDM9 - TE-Cooled Mount from Thorlabs. Laser diode input current was controlled using Thorlabs current controller LDC220C, laser diode temperature was controlled using Thorlabs temperature controller TED200C. The laser diode temperature was set so that the radiation emitted by the laser diode coincided with Yb^{3+} absorption maximum at 976 nm. Solution with UCNP was filled into UV fused quartz cuvettes (Thorlabs CV10Q3500F). UC luminescence was collected into the spectrometer Andor Kymera 328i-B1 coupled with Andor iStar CCD camera. All measured UC luminescence spectra were corrected according to the measurement system spectral response.

3.1.1. XRD Measurements

A XRD measurement was carried out determine the crystalline structure of synthesized nanoparticles. Before measurements, samples were dried out to obtain them in powder form. The diffraction peak measurement was compared with ICDD PDF-2 database entries. The results (Fig. 1) show that there are diffraction peaks that correspond to hexagonal crystalline phase β-$NaYF_4$ (PDF 00-028-1192), cubic α-$NaYF_4$ (PDF-01-077-2042), as well as NaCl (PDF 01-071-4661) in halite mineral form. Using semi-quantitative analysis, it was calculated that 50.9 % of the sample contained NaCl in halite mineral form, 23.8 % of the sample contained cubic $NaYF_4$ crystals, while 25.3 % of the sample contained desired lattice hexagonal doped $NaYF_4$ nanocrystals.

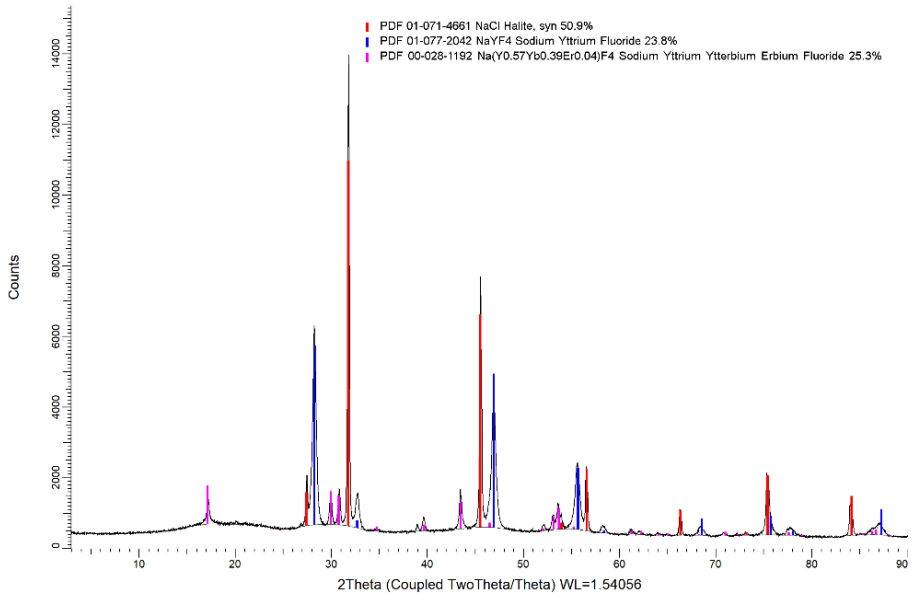

Fig. 1. XRD pattern of synthesized sample. Diffraction maximum positions from databases are given from β-$NaYF_4$ – pink, α-$NaYF_4$, – blue, NaCl in its halite mineral form – red.

To determine the effect of temperature and heating time on the crystalline structure of synthesized sample, additional synthesis was performed. Heating for 10 minutes at 300 °C for core nanoparticles and 5 minutes combined core and shell held at 300 °C, gave only cubic crystalline phase. Increasing the time for core and combined nanoparticles started to change crystalline phase from cubic to hexagonal. Figure 2 shows the presence of these crystalline phases. Our own experimental data and academic literature indicate that α-$NaYF_4$ nanocrystals are first formed, proceed by α → β conversion that occurs via a dissolution / recrystallization process, rather than through oriented aggregation of small α-phase UCNCs [23]. NaCl in the sample is a byproduct of a reaction between lanthanoid chlorides and NaF. It is also plausible to assume that NaCl may have formed due to side reactions with other compounds that are commonly found in RSO, such as linoleic acid, palmitic acid, stearic acid, esters, polyphenols, terpenoids, etc. [24].

3.1.2 STEM Measurements

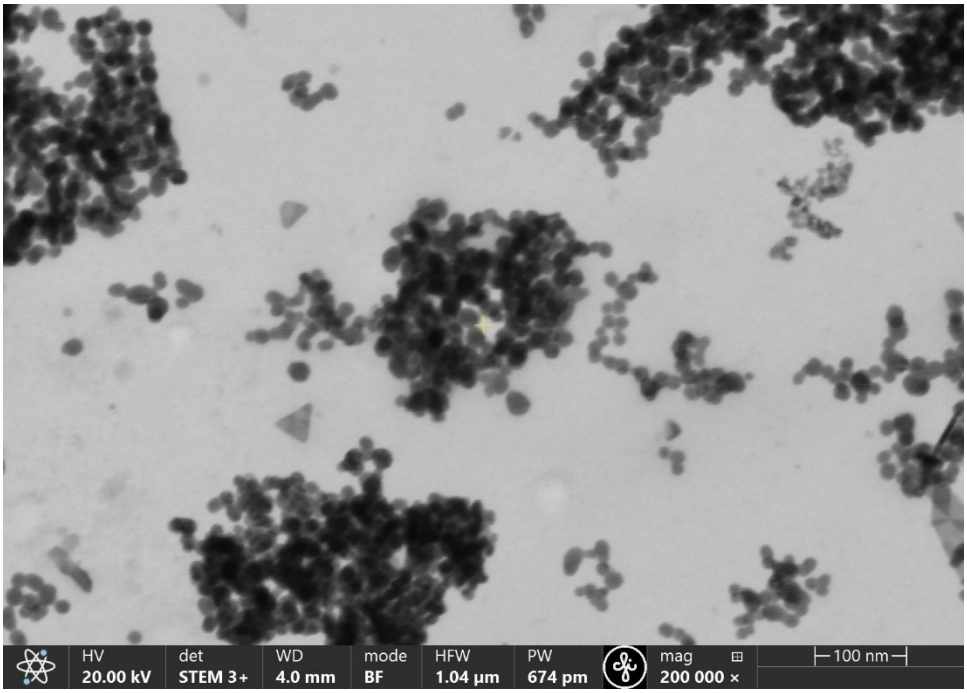

Fig. 2. STEM image of synthesized $NaYF_4$ nanoparticles doped with Yb^{3+},Tm^{3+}.

Using STEM it is possible to determine nanoparticle size and size distribution. Figure 2 shows that nanoparticles are agglomerated. Residual organic material after several rinsing processes can be also observed in Fig. 2, distorting the STEM image. Apart from the base material, there are also some plate-like crystals in the sample, which can be something that has crystallized from the solvent. These were quite resistant to e-beams, so these could be inorganic substances resulting from synthesis. Analysis

of nanoparticle size distribution shows that the mean size of synthesized nanoparticles is 17.2 ± 3.0 nm. STEM measurements allow determining synthesized nanoparticle morphology and size distribution, but not distinguishing core and shell part for nanoparticles in this study. This is explained by the fact that core and shell parts are made from the same base material – $NaYF_4$ only core part is doped with Tm^{3+} and Yb^{3+}, which only slightly affect $NaYF_4$ crystalline structure parameters [25]. Changes that have occurred by dopant introduction into base matrix cannot be detected by STEM measurements. The effect of the shell part on the dimensions of the nanoparticle can be determined by the electron microscopy measurement of nanoparticles obtained at different stages of synthesis processes [23].

3.1.3 Up-conversion Luminescence Measurements

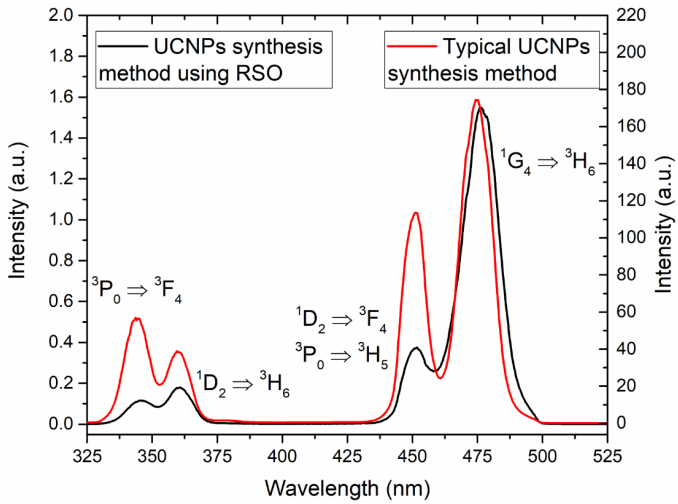

Fig. 3. Black line UC luminescence spectrum of synthesized $NaYF_4$ doped with Yb^{3+}, Tm^{3+} using RSO. Red line shows UC luminescence spectrum $NaYF_4$ doped with Yb^{3+}, Tm^{3+} synthesized with typical synthesis method. All spectra are recorded under 976 nm excitation. Tm^{3+} optical transitions for corresponding up-conversion luminescence bands are shown.

Distinguishing blue Tm^{3+} up-conversion luminescence can be observed with naked eye for synthesized $NaYF_4$:Yb^{3+},Tm^{3+} nanoparticles under excitation with 976 nm. Black line in Fig. 3 shows UC luminescence spectrum in blue and UV spectral regions, with Tm^{3+} luminescence bands in blue (476 nm and 454 nm) and UV (375nm and 340 nm) spectral regions: 476 nm - $^1G_4 - {}^3H_6$, 454 nm ($^1D_2 - {}^3F_4$, $^3P_0 - {}^3H_5$), 361 nm ($^1D_2 - {}^3H_6$) and 345 nm ($^3P_0 - {}^3F_4$) [26]. Other Tm^{3+} UC luminescence bands in red and infrared spectral region can also be observed, but the main focus is on UC luminescence bands in blue and UV spectral regions. Although XRD measurements show that $NaYF_4$ cubic and hexagonal phases coexist in the synthesized sample (23.8 % and 25.3 %, respectively), UC luminescence mainly occurs from $NaYF_4$ hexagonal phase due to higher efficiency of UC process since the data found in the literature indicate that hexagonal nanoparticle UCL is a factor of 10^4 brighter than that obtained from the cubic

phase nanoparticles [13].

For comparison, Fig. 3 also shows UC luminescence spectra (red line) for $NaYF_4$ core / shell nanoparticles doped with Yb^{3+}, Tm^{3+} which are synthesized with typical synthesis method [27]. It is possible to observe differences in the ratios of the different UC luminescence bands and in the overall UC luminescence intensity. Observed differences in UC luminescence spectra can be explained by two facts: (1) In this study, only part of synthesized $NaYF_4$ nanoparticles are in hexagonal phase which emits UC luminescence. This means that there are fewer nanoparticles which can emit UC luminesce. (2) In this study, the mean size of synthesized nanoparticles is 17.2 ± 3.0 nm, while in [27] the mean size of nanoparticles is 33.9 ± 4.6 nm. Smaller nanoparticle size means that energy transfer steps from Yb^{3+} to Tm^{3+} are less likely to occur. As a result, over all UC luminescence intensity will be lower compared to nanoparticles with greater size and Tm^{3+} is less likely to become excited to states with higher energy.

4. CONCLUSIONS

In this study, $NaYF_4$:Yb^{3+},Tm^{3+} nanoparticles (in cubic and hexagonal phase) with the size of 17.2 ± 3.0 nm were synthesized by means of thermal decomposition method using refined sunflower oil (RSO) as a substitute for oleic-acid and octadecene-1 that allowed reducing the overall cost of the synthesis method. Crystalline structure of synthesized nanoparticles was defined by the time of synthesis at 300 °C. During the study, 10 minutes at 300 °C core nanoparticles and 5 minutes combined core and shell held at 300 °C gave only cubic crystalline phase. Increasing the time for core and combined nanoparticles started to change crystalline phase from cubic to hexagonal. Characteristic Tm^{3+} up-conversion luminescence bands in blue and UV spectral regions could be observed under 976 nm excitation.

ACKNOWLEDGEMENTS

The research has been funded by the Latvian Council of Science, project "Up-conversion luminescence photolithography in organic compounds using nanoparticles/photoresist composition", project No. lzp-2019/1-0422.

Institute of Solid State Physics, University of Latvia as the Center of Excellence has received funding from the European Union's Horizon 2020 Framework Programme H2020- WIDESPREAD-01-2016-2017-TeamingPhase2 under grant agreement No. 739508, project CAMART².

REFERENCES

1. Auzel, F. (2004). Upconversion and Anti-Stokes Processes with f and d Ions in Solids. *Chemical Reviews, 104* (1), 139–174. https://doi.org/10.1021/cr020357g
2. Yang, D., Chen, D., He, H., Pan, Q., Xiao, Q., Qiu, J., & Dong, G. (2016). Controllable Phase Transformation and Mid-infrared Emission from Er3+-Doped Hexagonal-/Cubic-NaYF4 Nanocrystals. *Scientific Reports*, *6,* 29871. https://doi.org/10.1038/srep29871

3. Bing-Shuai, Z. H. O. U., Shi-Han, X. U., Song-Tao, H. U., Li-Heng, S. U. N., Jie-Kai, L. Y. U., Rui, S. U. N., … & Biao, D. O. N. G. (2022). Recent Progress of Upconversion Nanoparticles in the Treatment and Detection of Various Diseases. *Chinese Journal of Analytical Chemistry, 50* (2), 19–32. https://doi.org/10.1016/j.cjac.2021.08.003

4. Peng, X., Ai, F., Yan, L., Ha, E., Hu, X., He, S., & Hu, J. (2021). Synthesis Strategies and Biomedical Applications for Doped Inorganic Semiconductor Nanocrystals. *Cell Reports Physical Science, 2* (5), 100436. https://doi.org/10.1016/j.xcrp.2021.100436

5. Xin, N., Wei, D., Zhu, Y., Yang, M., Ramakrishna, S., Lee, O., … & Fan, H. (2020). Upconversion Nanomaterials: A Platform for Biosensing, Theranostic and Photoregulation. *Materials Today Chemistry, 17,* 100329. https://doi.org/10.1016/j.mtchem.2020.100329

6. Escudero, A., Becerro, A. I., Carrillo-Carrión, C., Núñez, N. O., Zyuzin, M. v., Laguna, M., … & Parak, W. J. (2017). Rare Earth Based Nanostructured Materials: Synthesis, Functionalization, Properties and Bioimaging and Biosensing Applications. *Nanophotonics, 6* (5). https://doi.org/10.1515/nanoph-2017-0007

7. Liu, Y., Tu, D., Zheng, W., Lu, L., You, W., Zhou, S., … & Chen, X. (2018). A Strategy for Accurate Detection of Glucose in Human Serum and Whole Blood Based on an Upconversion Nanoparticles-Polydopamine Nanosystem. *Nano Research*, *11* (6), 3164–3174. https://doi.org/10.1007/s12274-017-1721-1

8. Li, Z., Lv, S., Wang, Y., Chen, S., & Liu, Z. (2015). Construction of LRET-Based Nanoprobe Using Upconversion Nanoparticles with Confined Emitters and Bared Surface as Luminophore. *Journal of the American Chemical Society*, *137* (9), 3421–3427. https://doi.org/10.1021/jacs.5b01504

9. Hlaváček, A., Farka, Z., Hübner, M., Horňáková, V., Němeček, D., Niessner, R., … & Gorris, H. H. (2016). Competitive Upconversion-Linked Immunosorbent Assay for the Sensitive Detection of Diclofenac. *Analytical Chemistry*, *88* (11), 6011–6017. https://doi.org/10.1021/acs.analchem.6b01083

10. Chen, H., Tang, W., Liu, Y., & Wang, L. (2022). Quantitative Image Analysis Method for Detection of Nitrite with Cyanine Dye-NaYF4:Yb,Tm@NaYF4 Upconversion Nanoparticles Composite Luminescent Probe. *Food Chemistry*, *367,* 130660. https://doi.org/10.1016/j.foodchem.2021.130660

11. Zuo, J., Wang, W., Zhang, D., Wang, X., Ma, Y., Li, P., ... & Zhang, H. (2022). Ultra-Sensitive Water Detection Based on NaErF4@NaYF4 High-Level-Doping Upconversion Nanoparticles. *Applied Surface Science*, *575,* 151701. https://doi.org/10.1016/j.apsusc.2021.151701

12. Yang, C., Li, Y., Wu, N., Zhang, Y., Feng, W., Yu, M., & Li, Z. (2021). Ratiometric Upconversion Luminescence Nanoprobes for Quick Sensing of Hg2+ and Cells Imaging. *Sensors and Actuators, B: Chemical*, *326*, 128841. https://doi.org/10.1016/j.snb.2020.128841

13. Balabhadra, S., Reid, M. F., Golovko, V., & Wells, J. P. R. (2020). A Comparison of the Yb3+ Absorption and Upconversion Excitation Spectra for Both the Cubic and Hexagonal Phases of NaYF4:Yb3+/Er3+ Nanoparticles. *Optical Materials*, *107*, 110050. https://doi.org/10.1016/j.optmat.2020.110050

14. Krämer, K. W., Biner, D., Frei, G., Güdel, H. U., Hehlen, M. P., & Lüthi, S. R. (2004). Hexagonal Sodium Yttrium Fluoride Based Green and Blue Emitting Upconversion Phosphors. *Chemistry of Materials*, *16* (7), 1244–1251. https://doi.org/10.1021/cm031124o

15. Hong, E., Liu, L., Bai, L., Xia, C., Gao, L., Zhang, L., & Wang, B. (2019). Control Synthesis, Subtle Surface Modification of Rare-Earth-Doped Upconversion Nanoparticles and their Applications in Cancer Diagnosis and Treatment. *Materials Science and Engineering C, 105*, 110097. https://doi.org/10.1016/j.msec.2019.110097

16. Ansari, A. A., & Sillanpää, M. (2021). Advancement in Upconversion Nanoparticles Based NIR-Driven Photocatalysts. *Renewable and Sustainable Energy Reviews, 151*, 111631. https://doi.org/10.1016/j.rser.2021.111631
17. Zhou, J., Liu, Q., Feng, W., Sun, Y., & Li, F. (2015). Upconversion Luminescent Materials: Advances and Applications. *Chemical Reviews, 115* (1), 395–465. https://doi.org/10.1021/cr400478f
18. He, M., Huang, P., Zhang, C., Chen, F., Wang, C., Ma, J., … & Cui, D. (2011). A General Strategy for the Synthesis of Upconversion Rare Earth Fluoride Nanocrystals via a Novel OA/Ionic Liquid Two-Phase System. *Chemical Communications*, *47* (33), 9510–9512. https://doi.org/10.1039/c1cc12886h
19. Dinic, I. Z., Rabanal, M. E., Yamamoto, K., Tan, Z., Ohara, S., Mancic, L. T., & Milosevic, O. B. (2016). PEG and PVP Assisted Solvothermal Synthesis of NaYF4:Yb3+/Er3+ Up-conversion Nanoparticles. *Advanced Powder Technology*, *27* (3), 845–853. https://doi.org/10.1016/j.apt.2015.11.010
20. Mehrdel, B., Nikbakht, A., Aziz, A. A., Jameel, M. S., Dheyab, M. A., & Khaniabadi, P. M. (2022). Upconversion Lanthanide Nanomaterials: Basics Introduction, Synthesis Approaches, Mechanism and Application in Photodetector and Photovoltaic Devices. *Nanotechnology, 33* (8), 082001. https://doi.org/10.1088/1361-6528/ac37e3
21. Min, Y., Ding, X., Yu, B., Shen, Y., & Cong, H. (2023). Design of Sodium Lanthanide Fluoride Nanocrystals for NIR Imaging and Targeted Therapy. *Materials Today Chemistry*, *27*, 101335. https://doi.org/10.1016/J.MTCHEM.2022.101335
22. Pawar, R. V., Hulwan, D. B., & Mandale, M. B. (2022). Recent Advancements in Synthesis, Rheological Characterization, and Tribological Performance of Vegetable Oil-Based Lubricants Enhanced with Nanoparticles for Sustainable Lubrication. *Journal of Cleaner Production*, *378*, 134454. https://doi.org/10.1016/J.JCLEPRO.2022.134454
23. Suter, J. D., Pekas, N. J., Berry, M. T., & May, P. S. (2014). Real-Time-Monitoring of the Synthesis of β-NaYF4:17% Yb,3% Er Nanocrystals Using NIR-to-Visible Upconversion Luminescence. *Journal of Physical Chemistry C*, *118* (24), 13238–13247. https://doi.org/10.1021/jp502971j
24. Gotor, A. A., & Rhazi, L. (2016). Effects of Refining Process on Sunflower Oil Minor Components: A Review. *OCL*, *23* (2), D207. https://doi.org/10.1051/ocl/2016007
25. Sarakovskis, A., Grube, J., Mishnev, A., & Springis, M. (2009). Up-conversion Processes in NaLaF4:Er3+. *Optical Materials*, *31* (10), 1517–1524. https://doi.org/10.1016/J.OPTMAT.2009.02.015
26. Grube, J. (2022). Up-conversion Luminescence Processes in NaLaF4 Doped with Tm3+ and Yb3+ and Dependence on Tm3+ Concentration and Temperature. *Appl. Spectrosc. 76*, 189–198. https://doi.org/10.1177/00037028211045424.
27. Perveņecka, J., Teterovskis, J., Vembris, A., Vītols, K., Tropiņš, E., Vīksna, V. T., … & Grūbe, J. (2023). An Innovative Approach to Photolithography for Optical Recording of High-Resolution Two-Dimensional Structures in a Negative SU8 Photoresist by Activation of Up-conversion Luminescence in Yb3+ and Tm3+ Doped NaYF4 Nanoparticles. *Nano-Structures & Nano-Objects, 33*, 100932. https://doi.org/10.1016/J.NANOSO.2022.100932

sciendo

LATVIAN JOURNAL OF PHYSICS
AND TECHNICAL SCIENCES
2023, N 5

DOI: 10.2478/lpts-2023-0029

THE ROLE OF DECENTRALIZED ELECTRODE BOILER IN ANCILLARY SERVICES AND DISTRICT HEATING: A FEASIBILITY ASSESSMENT

K. Gicevskis*, O. Linkevics

Faculty of Electrical and Environmental Engineering,
Riga Technical University,
12/1 Azenes Str., Riga, LV-1010, LATVIA
*e-mail: karlis.gicevskis@edu.rtu.lv

This article evaluates the feasibility of using electrode boiler in grid ancillary services and district heating scenarios. Electrode boilers in the context of electricity grid management can be considered as a relatively new technology. This study assesses the technical and economic viability of electrode boiler by considering various factors such as energy demand, technical feasibility, economic viability, and regulatory market conditions. The simplified mathematical model has been developed for simulation of electrode boiler use for grid services and heat production. The results have shown that electrode boiler have the potential to be a cost-effective solution for heating and grid balancing services in certain scenarios. However, it may not be applicable or economically viable in all situations or regions; thus, further research and development is needed to fully realize their potential.

Keywords: *Balancing markets, CHP, electrode boiler, heat and power production.*

1. INTRODUCTION

It is widely acknowledged that combined heat and power plants (CHPs) can play a significant role in providing resilient energy systems. This is due to their ability to switch generation between electricity and heat, as well as operate in cyclic modes [1], [2]. Considering the rapid development of renewable energy sources and the emergence of new balancing markets, there is still a need for a comprehensive study on individual power-to-heat technologies that could further enhance the flexibility provided by CHPs. One such technology is the electrode boiler (EB).

EB is a device that uses electricity to generate heat for individual or district heating systems, or other industrial processes. Regarding electrode boilers, two types are

typically distinguished: those with an electric heater (known as electric resistance boilers) and those with electrodes. Due to their larger capacity, electrode boilers are most often used for district heating purposes. EBs can provide hot water as well as steam with efficiencies up to 99 % (η_{avg}^{EB}) and capacity of 5–70 megawatt (MW) [3], [4]. Other characteristics of electrode boilers are shown in Table 1.

Table 1. Electrode Boiler Characteristics [2], [5]

Parameter	Electrode boilers	
Ramp rate up/down, s	from less than 30 s	
Operating temperature level input, °C	10-110	
Operating temperature level output, °C	water: 70–140, steam: < 300 at 45 bar	
Investments for different EB capacities, million EUR/MW	Voltage and installed capacity	Net investments
	400 V and 1–3 MW	0.13–0.16
	10 kV and 10 MW	0.06–0.09
	10 kV and 20 MW	0.05–0.07
Total operations and maintenance (O&M)	-	
Fixed O&M, EUR/MW per year	1100	
Variable O&M, EUR per megawatt hour (MWh)	0.5	

As it can be seen in Table 1, the investments are decreasing with the increasing of EB capacity. To address potential cost fluctuations, including those attributed to inflation, this publication will incorporate a sensitivity analysis, considering cost adjustments of +15 % and +30 % for EB investments. Besides, valuable characteristics mentioned in Table 1, integrating EBs in CHPs is often associated with accommodation of large shares of variable renewable energy. Study [6] argues that despite an increased need for balancing renewables and the technology being available, initiatives to use them, for example, in Sweden district heating systems as flexibility sources are rare because the potential gain is considered low and unpredictive.

Nevertheless studies [7]–[10] emphasize importance of flexibility services provided by EBs. Most efforts of reviewed studies were focused on the electricity day-ahead market. Even though the number of works studying the participation in the balancing markets is limited, EBs still demonstrate the potential to increase the flexibility provided by CHPs, due to their high ramp rate from minimum to full load and high efficiency.

In this publication, the installation of EB is evaluated. The aim is to assess different EB capacities and the potential benefits from participating in heat and Baltic balancing markets. More specifically, restoration reserves with manual activation (mFRR) are evaluated in this paper, while EB is flexible enough to provide restoration reserves with automatic activation (aFRR) or even frequency containment reserve (FCR). Unlike previous research on district heating system in Riga [2], the use of EB is going to be investigated regarding the provision of ancillary services and heat supply. The proposed methodology considers income from both heat and ancillary services in the Baltic mFRR market.

The remaining part of this publication is structured as follows: Section II provides an overview of the current situation and CHP operation, as well as outlines the research problem and formulates the hypothesis. Section III presents and explains the math-

ematical model used for evaluation and calculation. Section IV presents results of mathematical simulation and feasibility assessment. Finally, Section V draws up the main conclusions of the research.

The study provides a reference for interested parties, including policy makers, foreseeing the landscape for power to heat system development.

2. AN OVERVIEW OF THE CURRENT SITUATION

A. Insight into the Energy Sector of Latvia and Other Baltic States

As studied in [11], [12], the Baltic States for the period up to 2030 can face the following: (1) supply of electricity balancing reserves is expected to decrease because the oldest conventional generators are expected to exit the market; (2) due to high geopolitical tensions in relations with ongoing war from Russia since February 2022, natural gas prices hit records – in the Netherlands Title Transfer Facility reached 345 EUR/MWh in March 2022; (3) the growing share of intermittent and distributed generation in the Baltic power system; (4) rising price of carbon dioxide (CO_2) emission allowances; (5) synchronisation of the Baltic power system with the grid of Continental Europe, which will further increase demand for balancing reserves – frequency containment reserves and automated/manual frequency restoration reserves (mFRR and aFRR).

According to a balancing roadmap of the Baltic transmission system operators (TSOs), TSOs have committed to implement and make operational European platform for the exchange of balancing energy from mFRR (the so-called MARI platform) and exchange of balancing energy from aFRR (the so-called PICASSO platform). Baltic TSOs have to join MARI platform no later than 24th July 2024, and the introduction of PICASSO is planned to be concluded by the end of 2024. To ensure necessary reserves for operation of the Baltic States, Baltic TSOs also plan to procure reserves (FCR, aFRR, mFRR) as capacity products. Procurement of all three types of reserves will start at the end of 2024. The main parameters for all three types of reserves are shown in Table 2 [13].

Table 2. Three Types of Reserves – FCR, aFRR and mFRR

Standard product	**FCR**	**aFRR**	**mFRR**
Activation type	Automatic	Automatic	Manual
Activation time	< 30 s (2 s reaction)	< 5 min	< 12.5 min
Minimum volume	1 MW		
Direction	Symmetrical	Up and down	
Preparation period	0 min	0 min	< 7 min
Linking of bids	No		Yes
Activation command	- (based on local frequency measurement)	Signal (from TSO frequency restoration controller)	Message (WebService)

This study considers EB aligned integration in JSC Latvenergo natural gas combined heat and power plant one and two (CHP-1 or CHP-2) operation. Both CHPs not only hedge Latvia against possible shortages of electricity supply, but also provide heat energy for the right bank of Riga district heating system. CHP-1 has two gas turbines (P = 158 MW and Q = 145 MW) combined with three gas heat only boilers (HOB, 3 × 116 MW). While CHP-2 consists of two combined-cycle gas turbines CHP - 2/1 (P = 412 MW and Q = 275 MW) and CHP - 2/2 (P = 419 MW and Q = 270 MW) combined with five gas HOBs (Q = 5 × 116 MW) [2].

B. Definition of the Problem and Formulation of the Hypothesis

In [2], two hypotheses were proposed: (A) Replacing natural gas fired boilers with EB can lower power plant production costs during periods of low electricity price in Europe's power market – Nord Pool; (B) Using EB can enhance the competitiveness of CHP plants. Both hypotheses generated positive incomes, although Hypothesis B was with lower income, making the installation of EB less attractive, while Hypothesis A showed more promise. This time, we will evaluate the benefits of providing regulation services to the transmission system operator through an EB. Therefore, the authors state the following hypothesis: The use of EB can not only reduce the heat production costs of CHPs, but also generate revenues from the Baltic balancing market, more precisely mFRR market, thus confirming the economic feasibility of EB integration in CHP operation, and making EB application more attractive.

C. The Baltic Balancing Market Volumes and Prices

Since 1 January 2018, a single balancing market has been operating in the Baltic States. Operation of the common Baltic balancing market takes place using balancing energy products: Baltic mFRR standard product and Baltic emergency reserve (ER) mFRR product. The total activated energy from mFRR and ER mFRR products in the Baltic balancing market for the four years can be seen in Fig. 1. On average, upward balancing electricity was activated in the amount of 193361 MWh during these years, and 210355 MWh for downward regulation.

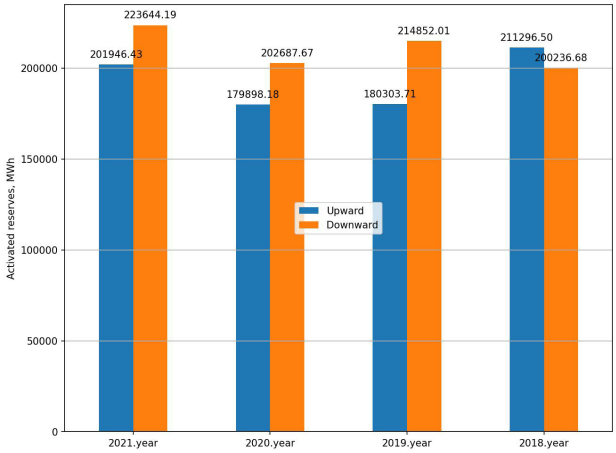

Fig. 1. Activated mFRR and ER mFRR volumes in the Baltic balancing market [14].

This study assumes that the EB will only be used for downward mFRR regulation, and the balancing market data and CHPs operation calculations are based on the year 2021. The reason for choosing 2021 is that CHPs units have been operating less than usual since 2022, due to the uncertainty surrounding gas availability following Russia's invasion of Ukraine.

Figure 2 shows the average annual reserve prices from normal activations for both upward and downward regulation in all three Baltic countries. The price of the ER mFRR specific product is not available on the Baltic Coba platform and not included in these statistics.

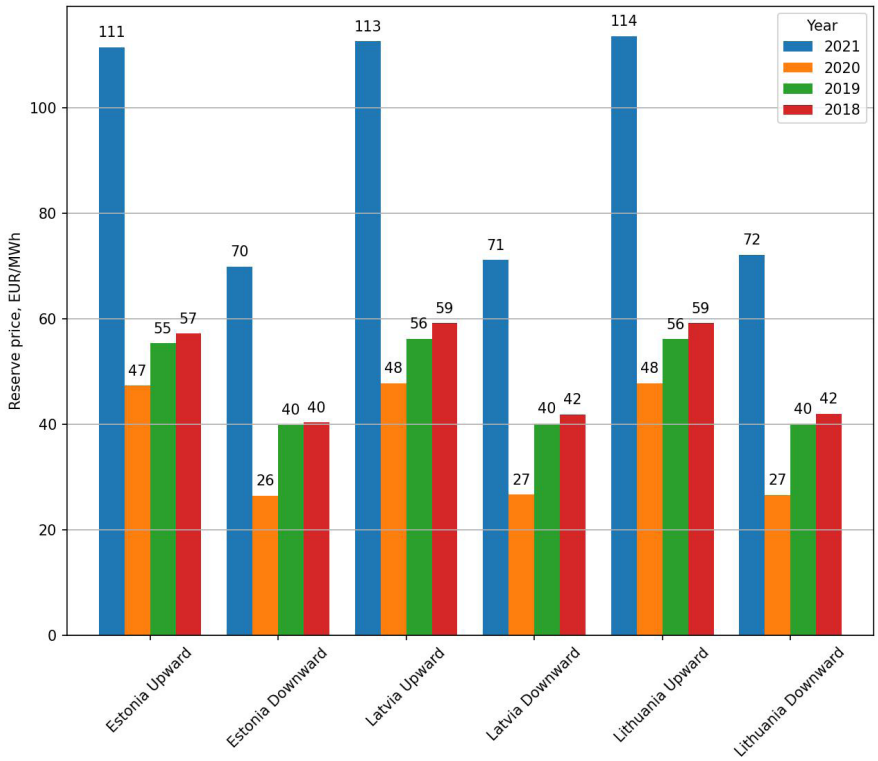

Fig. 2. Average annual reserve prices from normal activations [14].

It can be observed in Fig. 2, the downward reserve price is relatively lower than the upward reserve price. The EB can theoretically be used in the upward direction, but this study will not consider it. According to the Baltic balancing market rules, downward activation (or negative balancing energy) is balancing energy bid activation to reduce generation or increase consumption.

D. Future Research Prospects

The growth strategy of JSC Latvenergo focuses on ambitions plans which include the development of new renewable energy capacities, i.e., solar, wind parks. The com-

pany plans to implement renewable energy projects domestically and abroad, aiming for a capacity of 600 MW by 2026 and 2300 MW by 2030 [15]. Such a plan could be a reason to further analyse the use of EB to balance the ambitious renewable capacities in the portfolio of JSC Latvenergo. It is not under consideration in this study as the plans have not been implemented yet. In the future, opportunities to use EB in aFRR and FCR markets can also be explored.

3. METHODOLOGY FOR MATHEMATHICAL MODEL

As it has been mentioned above, the plan is to operate an EB in the Baltic balancing market where the mFRR product price and demand vary continuously. The aim is to replace HOB operation with EB. It is assumed that EB will use mFRR downward product to minimize the cost of heat energy, while at the same time generating additional revenues from the Baltic balancing market. Apart from economic benefits, replacement of HOB with EB could potentially reduce CO_2 emissions.

To evaluate the proposed hypothesis, a calculation model was created. The calculation principles of EB operation are shown in Fig. 3. Cycle is assumed to be one year. At the start of cycle, the inputs are defined. The inputs to the algorithms include data such as:

- actual heat load data of heat only boilers in CHP-1 and CHP-2 plant per time unit *i* (Q_i^{HOB}). For the relevant season, in the range of 0–546 MW, totalling 5751 hours a year;
- demand and price data for mFRR product per time unit *i* (A_i^{mFRR}, P_i^{mFRR}). In 2021, the demand amounted to 223644 MWh, with an average price of 71 EUR/MWh;
- the price of natural gas per month *m* (P_m^{NG}) was in the range of 0.226–1.237 EUR/m3;
- Nord Pool day-ahead electricity price per time unit *i* (P_i^E). In the range of -1.41 to +1000.07 EUR/MWh. On average, 118 EUR/MWh. Transmission costs and electricity taxes are excluded in calculations;
- the carbon dioxide price per time unit *i* ($P_i^{CO_2}$) ranged from 33.54 to 79.097 EUR/t;
- the average efficiency of the HOB (η_{avg}^{HOB}) was assumed to be 0.995;
- the carbon dioxide emission factor of natural gas (E_{CO_2}) was assumed to be 0.201 t/MWh;
- investments in CAPEX were assumed to be 0.08 million euros per MW, while fixed OPEX standed at 1,100 euros per MW and variable OPEX was 0.5 euros per MWh a year.

All data sets were sourced from 2021 to ensure that the analysis would remain unaffected by parameter spikes that emerged from 2022 onwards, such as increased electricity and gas prices, gas savings in CHPs, etc.

As the outputs of the algorithms include the heat production costs from gas boilers and the EB, it is necessary to determine whether there is potential to use electrode boiler, as well as EB operational costs and potential income together or independently from HOB replacement and mFRR market. Thus, all algorithms ensure evaluation of the formulated hypothesis.

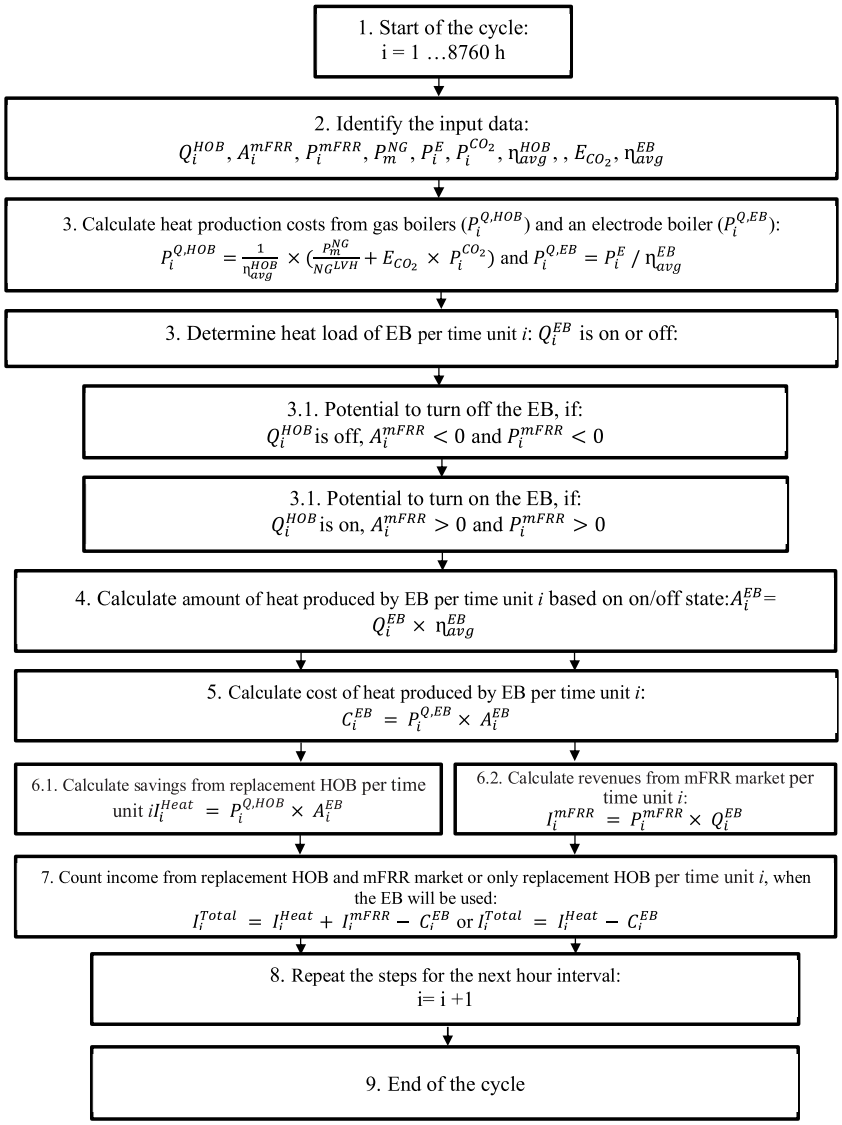

Fig. 3. The calculation principles of EB operation.

4. FEASIBILITY ASSESSMENT RESULTS

Based on an analysis and the operational patterns of CHP-1 and CHP-2, the results have been obtained for various EB capacities, starting from 10 to 100 MW.

The use of EB not only reduces the heat production costs of CHPs, but also generates revenues from the Baltic balancing market (Fig. 4). Figure 4 (a) represents the scenario where the EB operates and receives savings from HOB replacements and revenues in the mFRR market. Figure 4 (b) represents the scenario where the EB can also be used for HOB replacement when it is beneficial, even if there is no demand for the mFRR product during a specific hour.

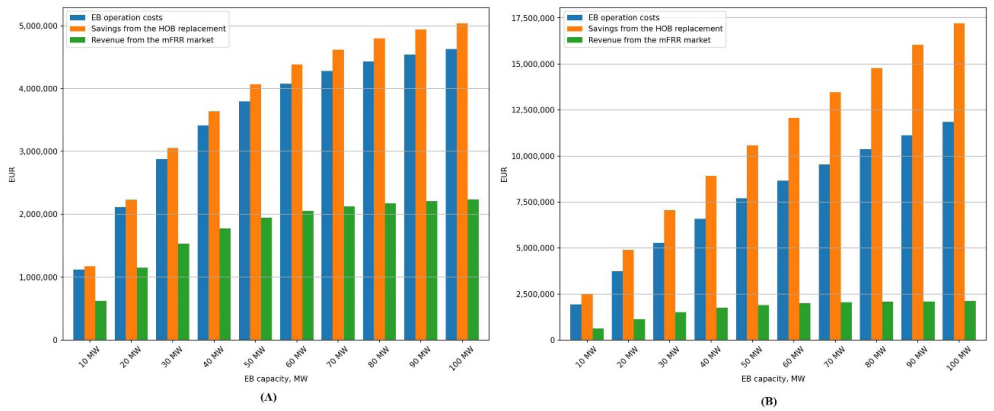

Fig. 4. Operation of EB in line with the formulated hypothesis.

Figure 4 shows that in both scenarios – A and B – the overall income of using an EB is significantly enhanced. Scenario B demonstrates that the EB should be utilized not only when there is a demand for the mFRR product, but also in other situations where it can effectively maximize savings from HOB replacement. Furthermore, Figure 5 illustrates the EB variations in heat production, income, and working hours between scenarios A and B. This serves as further confirmation that the EB should be employed not solely when there is a demand for the mFRR product, but also in other hours where it can significantly optimize savings by replacing HOBs.

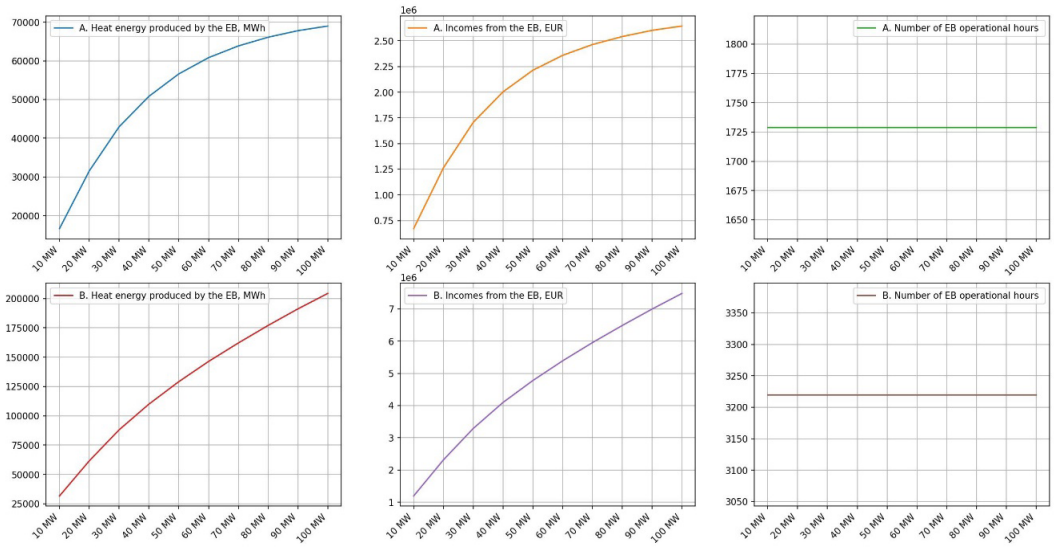

Fig. 5. Operation of EB in two scenarios A and B.

Figure 6 illustrates the broader characteristics for various EB capacity levels. It showcases the project economic indicators, which are expressed as net present value (NPV), internal rate of return (IRR) and the number of years it would take for the project to payback.

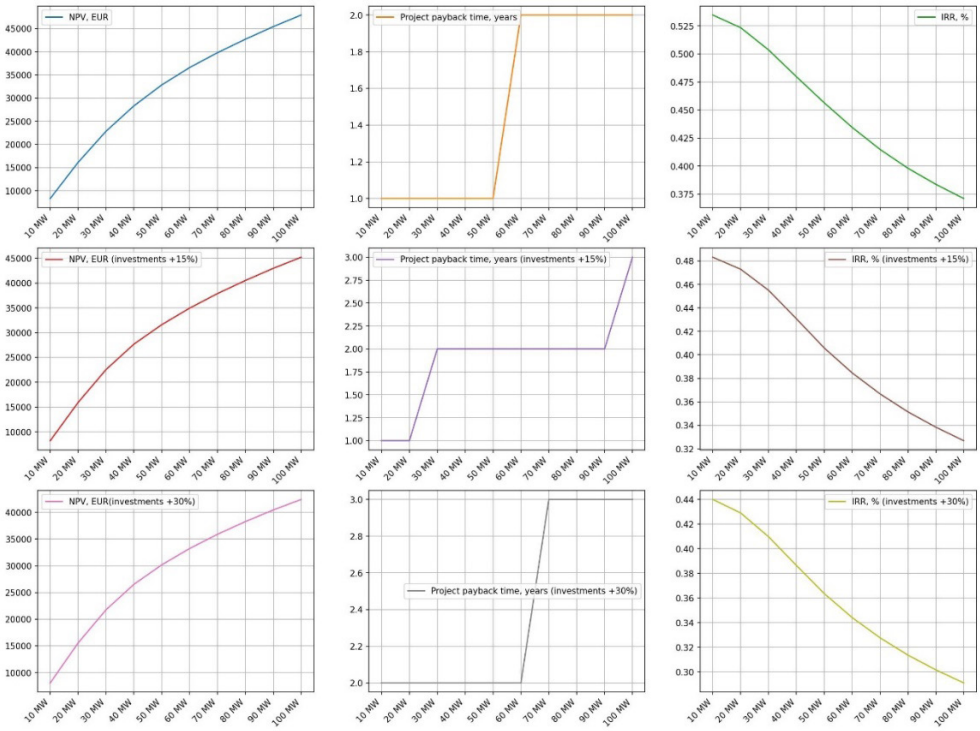

Fig. 6. Characteristics of EBs at different capacity.

It is worth noting that once the EB capacity reaches 50–60 MW, there is no significant increase in the amount of thermal energy produced, revenues from mFRR market (Figs. 5 and 6). Even more, the payback indicators of the project increase from such capacity. As a result, the authors suggest that developing an EB of this size (50–60 MW) would be advantageous.

Figure 7 shows the hours of operation for both the HOBs and EB (with 50 MW capacity) throughout the year.

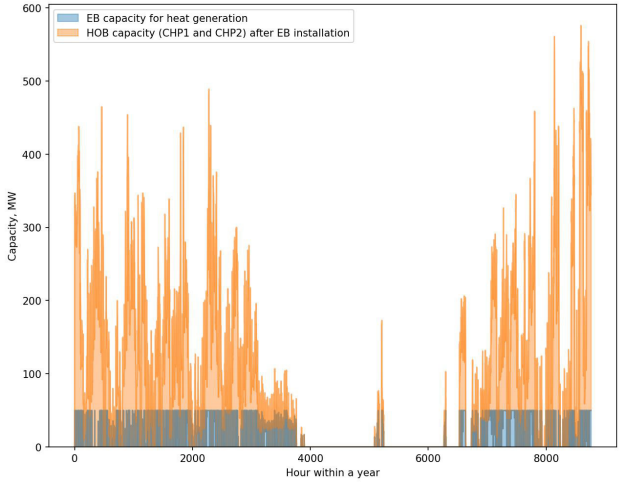

Fig. 7. HOB and EB capacity on an annual basis.

The HOB capacity is denoted in orange, while the EB capacity is shown in blue. Figure 7 demonstrates that the performance of the EB is reliant on the nature of the HOBs. Additionally, it indicates that the utilization of the EB could be even further enhanced if there were possibility to increase EB capacity or it could be profitable to operate under another heat or electricity market conditions.

5. DISCUSSION AND CONCLUSION

EBs have the potential to play an important role in ancillary services and district heating, offering a reliable and efficient solution for meeting energy demands. However, to assess their feasibility, a comprehensive evaluation is necessary, considering various factors such as energy demand, technical feasibility, economic viability, and regulatory market conditions. This paper considered the economic feasibility of EBs in ancillary services and district heating, providing a framework for decision making and helping to ensure that this technology could be deployed effectively.

The formulated hypothesis was proven, i.e., the use of EB can both reduce the heat production costs of CHPs and generate revenues from the Baltic balancing market. The magnitude of the income depends on the chosen EB capacity. In the authors' opinion, the EB with capacity of 50–60 MW can be sufficient, as there are no further significant improvements in economic characteristics. In addition, the use of the EB for balancing the portfolio of JSC Latvenergo, as well as the participation in the FCR and aFRR market, can even more increase the efficiency of EB use, thus also the feasibility. Furthermore, it is crucial to enhance the research by performing a comprehensive evaluation of various cost factors, including but not limited to the expenses associated with network connectivity, the initial and operational cost of the EB itself. Considering these factors, the feasibility can be assessed more precisely.

ACKNOWLEDGEMENTS

The research has been supported by the European Social Fund within Project No 8.2.2.0/20/I/008 "Strengthening of PhD Students and Academic Personnel of Riga Technical University and BA School of Business and Finance in the Strategic Fields of Specialization" of the Specific Objective 8.2.2 "To Strengthen Academic Staff of Higher Education Institutions in Strategic Specialization Areas" of the Operational Programme "Growth and Employment".

REFERENCES

1. Guzs, D., Utans, A., Sauhats, A., Junghans, G., & Silinevics, J. (2022). Resilience of the Baltic Power System When Operating in Island Mode. *IEEE Transactions on Industry Applications, 58* (3), 3175–3183. doi: 10.1109/TIA.2022.3152714.

2. Ivanova, P., Sauhats, A., & Linkevics, O. (2017). Cost-benefit analysis of electric boiler at combined heat and power plants. In *IEEE 58th International Scientific Conference on Power and Electrical Engineering of Riga Technical University (RTUCON)*, (pp. 1–6), Riga, Latvia, 2017. doi: 10.1109/RTUCON.2017.8124747.
3. Parat. (n.d.). *Parat Electrode Boiler*. Available at https://www.parat.no/en/references/industry/parat-electrode-boiler/
4. AEA. (n.d.). *Electric Boiler – High Voltage Solutions*. Available at https://www.aea.dk/el-kedler/
5. Salman, C.A., Li, H., Li, P., & Yan, J. (2021). Improve the Flexibility Provided by Combined Heat and Power Plants (CHPs) – A Review of Potential Technologies. *e-Prime – Advances in Electrical Engineering, Electronics and Energy, 1*. doi: https://doi.org/10.1016/j.prime.2021.100023
6. Fernqvist, N., Broberg, S., & Toren, J. (2023). District Heating as a Flexibility Service: Challenges in Sector Coupling for Increased Solar and Wind Power Production in Sweden. *Energy Policy, 172.* doi: https://doi.org/10.1016/j.enpol.2022.113332.
7. Gao, S., Jurasz, J., Li, H., Corsetti, E., & Yan, J. (2022). Potential Benefits from Participating in Day-ahead and Regulation Markets for CHPs. *Applied Energy, 306* (A). doi: https://doi.org/10.1016/j.apenergy.2021.117974
8. Javanshir, N., Syri, S., Tervo, S., & Rosin, A. (2023). Operation of District Heat Network in Electricity and Balancing Markets with the Power-to-Heat Sector Coupling. *Energy, 266*. doi: https://doi.org/10.1016/j.energy.2022.126423.
9. Boldrini, A., Navarro, J.P.J., Crijns-Graus, W.H.J., & van den Broek, M.A. (2022). The Role of District Heating Systems to provide Balancing Services in the European Union. *Renewable and Sustainable Energy Reviews, 154*. doi: https://doi.org/10.1016/j.rser.2021.111853
10. Corsetti, E., Riaz, S., & Riello, M. (2021). Modelling and Deploying Multi-Energy Flexibility: The Energy Lattice Framework. *Advances in Applied Energy, 2*. doi: https://doi.org/10.1016/j.adapen.2021.100030
11. Junghans, G., Silis, A., Marcina, K., & Ertmanis, K. (2020). Role of Balancing Markets in Dealing with Future Challenges of System Adequacy Caused by Energy Transmission. *Latvian Journal of Physics and Technical Sciences, 57* (3), 48–56. doi: https://doi.org/10.2478/lpts-2020-0015
12. Ansone, A., Jansons, L., Bode, I., Dzelzitis, E., Zemite, L., & Broks, A. (2022). Study on Potential Role and Benefits of Liquified Natural Gas Import Terminal in Latvia. *Latvian Journal of Physics and Technical Sciences, 59* (2), 37–54. doi: https://doi.org/10.2478/lpts-2022-0010
13. Elering. (n.d.). *Baltic TSOs, Baltic Balancing Roadmap*. Available at https://elering.ee/sites/default/files/2022-10/Baltic balancing roadmap 10.2022.pdf
14. Baltic Transparency Dashboard. (n.d.). *Current Balancing State.* Available at https://baltic.transparency-dashboard.eu/
15. Latvenergo. (n.d.). *The Development of Wind Farms is a Cooperation Opportunity for Latvian Entrepreneurs.* Available at https://latvenergo.lv/en/jaunumi/preses-relizes/relize/latvenergo-development-wind-farms-cooperation-opportunity-latvian-entrepreneurs

sciendo

LATVIAN JOURNAL OF PHYSICS
AND TECHNICAL SCIENCES
2023, N 5

DOI: 10.2478/lpts-2023-0030

BLENDING HYDROGEN WITH NATURAL GAS/ BIOMETHANE AND TRANSPORTATION IN EXISTING GAS NETWORKS

L. Zemite[1*], L. Jansons[1,2], N. Zeltins[1], S. Lappuke[2], I. Bode[3]

[1]Riga Technical University,
Faculty of Electrical and Environmental Engineering,
Institute of Power Engineering,
12-1 Azenes Str., Riga, LV-1048, LATVIA
[2]Riga Technical University,
Faculty of Engineering Economics and Management,
Institute of the Civil Engineering and Real Estate Economics,
6 Kalnciema Str. - 210, Riga, LV-1048, LATVIA
[3]Riga Technical University, Faculty of Civil Engineering,
Institute of Heat, Gas and Water Technologies
6a Kipsalas Str., Riga, LV-1048, LATVIA
*e-mail: laila.zemite@rtu.lv

The existing European Union (EU) natural gas network provides large capacity to integrate renewable (RGs) and low-carbon gases. Today, hydrogen contributes only a few percent to Europe's energy consumption and is almost exclusively produced from fossil fuels and used in the industry. Nevertheless, hydrogen has a significant role to play in emission reduction in hard-to-decarbonize sectors, in particular, as a fuel in transport applications and as a fuel or feedstock in certain industrial processes (steel, refining or chemical industries, the production of "green fertilizers"). Carbon dioxide (CO_2) in reaction with hydrogen can also be further processed into synthetic fuels, such as synthetic kerosene in aviation. In addition, hydrogen brings other environmental co-benefits when used as fuel, such as the lack of air pollutant emissions.

However, in transitional phase from fossil to RG, namely, renewable or green hydrogen, natural gas/biomethane and hydrogen blends, are needed to gradually replace natural in existing gas transmission and distribution networks. The gas networks are believed to be able to use natural gas/biomethane and hydrogen blends with 5–20 % of hydrogen by volume. Most systems and applications are able to handle it without a need for major infrastructure upgrades or end-use appliance retrofits or replacements. The promotion of hydrogen network such as

European Hydrogen backbone (EHB) is gaining momentum in Europe. To decarbonize the natural gas grids, the threshold of hydrogen in the existing grid systems must be increased, which can be done by means of wider natural gas/biomethane and hydrogen blending and simultaneous transportation in currently operational gas networks.

Keywords: *hydrogen, natural gas, biomethane, gas infrastructure, gas blends*

1. INTRODUCTION

Hydrogen is a colourless, non-toxic, odourless and tasteless gas that usually exists as a two-atom molecule. Hydrogen is the most common element in the universe, accounting for around 90 % of its mass and around 73 % of the visible universe's mass [1]. Hydrogen has three naturally occurring isotopes: hydrogen (^{1}H), deuterium (^{2}H) and tritium (^{3}H). Each has one proton and a different neutron count. Hydrogen has no neutrons, deuterium has one and tritium has two [2], [3]. Hydrogen is not usually found in pure form because it bonds easily with other elements. It is also the lightest known element with a density of 0.08988 grams per litre (gr/l) at 1 bar, and, consequently, the lightest known gas (density: 0,089 kg/m^3; relative density relative to air: 0.0695).

Hydrogen is gaining popularity very rapidly as an alternative source of clean fuel that can be used efficiently and widely with natural gas or biomethane, thus reducing greenhouse gas emissions (GHG) in several segments of the energy sector as well as energy-intensive industrial processes. Many companies plan to use hydrogen as part of their GHG reduction strategy, and, therefore, various natural gas/biomethane and hydrogen blending options and related challenges are being explored both at the industry level and within the framework of cooperation between industry and scientific institutions.

Hydrogen has several important properties that may affect its use in the energy sector:

- it connects with oxygen, creating water that is absolutely necessary for life processes and is not toxic;
- it has a high energy content per weight (almost three times higher than petrol), but the energy density per volume is quite low at standard temperature and at 1 ba pressure. The volume energy density can be increased by storing hydrogen at elevated pressure or by storing at extremely low temperatures as liquid;
- hydrogen is highly combustible; only a small amount of energy is needed to ignite it. It also has a wide range of flammability, meaning it can ignite forming 4 to 74 % of the air volume [4];
- hydrogen burns with a light blue, almost invisible flame, making hydrogen fires difficult to spot in daylight [5];
- combustion of hydrogen does not result in emissions of CO_2 and sulphur compounds. Under certain conditions, this may result in emissions of nitrogen oxides (NO_X) [6];
- hydrogen can be obtained from a wide range of sources, including renewables ones (RES) [7].

In order to make the simultaneous transport and use of natural gas, biomethane and hydrogen as safe as possible, it is necessary to take into account certain specific characteristics of hydrogen, such as:

- under standard conditions, hydrogen has a negative Joule–Thomson coefficient. This means that, unlike many other gases, hydrogen warms up slightly after expansion (pressure reduction) [8];

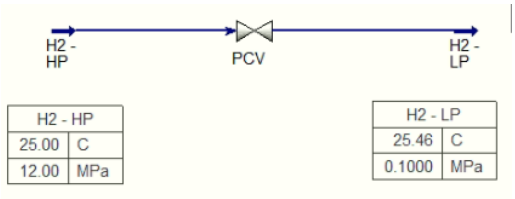

- hydrogen and methane have a negligible blending enthalpy that produces an unideal temperature. The figure below shows the excessive enthalpy of blending. In this case, hydrogen and methane are blended at 25 °C and the gas blend temperature is 21.6 °C instead of 25 °C, which would be expected [8].

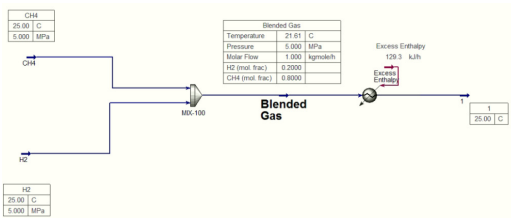

Developing renewable or green hydrogen, known as "renewable fuels of non-biological origin", is a priority for the EU. It plays an important role in decarbonizing these sectors of the economies of the EU Member States, where other alternatives could be impossible or more costly. It can be used to replace fossil hydrogen in transport and industrial processes and to create new industrial products such as "green fertilizers" and "green steel" [9], [10].

2. THE EU's HYDROGEN OUTLOOK

In 2020, the European Commission (EC) endorsed a hydrogen strategy for a climate neutral Europe, defining the conditions and actions for integrating clean hydrogen into the energy sector and the economy as a whole, and setting a green hydrogen production target by 2030. The strategy also notes that the introduction of renewable hydrogen into the existing gas supply network may be considered as the first step towards decarbonization of the EU's gas supply sector [11], [12]. Some EU countries have even set a hydrogen percentage target for blending with natural gas and biomethane into the existing gas networks.

As for 2022, hydrogen accounted for less than 2 % of Europe's energy consumption and was mainly used to produce chemicals such as plastic and mineral fertilizers. The breakdown of hydrogen consumption by industry in the EU Member States in 2019 is shown in Fig. 1. 96 % of this hydrogen came from fossil sources, namely natural gas, resulting in significant CO_2 emissions. To change the situation, the EC proposed to significantly increase a production potential of renewable hydrogen by producing 10 million tonnes (Mt) of it by 2030 and importing at least the same amount.

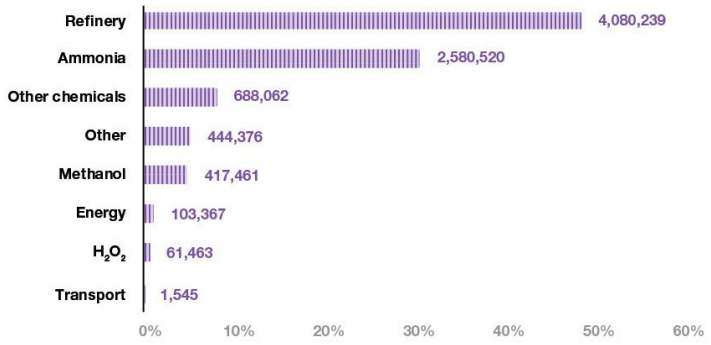

Fig. 1. Hydrogen consumption in the EU Member States (2019, by sector).

The *REPowerEU* framework, on the other hand, offers an updated vision for a more ambitious target of 15 Mt for the production and transport of renewable hydrogen, in addition to the 5.6 Mt already foreseen for *Fit-for-55* package, which are well above the EU hydrogen strategy targets. The new objectives require rapid acceleration of the development of integrated gas and hydrogen infrastructure across Europe, and the EHB initiative has developed such a framework program for 2035. It includes a vision of a hydrogen transport network of around 53 000 km in the EU by 2035 with significant potential for further growth and expansion [13]. Since the initial presentation of the EHB framework program, 31 countries in total have joined the initiative and the planned hydrogen transmission network has increased 110% in length. The 2040 framework programme provides for an investment of between 80 and 143 billion euros (EUR) in the development of a hydrogen transmission network of around 53 000 km. About 60 % of existing natural gas transmission pipelines are expected to be adapted to transport hydrogen, while about 40 % of the pipelines, including underwater ones, will be newly built.

EHB experts estimate that transporting hydrogen 1000 km by land pipeline would cost an average of 0.11–0.21 EUR/kg, making the piping system the most cost-effective solution for long-range transportation of large-scale hydrogen. On the other hand, if hydrogen were transported exclusively through underwater pipelines, the costs would be around EUR 0.17–0.32 per kg/1000 km [14].

There is currently no common technical and legal framework in the EU for the acceptable percentage of hydrogen for transportation and distribution of natural gas/biomethane and hydrogen blend in the public gas supply network. The permitted proportion of hydrogen in a gas blend in gas transmission networks varies from one EU Member State to another. For example, only 0.5 % is allowed in Sweden, 4 % – in Austria and Switzerland, 5 % to 10 % – in Germany (depending on the availability of gas infrastructure). On the other hand, it is permissible to introduce a gas blend with a hydrogen content of up to 12 % into the Dutch gas supply network.

In Latvia, in accordance with Cabinet of Ministers Regulations no. 567 "Regulation on the requirements for the introduction and transportation of biomethane and liquefied natural gas converted into a gaseous state into the natural gas transmission and distribution system", the proportion of hydrogen in the natural gas or natural gas/biomethane blend can be from $\leq 0.1 - \leq 2$ %. However, the highest indicated level can be reached only, if hydrogen is injected into the natu-

ral gas distribution or transmission system, which is not directly related to deliveries to other countries or the Incukalnas underground gas storage (UGS) facility [15]. It should be noted that the complete physical separation of one part of the transmission or distribution system of the country or region may not only be technically difficult, but in some cases physically impossible. Therefore, before deciding on the possibilities of increasing the hydrogen content in the Latvian gas supply system, it is also necessary to agree on the removal of the above-mentioned restrictions.

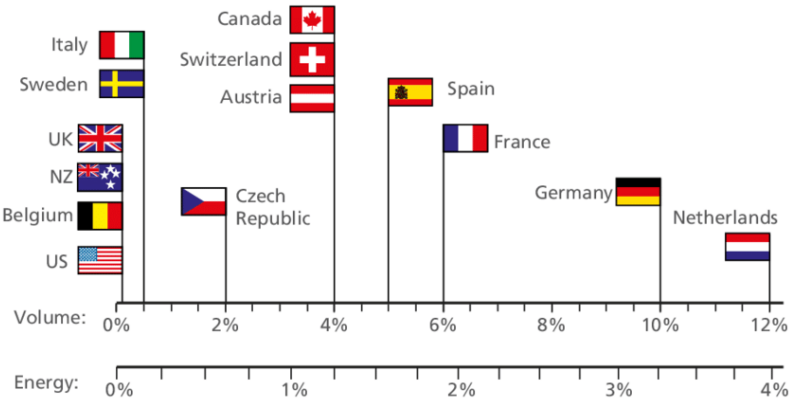

Fig. 2. Share of hydrogen in natural gas/biomethane blend in some countries (2023).

Preliminary studies carried out by the European Network of transmission system operators for gas (ENTSOG) and other organisations have shown that the transport of a natural gas and hydrogen blend is possible without modification of the pipeline, provided that the mass of hydrogen in the gas remains sufficiently low. According to one of the reports, it is possible to introduce up to 2 % of hydrogen "by default" into the gas supply system without making complete technical improvements [16]. Higher hydrogen concentrations, regardless of the network pressure regime, may require some infrastructure adjustments.

This need is linked to different physical and chemical characteristics of hydrogen and natural gas/biomethane, as blending hydrogen with natural gas/biomethane may affect:

- security of gas supply and increase the risk of gas leakage, as potential hydrogen leakage can be much faster and more voluminous than natural gas/biomethane leakage due to higher hydrogen leakage speeds than natural gas/biomethane (especially in high pressure mode);
- the integrity of the pipeline as hydrogen can cause metal fragility of the pipelines (hydrogen-induced cracking) or even damages of polyethylene pipes (especially in high pressure mode) [17];
- gas quality because the addition of hydrogen to natural gas changes the combustion properties and calorific value of the gas, which may directly affect the final consumption sector [18].

As it has been mentioned above, one of the main challenges for the harmonious development of the renewable hydrogen sector in the EU, including utilization of existing gas infrastructure, is a lack of a single standardization framework. However, the European Clean Hydrogen Alliance's *European Clean Hydrogen Alliance Roadmap on Standardization* provides a

comprehensive overview of the challenges and needs of standardization identified by members of the Alliance. The lack of uniform standards remains a major obstacle to the faster development of hydrogen technologies and to the attraction of investment at different stages of the hydrogen energy value chain. The roadmap covers all standardization needs of the hydrogen value chain, from production, distribution, transport and storage to final consumption in different economic sectors [19].

3. NATURAL GAS/BIOMETHANE AND HYDROGEN BLENDING AND ITS CHALLENGES

Over the past decade, several visions have been presented on possible transformation of the European gas supply network for transportation of 100 % hydrogen. For example, the EHB report states that five pan-European hydrogen supply and import corridors could emerge by 2030, connecting industrial clusters, ports and hydrogen valleys to key local and global hydrogen production and logistics centres. European hydrogen network could grow to more than 50 000 km by 2040, mainly by using existing natural gas infrastructure [20].

There are two options for transporting hydrogen through existing natural gas pipelines: as a blend with other gases (natural gas, biomethane, etc.) or as pure hydrogen, in both cases equipment is required to feed hydrogen into the gas network. The first option requires the addition of a certain amount of hydrogen to a gas pipeline that already transports natural gas or blends of natural gas/biomethane, producing a blend of hydrogen/natural gas/biomethane with a certain percentage of hydrogen in it. In the latter case, the complete replacement of natural gas or natural gas/biomethane blend with hydrogen as a new transport fuel is necessary [21]. Figure 3 shows the principal technical scheme for injection of hydrogen into the gas network and Fig. 4 outlines the same process with regulatory applications and major stages in hydrogen blending with natural gas/biomethane and delivery to end-users.

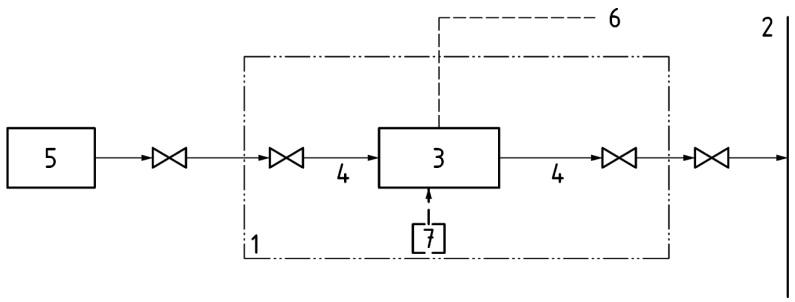

1. Gas supply station
2. Gas distribution or transmission system
3. Measurement and control point — pressure control/flow control/measurement etc.
4. Hydrogen pipeline (gas blend pipeline)
5. Production of hydrogen gas
6. Gas composition/flow information
7. Gas supply for forming a gas blend

Fig. 3. Principal technical scheme for injection of hydrogen into the existing gas network.

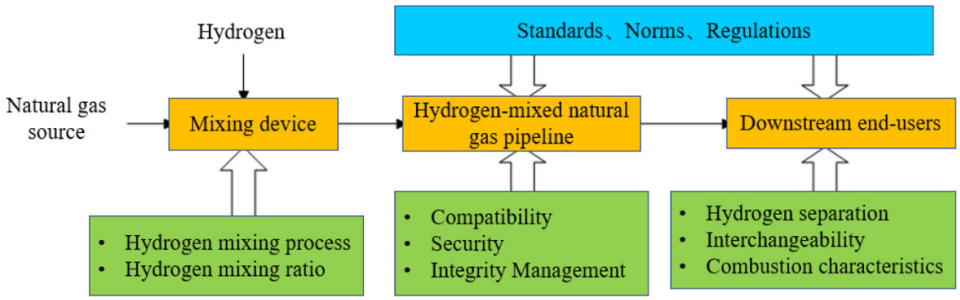

Fig. 4. Regulatory applications and major stages in hydrogen blending with natural gas/biomethane and delivery to end-users.

Also, the system for introducing hydrogen into an existing gas supply network or autonomous hydrogen network shall cover a wide range of measures, including pressure regulation, protection against overpressure, testing to ensure gas quality as required, gas measurement and, if necessary, odorization.

Numerous studies concerning the use of natural gas/biomethane and hydrogen blends have only taken into account the impact of hydrogen in the final consumption sector, in particular its combustion problems, by examining, for example, the impact of hydrogen on burner performance and the combustion process itself (capacity, efficiency, emissions, etc.). However, in order to test the readiness of the gas infrastructure for the new fuel and make the necessary adjustments, in-depth, comprehensive studies are needed on the impact of hydrogen on the materials that make up all network components and equipment. Such studies are particularly important for the transmission network, which consists of large diameter pipelines, and connects gas system entry points with many long-distance final consumers. The transmission system operates under high pressure conditions (≥ 50 ba), making possible hydrogen leaks potentially more dangerous than they would be in the distribution system [22].

The main risk factors associated with growing concentration of hydrogen in natural gas/biomethane and hydrogen blends are: leaks, as hydrogen can diffuse through many materials considered impermeable to other gases, buoyancy as hydrogen rises quickly under atmospheric conditions, flammability when mixed with air, – can easily ignite or/and explode, hydrogen-induced cracking as reduction in the ductility of a metal can occur due to absorbed hydrogen (steels, iron, nickel, titanium, cobalt, and their alloys) [23]. Also, hydrogen energy content is about one-third of the natural gas. Thus, not only more hydrogen-blended natural gas is needed to deliver the same amount of energy to users compared to pure natural gas but also a higher volumetric flow rate is required. Options for the latter include increasing operating pressure in a distribution system or replacing the existing pipelines with ones of larger diameter [24].

As it has been mentioned above, most metals from which existing gas transmission pipelines are made suffer from hydrogen-induced cracking, especially at high pressure. This may result in necessity to introduce more strict requirements in production of such pipelines, if they are not totally replaced with polyethylene analogues. Specially designed pipelines for the transmission of hydrogen may significantly increase construction costs per kilometer of the hydrogen transmission network in comparison with pipelines for transportation of

natural gas/biomethane [25].

Metal fragility caused by hydrogen is one of the main challenges for the wider use of hydrogen in the existing EU gas transmission network, where steel gas pipelines currently dominate. The risk of fragility depends heavily on the quality of the steel, in particular its microstructure, as well as the conditions under which the material has been exposed over a long period of time [26]. The literature explores the impact of metal fragility caused by hydrogen on carbon steels with quality up to API 5L X80 to determine the relationship between hydrogen concentration in the gas blend and the failure load of the gas pipeline [27].

Another important aspect of ensuring the safe and efficient use of gas pipelines is the prevention of critical gas leaks in valves and other elements of infrastructure. It is therefore essential to implement regular maintenance and inspection measures in a whole gas network, not only pipelines. Hydrogen is believed to leak at the same rate as natural gas in low and medium pressure systems (natural gas distribution system and autonomous, local natural gas supply systems), but as the system operating pressure increases, the leakage rate increases, too. Some studies have also attempted to predict potential leakage spots by highlighting cell connection sites as some of the most critical points [28].

A blend of natural gas/biomethane and hydrogen can potentially cause problems not only for the integrity of the pipelines but also for the safe use of other elements of the gas supply system, so system security requires much greater attention than in the case of separate transmission and distribution of natural gas/biomethane. A number of significant indicators for natural gas/biomethane and hydrogen are also different, such as the Wobbe Index, which may directly affect the accounting of the blend (accuracy of gas meters [29]) and burners used in gas heating appliances or industrial natural gas combustion systems. Furthermore, hydrogen has a lower calorific value than natural gas, thus blending hydrogen with natural gas will reduce the calorific value of a blend [30]. The change in the Wobbe Index and calorific value of the blend of natural gas/biomethane and hydrogen under the conditions of the different percentage of hydrogen in the gas blend is shown in Fig. 5.

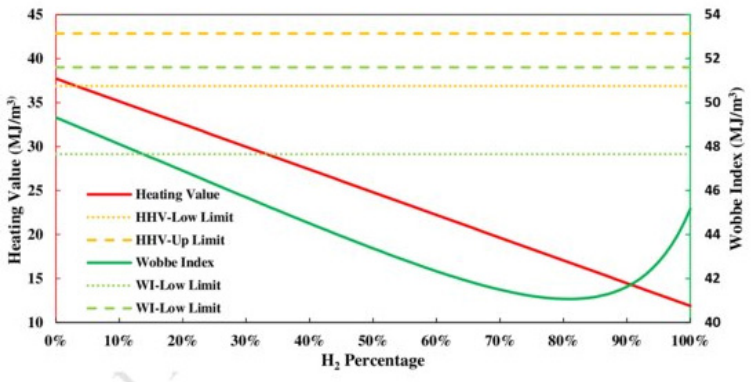

Fig. 5. The change in the Wobbe Index and calorific (heating) value of the blend of natural gas/biomethane and hydrogen [31].

4. DEBLENDING SOLUTIONS

Several technical solutions for the simultaneous transmission and distribution of hydrogen and natural gas/biomethane are currently offered on the European and global markets, including blending facilities of natural gas/biomethane and hydrogen, where the percentage of hydrogen in a gas blend can vary significantly. Such solutions are offered by manufacturers and suppliers such as "JLS International", "Emersons" [28], "Linde" and "Honeywell". Both stationary gas blending solutions and equipment with moving elements are available. Basically, both solutions are currently being offered for large diameter pipelines.

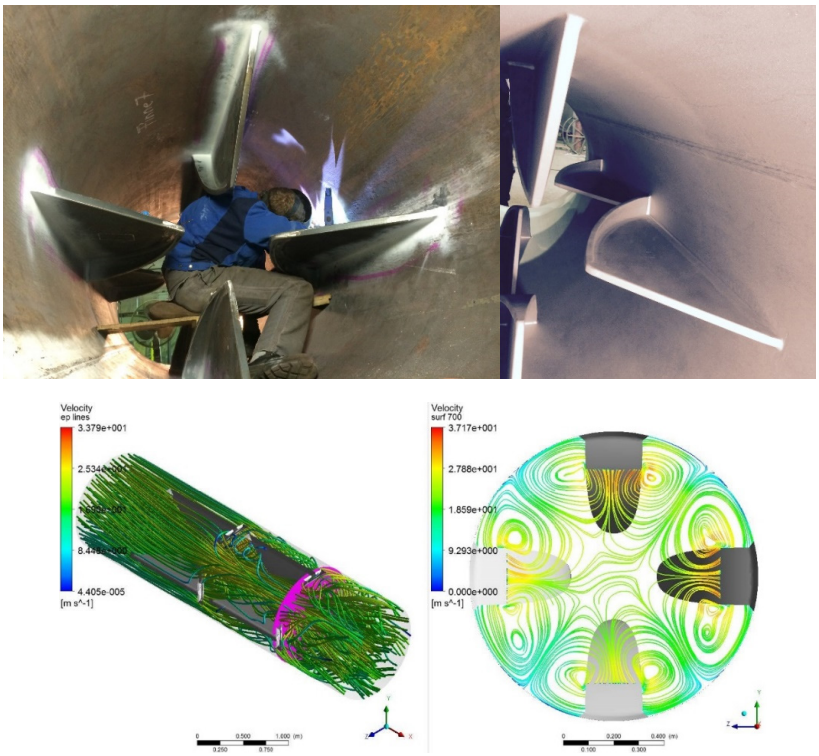

Fig. 6. Stationary, pipe-mounted, gas mixer assembly (upper images), gas mixer performance test (computer simulation) in different gas blending modes [32].

Stationary solutions are used not only for blending of natural gas/biomethane and hydrogen, but also for the addition of odorant or biomethane to natural gas. For example, "Emersons" and "Linde" offer integrated natural gas/biomethane and hydrogen blending solutions suitable for lower pressure regimes and smaller pipe diameters and, in particular, for the gas distribution network [33], [34]. The bulk of the gas distribution network today consists of polyethylene pipes, the use and maintenance of which are less complex than in the case of steel pipelines. Polyethylene pipelines have properties such as corrosion resistance, high elasticity and excellent low temperature toleration properties, which also make them more resilient to potential negative effects of hydrogen [35].

Fig. 7. "Emerson" *El Campo* natural gas/biomethane and hydrogen blending test facility.

Although the principles of blending natural gas/biomethane and hydrogen are similar to both small and large industrial solutions, some producers, such as "Honeywell", work at development of complex gas/biomethane to hydrogen grid solutions, where different scale applications coexist.

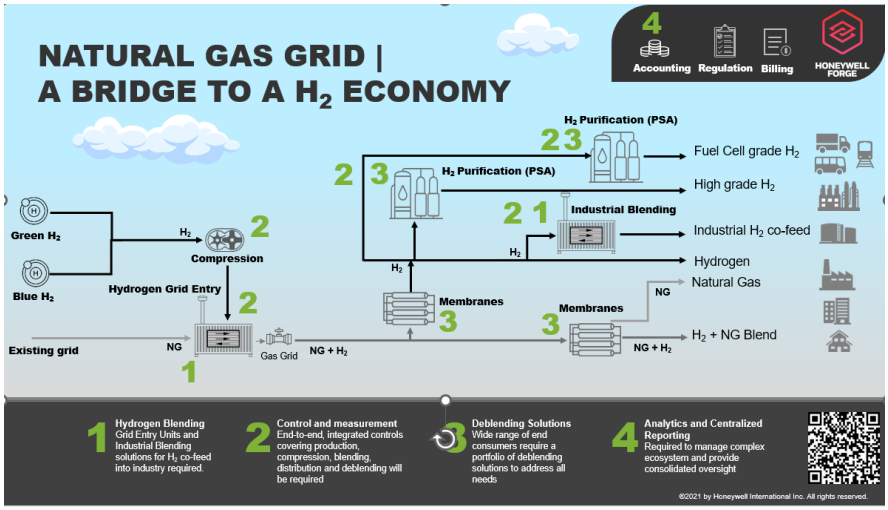

Fig. 8. "Honeywell" complex gas/biomethane to hydrogen grid solutions [34].

However, as the main function of the gas network is to supply gas resources to final customers, it may also be necessary to develop a universal natural gas/biomethane and hydrogen blend separation or deblending technology in the future. This will be necessary if certain categories of gas end-users connected to existing diversified gas supply networks could not, for objective reasons, receive and use a blend of natural gas/biomethane and hydrogen [36]. Currently, the hydrogen separation technology used is made almost exclusively for a high hydrogen concentration gas blend, and there is still room for research in sector of gas deblending with relatively low hydrogen content ($\leq 5 - 30$ %). Pressure oscillation adsorption and fractionated/cryogenic distillation systems are available on the market, but they are generally not cost-effective because they are energy-intensive, especially when the hydrogen content of the gas

blend is low. For this reason, membrane-based technologies are considered to be more prospective for ensuring high purity hydrogen flow in the future [37], [38].

5. CONCLUSIONS

Blending and transportation of hydrogen in existing gas networks are the most topical issues in decarbonization and diversification of the gas transportation infrastructure in the EU. At the moment, a few obstacles exist in terms of wider hydrogen application in the area, namely:

- a lack of harmonized, EU-wide regulatory framework governing natural gas/biomethane and hydrogen blending;
- different percentage of hydrogen acceptable for transportation and distribution in existing gas networks, which can vary significantly from country to country (from 0 up to 12%);
- existence of limitations preventing hydrogen bending with methane-based gaseous fuels, if there are possibilities for these bends be transported and traded abroad;
- existence of limitations preventing hydrogen bending with methane-based gaseous fuels, if there are possibilities for these bends to reach certain UGS facilities;
- limited possibility to use higher hydrogen percentage in natural gas/biomethane and hydrogen blends in the whole national gas transportation and distribution network (access only to local or autonomous sections of gas distribution networks);
- a necessity to develop a universal natural gas/biomethane and hydrogen blend separation or deblending technology/set of technologies suitable to certain categories of gas end-users connected to existing diversified gas supply networks, who, for objective reasons, cannot receive and use a blend of natural gas/biomethane and hydrogen.

REFERENCES

1. Origin of Element (n.a.). Available at https://www2.lbl.gov/abc/wallchart/chapters/10/0.html
2. Isotopes of Hydrogen (n.a.). Available at https://www2.lbl.gov/abc/wallchart/chapters/02/3.html
3. Libretexts. (n.a.). *Isotopes of Hydrogen*. Available at https://chem.libretexts.org/Bookshelves/Inorganic_Chemistry/Map%3A_Inorganic_Chemistry_(Housecroft)/10%3A_Hydrogen/10.03%3A_Isotopes_of_Hydrogen
4. Rhodes, R. (n.a.). *Explosive Lessons in Hydrogen Safety*. Available at https://www.nasa.gov/pdf/513855main_ASK_41s_explosive.pdf
5. Hydrogen Tools. (n.a.). *Hydrogen Flames*. Available at https://h2tools.org/hydrogen-flames
6. Douglas, C., Emerson, B., Lieuwen, T., Martz, T., Steele, R., & Noble, B. (2022). *NO_x Emissions from Hydrogen-METHANE Fuel Blends.* Strategic Energy Institute. Available at https://research.gatech.edu/sites/default/files/inline-files/gt_epri_nox_emission_h2_short_paper.pdf
7. US Department of Energy. (n.a.). *Hydrogen Production and Distribution*. Available at https://afdc.energy.gov/fuels/hydrogen_production.html
8. Ques10. (n.a.). *Fine Joules Thompson Coefficient and its Significance.* Available at https://www.ques10.com/p/33100/define-joules-thompson-coefficient-and-its-signifi/
9. EC. (n.a.). *Hydrogen*. Available at https://energy.ec.europa.eu/topics/energy-systems-integration/hydrogen_en

10. Savickis, J., Zeltins, N., & Jansons, L. (2019). Synergy between the Natural Gas and RES in Enhancement of Security of Energy Supply in the Baltic Countries (Problem Statement). *Latvian Journal of Physics and Technical Sciences*, *56* (6), 17–31. doi: 10.2478/lpts-2019-0032
11. Communication from the Commission to the European Parliament, the Council, the European Economic and Social Committee and the Committee of the Regions. (2020). *A Hydrogen Strategy for a Climate-neutral Europe*. European Commission, Brussels. Available at https://eur-lex.europa.eu/legal-content/EN/TXT/?uri=CELEX:52020DC0301
12. Conexus. (n.a.). *European Hydrogen backbone Initiative Develops a Vision for Hydrogen infrastructure*. Available at https://www.conexus.lv/press-releases/eiropas-udenraza-mugurkaula-iniciativas-ietvaros-izstradata-vizija-par-udenraza-infrastrukturu
13. EHB. (n.a.). *European Hydrogen Backbone Grows to Meet REPowerEU's 2030 Hydrogen Targets*. Available at https://ehb.eu/newsitem/european-hydrogen-backbone-grows-to-meet-repowereu-s-2030-hydrogen-targets
14. Jansons, L., Bode, I., Zemite, L., Zeltins, N., Geipele, I., & Kiesners, K. (2022). Securing Sustainable Energy Future: Green Hydrogen as a Part of Gaseous Fuel Diversification Risk Management Strategy. *Latvian Journal of Physics and Technical Sciences*, *59* (4), 53–70. doi: 10.2478/lpts-2022-0033
15. Cabinte of Ministers. (2022). *Requirements No 567. Regulation on the requirements for the introduction and transportation of biomethane and liquefied natural gas converted into a gaseous state into the natural gas transmission and distribution system*. Available at https://likumi.lv/ta/id/335532-noteikumi-par-prasibam-biometana-un-gazveida-stavokli-parverstas-saskidrinatas-dabasgazes-ievadisanai-un-transportesanai
16. Jansons, L., Zemite, L., Zeltins, N., & Geipele, I. (2023). Green and Sustainable Hydrogen in Emerging European Smart Energy Framework. *Latvian Journal of Physics and Technical Sciences*, *60* (1), 24–38. doi: 10.2478/lpts-2023-0003
17. DNV. (n.a.). *Switching a City from Natural Gas to Hydrogen*. Available at https://www.dnv.com/oilgas/perspectives/switching-city-from-natural-gas-to-hydrogen.html
18. EC. (2023). *European Clean Hydrogen Alliance Roadmap on Standardisation*. Available at https://ec.europa.eu/docsroom/documents/53721
19. EHB. (2022). *Five Hydrogen Supply Corridors for Europe in 2030*. Executive Summary. Available at https://ehb.eu/files/downloads/EHB-Supply-corridors-presentation-ExecSum.pdf
20. Abdalla, A. M., Hossain, S., Nisfindy, O. B., Azad, A. T., Dawood, M., & Azad, A. K. (2018). Hydrogen Production, Storage, Transportation and Key Challenges with Applications: A Review. *Energy Conversion and Management, 165*, 602–627. https://doi.org/10.1016/j.enconman.2018.03.088
21. Birkitt, K., Loos-Morrey, M., Sanchez, C., & O'Sullivan, L. (2021). Materials Aspects Associated with the Addition of up to 20 mol% Hydrogen into an Existing Natural Gas Distribution Network. *Inta. J. of Hydrogen Energy, 46* (23), 12290–12299. https://doi.org/10.1016/j.ijhydene.2020.09.061
22. Gao, Z., Xue, Y., Li, J., Xu, L., & Qiao, L. (2022). The Mechanism of the High Resistance to Hydrogen-Induced Strength Loss in Ultra-High Strength High-Entropy Alloy. *Metals, 12* (6), 971. https://doi.org/10.3390/met12060971
23. Bosch, C., Haase, T., Liessem, A., & Schroder, J. (2010). *Hic Performance of Heavy Wall Large-Diameter Pipes For Sour Service Applications under Fit-For-Service Conditions*. Paper presented at the CORROSION 2010, San Antonio, Texas. Available at https://onepetro.org/NACECORR/proceedings-abstract/CORR10/All-CORR10/NACE-10280/126975
24. EIGUS. (2014). *Hydrogen Pipeline Systems.* Doc 121/14. European industrial gases Association AISBL. Available at https://www.eiga.eu/ct_documents/doc121-pdf/

25. Webcorr. (n.a.). *Different Types of Corrosion. Recognition of Hydrogen-Induced Cracking (HIC)*. Available at https://www.corrosionclinic.com/types_of_corrosion/hydrogen-induced_cracking_HIC.htm
26. Briottel, L., Moros, I., & Lemoine, P. (2012). Quantifying the Hydrogen Embrittlement of Pipeline Steels for Safety Considerations. *International Journal of Hydrogen Energy, 37* (22). https://doi.org/10.1016/j.ijhydene.2012.05.143
27. Ronevich, A.J., Song, E.J., Somerday, B.P., & Marchi, C.W.S. (2021). Hydrogen-Assisted Fracture Resistance of Pipeline Welds in Gaseous Hydrogen. *International Journal of Hydrogen Energy, 46* (10), 7601–7614. https://doi.org/10.1016/j.ijhydene.2020.11.239
28. SwRI. (2023). *SwRI Investigates Accuracy of Flow Meters Measuring Hydrogen and Natural Gas Blends.* Available at https://www.swri.org/press-release/swri-investigates-accuracy-of-flow-meters-measuring-hydrogen-natural-gas-blends
29. The Engineering Toolbox. (n.a.). *Fuels – Higher and Power Calorific Values*. Available at https://www.engineeringtoolbox.com/fuels-higher-calorific-values-d_169.html
30. Zhao, Y., McDonell, V., & Samuelsen, S. (2019). Influence of Hydrogen Addition to Pipeline Natural Gas on the Combustion Performance of a Cooktop Burner. *The International Journal of Hydrogen Energy, 44* (23), 12239–12253. 10.1016/j.ijhydene.2019.03.100
31. Emersons. (n.a.). *Decarbonization in Natural Gas Applications.* Available at https://www.emerson.com/en-gb/automation/valves-actuators-regulators/decarbonization-in-natural-gas-applications
32. JLS International. (n.a.). *Gas Mixer and Flow Meter*. Available at https://www.jls-europe.de/products/static-mixer/gas-mixer.html
33. Emersons. (n.a.). *Expertise and Integrated Solution Support for your Hydrogen Blending Applications*. Available at https://www.emerson.com/documents/automation/product-brochure-hydrogen-%E2%80%93-natural-gas-blending-solutions-brochure-emerson-en-en-7838030.pdf
34. Linde (n.a.) *Hydrogen on Tap.* Available at https://www.engineering.linde.com/hiselect-for-hydrogen?utm_source=google&utm_medium=cpc&utm_campaign=EMEA-EN-SUCH+RLSA-HISELECT(exact)&utm_term=natural%20hydrogen&utm_medium=paid&utm_source=Google+Ads&utm_campaign=HISELECT_ContactForm&utm_term=natural%20hydrogen&gclid=CjwKCAjwsKqoBhBPEiwALrrqiO0v0mGR9bGAbTKHNLToS_MG1CkuZYMshmuVEBG_5lvZcKE3JLsJERoCJXcQAvD_BwE
35. IGRC. (2017). *Using the Natural Gas Network for Transporting Hydrogen – Ten Years of Experience*. Available at https://arkiv.dgc.dk/sites/default/files/filer/publikationer/C1703_IGRC2017_iskov.pdf
36. Honeywell. (2023). *Hydrogen Grid Injection & Point of Use (de -) blending*.
37. Jackson, C., Smith, G., & Kucernak, A.R. (2023). Deblending and Purification of Hydrogen from Natural Gas Mixtures Using the Electrochemical Hydrogen Pump. *International Journal of Hydrogen Energy*. https://doi.org/10.1016/j.ijhydene.2023.05.065
38. Shao, L., Low, B.T., Chung, T.-S., & Greenberg, A.R. (2009). Polymeric Membranes for the Hydrogen Economy: Contemporary Approaches and Prospects for the Future. *Journal of Membrane Science, 327* (1–2), 18–31. https://doi.org/10.1016/j.memsci.2008.11.019

sciendo

LATVIAN JOURNAL OF PHYSICS
AND TECHNICAL SCIENCES
2023, N 5

DOI: 10.2478/lpts-2023-0031

ANALYSIS AND IMPLEMENTATION OF ENERGY EFFICIENCY MEASURES IN MULTI-APARTMENT BUILDINGS IN LATVIA

A. Cimbale*[1], I. Amolina[2], I. Geipele[2], N. Zeltins[3]

[1] Ltd "Juridiskā koledža"
Kr. Valdemāra Str. 1c, Riga, LV-1010, LATVIA
[2] Riga Technical University,
Institute of Civil Engineering and Real Estate Economics,
6-210 Kalnciema Str., Riga, LV-1048, LATVIA
[3]Riga Technical University,
Faculty of Power and Electrical Engineering, Institute of Power Engineering
12-1 Azenes Str., Riga, LV-1048, LATVIA
*e-mail: a.cimbale@inbox.lv

A simplified life cycle of any product or service consists of three main stages – manufacturing, including obtaining, transformation, combination of raw materials; transportation, as well as packaging; consumption from purchase up to actual use. Energy is not an exception, it is also an item offered by the market in different forms, and everyone in need of it has the right to buy it in case the price is acceptable. Heat power is one of the energy types required by households and important for proper maintenance. Without heating, as well as electricity, modern houses cannot function appropriately, are not attractive to their inhabitants, do not provide comfort and safety. Nevertheless, heat power often is considered as a by-product of electricity production, nowadays a swift price increase for both types of energy is inevitable.

Energy efficiency is the level of appropriate usage of energy resources, which can be determined as the relation between final product type, quality, quantity and consumption of energy necessary to create this product [1].

Indirectly energy efficiency impacts health of the society in general and each individual in particular. Renovated energy efficient apartment buildings have a better ventilation system and microclimate. The problem of moisture and mold is at least partly solved, comfort is reached by consuming less energy, especially, heat power [2].

The aim of the paper is to research the impact of different energy efficiency increasing measures on heat consumption in multi-apartment buildings.

Keywords: *Construction costs, energy efficiency, renovation of residential houses, thermal energy savings.*

1. INTRODUCTION

The term "energy efficiency" during the past 20 years has become one of the most popular key words in different professional branches and spheres of life. Its wide use and sometimes unreasonable replication in mass media, social networks, official statements, and advertisements of maintenance companies create doubts and sceptical mood, rather than the will to participate, make the environment better, thus caring for the future of the society and next generations. Energy efficiency has become a thing used inappropriately, a thing that is unable to find its true owner – an owner who is capable of understanding and correctly using the benefits.

The field of the research is narrower than the term "energy efficiency" in general. It concentrates mostly on improvements of this parameter in multi-apartment buildings. In accordance with this statement, let us observe the definition provided by the Law on the Energy Performance of Buildings: "energy performance of a building – the relative amount of energy which characterises the necessary energy consumption for the supply of heating, ventilation, cooling, lighting and hot water in the typical operating conditions of a specific type of building" [3].

Consulting company Copenhagen Economics cooperates with governmental and non-profit organisations in Europe, and in 2012 precisely defined the benefit of high-quality renovation in different times of buildings, including multi-apartment buildings. Evaluating the process from economical perspective a wider range of positive effects can be determined – public and private can prevail over the development of the energy production and consumption branch. Needless to say, that the reduction of energy and consumption of combustibles decrease the expenses of every household, as well as has a positive impact on the societies balance of expenditures. However, the state in general goes through the reduction of income from taxes, excises and tolls, the budget indicates less expenditures related to the energy production sector.

Building-energy-use factors could be divided into two types according to their effect on energy efficiency: efficiency-correlated factors (which will affect the energy use efficiency) and non-efficiency-correlated factors (which will not affect the energy use efficiency) [4].

In the modern highly developed society, many persons own some kind of immovable property, which they often want to alter by reconstructing and renovating it, as well as implementing energy efficiency measures. Foreign investors fund construction of new projects in Latvia. Many such companies have been established in the country and are performing deals in this field, most of them complete personal projects, building whole villages, blocks of multi-apartment buildings or commercial spaces [5], as well as participating in energy efficiency projects.

Reducing the heat power supply chain to plain commerce is easy to draw a line between the supplier and the customer. The supplier oversees the condition of the power plants and the distribution grid. To increase the efficiency coefficient, existing elements of the power plants are exchanged by new ones, heat is being removed from flue gasses, combustible diversification is being implemented. To increase safety and decrease heat losses in the transportation segment, the grid is being modernized, using, for example, pre-insulated pipes. It is crucial to emphasise that manufacturers

have their limits. One day the line will be reached – the maximal level of modern technologies together with inadequate expenses of such will not allow to proceed with improvements. Currently, we are travelling towards economic and technological dead-end. Long ago thoughtful, knowledgeable, and acting customers had to appear in this system. The next stage of improvements must be made by consumers.

The consensus in the academic literature is that energy efficiency is associated with transaction value premiums [6].

It is worth mentioning that the implementation of energy efficiency measures gives general benefits to the market as well. Complete or partial renovation revives the housing stock and stimulates the development of the construction branch. Refurbished and renovated houses become a popular and highly valued product on the real estate market.

The aim of the research is to determine the impact of different energy efficiency increasing measures on heat consumption in multi-apartment buildings. To achieve the aim, several tasks have been formulated:

1. to find, if it exists, or create a methodology that would allow determining the impact of single refurbishment works and repairs in multi-apartment buildings on heat power consumption;
2. to accumulate as much data of houses as possible where any kind of repairs having impact on energy efficiency have been done;
3. to use the obtained data to calculate the reduction of heat consumption taking into account different types of buildings;
4. to make conclusions and suggestions to improve the process.

To complete the research, the authors have applied the analytical statistical, inductive, and qualitative methods. Considering the wide area of the research, the authors have decided to narrow down the time period till 2015–2022; the observed objects – multi-apartment buildings (mostly, prefabricated mass-housing repeated projects) located in Riga, Latvia.

2. ENERGY EFFICIENCY AND SUSTAINABLE DEVELOPMENT

Since 1995, numerous legislative acts have been adopted and entered into force in the field of administration of residential houses and multi-apartment buildings in Latvia. These acts in this field are regularly revised and modernized, even replaced by more actual and suitable ones. Since 2009, energy efficiency projects in residential objects have been started. Even having different repayment terms, all projects have the same characteristic parameters – decrease of heat power costs, rising of comfort and quality of space, balanced heat power supply and heat losses, increased value of the property, developed image of the object, preservation of envelope of the building, prolong life cycle, each of them leading towards sustainable exploitation of the house.

In an indirect way, energy efficiency has a positive impact on health of the society in general and each individual in particular. Renovated multi-apartment buildings have better ventilation systems and arranged microclimate. The problem of humidity and mould are at least partly resolved, and comfortable everyday life is provided reducing the consumption of energy, especially, of heat power [2].

The market also gains profit from

implementation of energy efficiency measures. Renovation revitalizes the immovable property fund and leads to the development of the construction field. Arranged and refurbished houses become an attractive and popular product on the real estate market.

In 2013, the United Nations Economic Commission completed an analysis on multi-apartment residential buildings in different countries, including Latvia, and drew several conclusions, among other – determined the existence of components forming an energy efficient building. Those are:

1. awareness of energy consumption and behaviour change in residents;
2. retrofitting existing housing to achieve high energy efficiency standards;
3. high energy standards for newly built homes;
4. energy-efficient utility systems providing services to housing;
5. low-energy housing management systems;
6. replacement of inefficient equipment, appliances, and lighting systems;
7. good environmental quality in spatial planning;
8. environmentally friendly building practices;
9. a minimized carbon footprint for the housing sector;
10. housing energy affordability [7].

This list is not only a pure conclusion – it can be used as an indicator list to take into account energy efficiency measures in multi-apartment buildings. These parameters must be researched before starting a single or several repairs decreasing energy consumption in the house, as well as after the signing of acceptance-handover act.

The will to improve, preserve and develop a person's dwelling is characteristic for every resident of an apartment even without consideration of global profit and public bidding. Many apartment owners consider the option to consume less without any crucial loss of comfort. Only some of them understand that to save up in future one should be ready to spend a little bit more today. Every multi-apartment building manager asked to name the most often heard reasoning for not renovating the house named the problem of lack of information, the fast spreading of false and unfounded information, concerns in other areas of life. This situation becomes worse due to negative experience related to maintenance of the building (dishonest residential house administrator, wasted funds of the community of apartment owners, low-quality refurbishment works and repairs, etc.).

In many developed countries, energy efficiency has become an indispensable part of housing policies, planning, design, and construction [8].

Sustainability and sustainable development have the chance to become more popular and attractive to society giving an impulse and solutions for optimization of energy supply. Sustainable development combines progress and the ability to preserve the current life level, keeping in mind that the most nature sources are exhaustible, those must be spared to allow next generations to live the same full-fledged life. There are several types of development to consider – besides the sustainable development there are two more types. The state of balance represents the situation of almost equal consumption and replenishment that leads to economy of stability, but in case of consumption overwhelming replenishment the society floats towards degradation and deficit.

The term of sustainable development is much wider than the idea of energy efficiency. The preservation or degradation of the environment is related not only to regulated and controlled production of different

energy types and amounts, consumption of fossil fuels, and use of non-conventional and alternative energy sources, but also to rational use of water sources, forward-looking waste recycling and disposal, implementation of design based on repetitive use, life cycle analysis with the aim to prolong the lifespan of products and services and many other activities. In the 2030 Agenda on Sustainable Development, homes are included as the base for a person's safety, qualitative development and education, preservation of cultural and historical values, step-by-step development of urban environment, stimulus to reduce energy consumption. Modern society must care not only about energy efficiency and the reduction of heat losses, but also about the complex arrangement of housing. Investing money in all the above-mentioned aspects might lead not only towards economy in future, but also help restrain many palpable problems – reduce number of different types of waste, repetition of emergency situations in buildings, dangers related to exploitation of buildings, etc.

Unfortunately, it is easily determined that the communities of apartment owners continue to ineffectively use different types of resources (heat but no insulate, complete local repairs instead of replacing the whole engineering system, perform arbitrary construction and for this reason do not provide access to their apartments to the maintenance company or other officials to perform mandatory checks etc.). Currently, communities of apartment owners selfishly stimulate the degradation of their life and property. Possibly, these harsh words would reach the aim audition and make them rethink their future.

3. HEAT POWER CONSUMPTION REDUCTION DUE TO PERFORMANCE OF DIFFERENT REPAIRMENTS

The authors of the research have obtained data and analysed repairs and maintenance works in several multi-apartment buildings (both municipal and private), as well as plans developed for future periods. As a result, they have concluded which works are the most popular among apartment owners and administrators. Thus, the mostly performed repairs are the following:

1. replacement of windows and doors;
2. replacement of the surface of the rooftop;
3. insulation of the overlap between the basement and the first floor or the attic and the last floor;
4. hermitization of junctures between panels;
5. exchange of the horizontal and vertical pipelines of cold, hot water and sewage;
6. renovation and modernization of the heating system;
7. modernization of the lighting and electricity supply systems;
8. repairs of the balconies and loggia;
9. insulation of the façade.

The above-mentioned list on types of repairs required by a dwelling house can be prolonged with works chosen rarely, but crucial for a particular object (development of a construction project, renovation of the fire extinguishing system, adjusting of a junction point of a commercial meter, connection of centralized water supply system and sewerage services, etc.). The authors have attempted to limit this list using one important factor – whether the chosen repair or maintenance work somehow reduces the consumption of heat power or electricity.

The plan of required repairs in a multi-apartment building is determined not only by the administrator, whose decisions are made based on annual and random inspections, and the community of apartment owners, but also many other factors have an impact on the final document. Often the developed plan is adjusted due to the offer to receive co-funding from a local authority or European Union funds.

Municipal and governmental bodies have massive impact on the plan, their instructions, acts, and decisions make required alterations. Cooperation among communities of apartment owners, administrators and municipal building authorities, the State Fire and Rescue Service of the Republic of Latvia, State and Municipal Police, in Riga – Administration of Building Arrangement, lead to crucial changes in the plan of repairs of a particular house.

To sum up, the plan of repairs and maintenance works is developed in accordance with the requirements stated in the legislative acts. Regulations of the Cabinet of Ministers No. 384 "Building Standard for Technical Survey of Buildings LBN 405-21" state that the technical survey (or the general inspection) must be done periodically during the exploitation of a buildings, but not less than once every 10 years for public and multi-apartment buildings corresponding to the second and third groups in accordance with General Construction Regulations [9]. Also, Regulations of the Cabinet of Ministers No. 907 "Regulations Regarding the Survey, Technical Servicing and Current Repairs of the Residential House" and particularly Section 16 reminds that the technical survey of a building shall be performed if the average lifetime referred to in Annex 2 to this Regulation has passed since the residential house and the buildings (structures) belonging thereto were put into operation or in accordance with the relevant residential house solidity group for the respective part of the building or built-in building wares [10]. The administrator has to follow attentively the lifetime of the building to create corresponding funds and to order the preparation of the technical survey. In this case the technical survey is not only a position in the plan of repair and maintenance works, but also the most important source of information for further development of the multi-apartment building.

The factors determining the planned and performed repairs in 2022 were the real potential to decrease heat power consumption, taking in account tariffs in different municipalities in Latvia and the prices for repairs in correlation with funds created by communities of apartment owners. Thus, it is important not only to compile the list of necessary repairs and maintenance works, but also to create this list in accordance with crucial priorities to ensure maximal effect – the limited amount of money must give maximal positive effect on the object. The community of apartment owners and the administrator have to evaluate all required works and their effect on energy efficiency to achieve this goal.

In the face of the unprecedented challenges posed by the negative influence of energy dependence on fossil fuels on the environment, energy efficiency contributes in a cost-effective way to reducing greenhouse gas emissions and therefore to mitigating climate change. The most effective way to persuade the management team for improving an energy management program is to present results through energy efficiency calculations and statistical analysis of energy consumption and energy costs [11].

4. METHODOLOGY

The authors of the research have tried to find different criteria to divide into groups the repairs needed by an apartment building. Classifying mostly depends on local legislative acts, which means that the offered system might not be appropriate for any other country except Latvia but it might show the basic principles useful for other scientists working in this field. Conceptually, the massive of the repairs can be related to:

1. expenses and their source;
2. confirmation, approval, and technical documentation needed beforehand the construction works;
3. result in form of reduction of heat loses and increase of energy efficiency parameters of the building.

The parameter of expenses is not only variable but depends on many social and economic aspects – the wealth level of the apartment owners, possible and available co-funding programs, amount, and type of repairs needed, the novelty and complications of the chosen repair methods impacting both the price and availability on the market. The process of confirmation of repairs also might be an additional complication before fast and effective implementation, and a classification parameter. Most of the repairs performed in multi-apartment buildings do not require any kind of agreement received from the Riga City Council Department of City Development in case of Riga or similar organisations in case of other cities of Latvia, but if more complex repairs are chosen, many different alterations are going to be done, and more detailed documentation must be prepared. In the context of this research, the parameter of energy efficiency is crucial due to the policy of the country, European Union, and the whole world. The shortage of resources determines the necessity to evaluate repairs not only as an instrument to prolong the lifespan of an object, but as a tool to allow the building to serve society as long as possible, consuming less energy in comparison with the present amount.

The authors of the research have made several attempts to find a universal methodology to calculate mostly precise the reduction of energy consumption following different repairs completed in multi-apartment buildings. The most logical way to find the efficiency degree of any repair is to compare heat consumption of a building during winter before the works and during winter after them. However, this "easy" method has many important drawbacks. The most important variable parameter is the duration of the real, not the calendar winter. The real winter or namely the heating season duration alters every year. Also, the air temperatures are very different during this season. During a very long heating season the temperatures might drop only till -5 °…+5 °C, but a rather short winter might bring temperatures lower than -10 °C on a constant basis. The combination of temperatures and duration has a significant impact of the overall energy consumption of the building.

The most appropriate for this occasion calculation attempt was made by two Ukrainian engineers Aleksandr Gut and Aleksej Zhdanov in 2016. They offer to calculate a correction coefficient that gives the required precision to an ordinary comparison of heat consumption during any period. The coefficient is determined using the following formula:

$$K = \frac{GDD_{year+1}}{GDD_{year}}, \quad (1)$$

where
K – correction coefficient of heat power consumption;
GDD_{year+1} – degree day amount in the year / winter / single winter month after the repairs;
GDD_{year} – degree day amount in the year / winter / single winter month before the repairs (AW Therm, AW Therm.2023.).

The degree day amount in Riga is determined by the local district heating company JSC "Rīgas siltums" and their collected data has been used to perform calculations for the capital of Latvia. All multi-apartment houses whose data have been used in this research are located in Riga and receive heat power from JSC "Rīgas siltums".

The heat power consumption reduction is calculated in the following way:

$$I = \frac{Q_{2015} - Q_{2016}}{Q_{2016}} \times 100\%, \quad (2)$$

where
I – the economy or reduction of heat power, %;
Q_{year} – heat power consumption in the year / winter / single winter month before the repairs, J;
Q_{year+1} – heat power consumption in the year / winter / single winter month after the repairs, J.

Therefore, the corrected economy or reduction of heat power is equal to:

$$I_{corrected} = IK, \quad (3)$$

where
$I_{corrected}$ – the corrected economy or reduction of heat power, %;
I – the economy or reduction of heat power, %;
K – correction coefficient of heat power consumption [12].

To show the usage of this method and its reliance to any kind of repairs performed in multi-apartment buildings, the authors provide further an example. The research is based on most common repairs completed in typical, concrete panel houses. The repairs in the field of interest of the corresponding research theoretically might positively affect energy efficiency of an object and reduce heat losses. Such works are insulation of the envelope of the building, exchange of doors and windows, hermetization of junctures between panels, renovation of foundation and plinth. These works are not only important to minimize energy consumption, but also very popular among maintenance companies and apartment owners' communities as they prolong the lifespan of the corresponding object. In October 2016, one house in Riga underwent the insulation works of both end walls or being more precise – firewalls. The house corresponds to 602 series, which is common not only in Riga, but overall, in Latvia.

First, the correction coefficient of heat power consumption has been calculated:

$$GDD_{2016\ january} = 218 \times (20 - -2.7) = 4948.6. \quad (4)$$

$$GDD_{2017\ january} = 204 \times (20 - -1.6) = 4406.4. \quad (5)$$

$$K_{2016\ january}/_{2017\ january} = \frac{4406,4}{4948.6} = 0.89. \quad (6)$$

The economy or reduction of heat power comparing January 2016 and January 2017:

$$I = \frac{132.95-121.8}{121.8} \times 100\% = 9.15\%. \quad (7)$$

Using the correction coefficient, the actual reduction is equal to:

$$I_{2016\ january/2017\ january} = 9.15 \times 0.89 = 8.14\%. \quad (8)$$

In this case after completing the repairs – the insulation of both firewalls has allowed to achieve 8.14 % reduction of heat consumption. Performing analogical calculations, positive results were received for other types of refurbishments.

5. TYPES OF REPAIRS ANALYSED

The multi-apartment buildings in Latvia are maintained by different bodies. There are state and municipal companies providing the obligatory variety of services, private companies acting upon a contract, cooperatives, and partnerships of apartment owners. Analysing the most common repairs chosen by these maintenance bodies, the authors have come to one main conclusion – the choice of repair type does not depend on the person providing maintenance, but it depends on the type, lifespan, construction features and other technical aspects of the building. Still, the most widespread multi-apartment buildings were constructed in accordance with types or series, replicating not only the facades and internal utilities, but also making mistakes and disadvantages common and repeated.

The list of works mentioned in Section 3 of this paper presents the most popular works, but not all of them result in energy saving and are not related to energy efficiency. Still, most of them provide benefits to the energy balance of the building, so they can be evaluated using the methodology described above.

Insulation of the end walls of the building is not the most popular nowadays, but still perceived by many people as the most efficient work. Often it is chosen in such cases as damage of the brick or panel end walls, freezing through the end walls, moisture and mould in apartments through the end walls. The work is relatively complicated, expensive and voluminous, scaffolding is required, but the changes in the façade have to be agreed upon by the community of apartment owners and local construction authorities. As a major drawback of this construction work, thermal bridges can be named. Even in case of very qualitative insulation material and perfectly completed work, heat finds alternative ways to leave the building through its envelope. A very common solution can be observed in Fig. 1.

Fig. 1. Insulated end wall of a multi-apartment building corresponding to 602M series in micro district Pļavnieki in Riga.

The authors of this research have determined several objects where insulation of end walls has been performed using different construction technologies. Without evaluation of these technologies, the quality of the performed works, expenses, the research concentrates purely on the reduction of energy consumption after the completion of the repairs. As can be seen in the previous section, an important part in the calculus is played by the degree days. In accordance with Latvian construction acts and standards, let us assume that the room temperature was equal to 20 °C, but the degree day amount before the year 2019 was equal to 203 days, but after – 197 days. The actual degree day value for all years appearing in the calculations has been determined for Riga by the local heat supply company JSC "Rīgas Siltums". However, it is worth mentioning that the factual duration of the heating season may differ due to the right of the apartment owner communities to determine this parameter. The company determines the length of this season choosing two dates – when 50 % of all houses using the service have started heat consumption and when 50 % of all houses have rejected taking any energy for heating purposes.

Further on, these data become a constant during the calculation. The actual heat consumption by different objects using district heating provided by JSC "Rīgas Siltums" is summed up on their homepage and offered to the public.

Table 1. Comparison of Heat Power Consumption in Multi-apartment Buildings with Insulated End Walls

No.	Address	Year of construction works	Type / series of building	Heat power consumption in January in the year before the repairs, Q_{year}, MWh	Heat power consumption in January in the year after the repairs, Q_{year+1}, MWh	Economy or reduction in heat power, I, %	Corrected economy or reduction in heat power, $I_{corrected}$, %
(1)	(2)	(3)	(4)	(5)	(6)	(7)	(8)
1	House 1	2016	602	132.95	121.8	9.15	8.14
2	House 2	2017	464	59.82	57.38	4.25	4.68
3	House 3	2017	119	72.92	67.63	7.82	8.61
4	House 4	2018	602 (old)	169.7	185.96	**-8.74**	**-6.86**
5	House 5	2018	464	74.15	80.74	**-8.16**	**-6.40**
6	House 6	2018	467	123.52	128.94	**-4.20**	**-3.30**
7	House 7	2019	464	62.44	45.34	37.72	29.72
8	House 8	2019	316/318	63.64	54.49	16.79	13.23

The authors are willing to emphasise that for the comparison of the heat consumption reduction the addresses of the buildings are not required, as well as the representatives of the communities of the apartment owners have agreed to provide information in case the data would be published without particular addresses. To make the calculus simpler, as well as to test the offered methodology the data have been analysed not for a quarter of the year, but only for one month – January. All houses summed up in Table 1 have undergone insulation works in summer or autumn – the earliest month was June but the latest October. For example, House 1 has insulated the end walls in October of 2016, so the comparison of heat energy consumption in January 2016 and in January 2017 is more than accurate.

Economy or reduction in heat power, I, % and corrected economy or reduction in heat power, $I_{corrected}$, %, for Houses 4, 5 and 6 are negative. All three houses have a different number of floors, heating surfaces, belong to different series, but are located in the same part of the city of Riga – Kurzeme Suburb (left bank of Daugava, northern part of the city). This poor result caused the authors to observe deeper the three cases. In the subsequent years, the objects provided better results. It is likely that such a deviation might be related to the quality of the works, chosen materials, overall state of these multi-apartment buildings. Altogether the houses that have shown an actual reduction in energy consumption provide an average success of 12.88 %.

Slightly popular than the previous work is hermetisation of junctures between panels. This kind of work does not require any complicated documentation or special agreements with the local building authority. It can be performed locally, even in winter. The most common technology used to perform this works consists of several stages. The quality of the result depends mostly on the first stage – preparation of the surface. The previous filling of the junctures must be mechanically removed, thus cleaning the space between panels and the surface of the elements. During the exploitation of the construction the façade is covered with different kind of substances that might originate from impure rain, snow, air, etc. For this reason, the surface has also to be degreased, dust and dirt have to be removed, even ice and condensate have to be cleaned. The second stage consists mostly of priming. The priming has to correspond to the material that will be used for filling or hermetization. After priming the space between the panels is filled with a special cord and polyurethane hermetization mixture. The layer must be 10–12 mm deep [13]. Main complications include the necessity to act very high and to preserve the cleaned surface from moisture. The main aim of this repair or construction work is to preserve the concrete panels and metal armature from damage and corrosion.

The authors succeeded in finding 27 multi-apartment buildings in Riga, which used hermetization of junctures and completed this work in 2016 and 2017. Among them, there were objects corresponding to different series of concrete bulk construction, such as 602, 119, 464, 467A, 467, 103, 104 and 101 series. To ensure adequate analysis and comparison, 16 houses of the 119 and 602 series were chosen. Houses of these types have a list of crucial similarities – the same floor number (9), the same number of apartments in a single section (36), similar explication of rooms in the apartment, etc.

Table 2. Comparison of Heat Power Consumption in Multi-apartment Buildings of the 119 Series where Hermetization of Junctures was Performed

No.	Address	Year of construction works	Type / series of building	Heat power consumption in January in the year before the repairs, Q_{year}, MWh	Heat power consumption in January in the year after the repairs, Q_{year+1}, MWh	Economy or reduction in heat power, I, %	Corrected economy or reduction in heat power, $I_{corrected}$, %
(1)	(2)	(3)	(4)	(5)	(6)	(7)	(8)
1	House 119 1	2016	119	59.6	50.77	17.39	15.49
2	House 119 2	2016	119	413.15	346.04	19.39	17.27
3	House 119 3	2017	119	201.84	186.98	7.95	8.74

It is impossible to search for rules and repetitions in case of only three examples. Without calculating the average heat consumption reduction, it is easy to conclude that this kind of construction works gives a very palpable effect, especially when all four façades of the building are handled. The researchers paid attention to the second house – house of 1119 2 series – due to a large number of apartments its heat consumption is huge, so the reduction is also massive evaluating absolute values. There are 200 apartments in this building, it has a big construction and façade surface. The savings in relation with a single apartment are not outstanding, even similar to the other cases, but the absolute reduction in fuel consumption is important for the district heating operator and economy in general.

Table 3. Comparison of Heat Power Consumption in Multi-apartment Buildings of the 602 Series where Hermetization of Junctures was Performed

No.	Address	Year of construction works	Type / series of building	Heat power consumption in January in the year before the repairs, Q_{year}, MWh	Heat power consumption in January in the year after the repairs, Q_{year+1}, MWh	Economy or reduction in heat power, I, %	Corrected economy or reduction in heat power, $I_{corrected}$, %
(1)	(2)	(3)	(4)	(5)	(6)	(7)	(8)
1	House 602 1	2016	602	125.15	108.33	15.53	13.83
2	House 602 2	2016	602	188.8	169.82	11.18	9.95
3	House 602 3	2017	602	227.29	215.97	5.24	5.77
4	House 602 4	2017	602	103.76	98.22	5.64	6.21
5	House 602 5	2017	602	118.3	113.31	4.40	4.85
6	House 602 6	2017	602	249.16	248.58	0.23	0.26
7	House 602 7	2017	602	239.42	228.74	4.67	5.14
8	House 602 8	2017	602	199.77	190.35	4.95	5.44
9	House 602 9	2017	602	146.38	139.37	5.03	5.53
10	House 602 10	2017	602	172.41	170.51	1.11	1.23
11	House 602 11	2017	602	114.35	108.75	5.15	5.67
12	House 602 12	2017	602	169.15	158.3	6.85	7.54
13	House 602 13	2017	602	156.15	156.82	-0.43	-0.47

As presented in Table 3, the hermetization of junctures did not provide the same positive effect to all houses of the 602 series. The corrected heat power consumption balances between -4.7 % and 13.83 %. Several reasons might cause this effect – different quality of performed works, bigger heat losses through other elements of the envelope (for example, through the overlap between the basement and the first floor or the attic and the last floor, windows of the apartment, etc.), not balanced heating system. The average calculated value of economy is equal to 9.96 %. This work can be offered to administrators and representative of communities of apartment owners, because it does no only preserve elements of the building, but also develops the quality of it. The table with the comparison of all 27 buildings of different series is not provided in this paper, but the average heat consumption reduction for all objects is equal to 8.73 %, which is also sufficient with regard to investments.

The insulation of the attic, or being more precise – the insulation of the overlap between the attic and the last floor is one more work that is important for the multi-apartment building. Although it is laborious and expensive, it is still often chosen by communities of apartment owners instead of overall renovation. The process of this work does not depend on the insulation material chosen; the steps are the following:

1. It has to be evaluated if the vapour insulation film or the barrier has to be applied.
2. The necessity of the wind barrier should be evaluated.
3. Then footbridges are created.
4. Pipelines in the attic are insulated.
5. All insulation material is applied [14].

For the insulation of the overlap of the attic, a wide variety of materials are used, such as mineral wool, polystyrene foam, polyurethane foam, ecowool, straw, expanded clay, wood shavings, plywood, veneer, mineral wool, basalt. Material also differs in form, e.g., in bulk, rolls, plates. The choice depends on the will of the customer, budget of the project, calculated heat losses, the quality and bearing capacity of the overlap.

This work was performed in 52 different houses representing very different types and series. Thirteen objects that underwent this repair are wooden, built before World War II or represent the monumental Stalinist architecture of the 1940s and 1950s. These buildings are mostly unique and incomparable with each other. Other multi-apartment building among these 52 correspond to different series, mostly 316/318, 119, 464 series.

Within the 316/318 series, there are various buildings constructed in the 1960s. However, they have several unified parameters – there are built from silicate bricks with overlaps from reinforced concrete. The number of these houses was 13, but the calculated heat power consumption loss was within 8.51 % and 34.98 % (see Table 4). The average value is equal to 20.27 %. Such a fabulous result can be easily explained – the normative lifespan of these buildings is equal to 60 years, and they have a very high depreciation. It has been determined that most losses of heat occur through the overlap of the attic and finally the roof. Despite the insulation the warm air rises up, and still finds a way out from the building. The insulation of the attic is very effective but cannot prevent all the heat losses that leads us to the conclusion that single works might be good, but complex renovation is better.

Table 4. Comparison of Heat Power Consumption in Multi-apartment Buildings of the 316/318 Series with the Insulation of the Overlap between the Attic and the Last Floor

No.	Address	Year of construction works	Type / series of building	Heat power consumption in January in the year before the repairs, Q_{year}, MWh	Heat power consumption in January in the year after the repairs, Q_{year+1}, MWh	Economy or reduction in heat power, I, %	Corrected economy or reduction in heat power, $I_{corrected}$, %
(1)	(2)	(3)	(4)	(5)	(6)	(7)	(8)
1	House 1	2017	316/318	54.5	44.97	21.19	23.32
2	House 2	2016	316/318	90.76	67.22	35.02	31.18
3	House 3	2016	316/318	108.94	86.34	26.18	23.31
4	House 4	2016	316/318	74.47	61.79	20.52	18.27
5	House 5	2016	316/318	75.87	69.25	9.56	8.51
6	House 6	2016	316/318	72.4	64.79	11.75	10.46
7	House 7	2016	316/318	93.7	81.64	14.77	13.15
8	House 8	2016	316/318	97.46	82.88	17.59	15.66
9	House 9	2016	316/318	113.84	97.84	16.35	14.56
10	House 10	2019	316/318	83.39	66.1	26.16	20.61
11	House 11	2019	316/318	59.5	47.76	24.58	19.37
12	House 12	2019	316/318	60.42	43.69	38.29	30.17
13	House 13	2019	316/318	88.31	61.16	44.39	34.98

Table 5. Comparison of Heat Power Consumption in Multi-apartment Buildings of the 119 Series with the Insulation of the Overlap between the Attic and the Last Floor

No.	Address	Year of construction works	Type / series of building	Heat power consumption in January in the year before the repairs, Q_{year}, MWh	Heat power consumption in January in the year after the repairs, Q_{year+1}, MWh	Economy or reduction in heat power, I, %	Corrected economy or reduction in heat power, $I_{corrected}$, %
(1)	(2)	(3)	(4)	(5)	(6)	(7)	(8)
1	House 1	2017	119	226.6	206.8	9.57	10.53
2	House 2	2017	119	184.57	152.36	21.14	23.26
3	House 3	2017	119	205.7	179.01	14.91	16.40
4	House 4	2016	119	184.57	158.56	16.40	14.61
5	House 5	2016	119	946.22	783.06	20.84	18.55
6	House 6	2016	119	416.65	334.17	24.68	21.98
7	House 7	2016	119	162.27	135.5	19.76	17.59
8	House 8	2018	119	293.72	288.71	1.74	1.36
9	House 9	2019	119	79.46	53.18	49.42	38.94
10	House 10	2019	119	151.3	106.3	42.33	33.36

Out of 52, ten multi-apartment buildings, where the insulation of the overlap between the last floor and the attic was done, are of the series 119. These ten houses show a very impressive dispersion of results – the economy fluctuates between 1.36% and

38.94% (see Table 5). The average value of the reduction of energy consumption is comparable with the result obtained by the 316/318 series – equal to 19.66 %. It is important to emphasise that houses of the 119 series were built in the 1980s using the most modern technologies on the construction market. The panels have an internal integrated insulation layer which actually has worn out during exploitation and the most apartment owners and inhabitants have voiced the opinion that the houses are not very warm and comfortable, especially during late autumn and early spring.

Also nine apartment buildings of the 464 series were researched. This type of houses is very "fruitful" – it has very many subtypes, including 464A used mostly in Latvia (it can be determined by a smaller window in kitchen in comparison with other ordinary windows of the rest of the rooms).

Table 5. Comparison of Heat Power Consumption in Multi-apartment Buildings of the 464 Series with the Insulation of the Overlap between the Attic and the Last Floor

No.	Address	Year of construction works	Type / series of building	Heat power consumption in January in the year before the repairs, Q_{year}, MWh	Heat power consumption in January in the year after the repairs, Q_{year+1}, MWh	Economy or reduction in heat power, I, %	Corrected economy or reduction in heat power, $I_{corrected}$, %
(1)	(2)	(3)	(4)	(5)	(6)	(7)	(8)
1	House 1	2016	464	106.91	94.07	13.65	12.15
2	House 2	2016	464	91.26	77.06	18.43	16.41
3	House 3	2016	464	101.03	86.29	17.08	15.21
4	House 4	2016	464	100.06	87.38	14.51	12.92
5	House 5	2016	464	97.29	82.49	17.94	15.98
6	House 6	2019	464	106.47	75.26	41.47	32.68
7	House 7	2019	464	76.92	55.16	39.45	31.09
8	House 8	2019	464	93.98	69.03	36.14	28.48
9	House 9	2019	464	72.64	55.21	31.57	24.88

The results of the nine buildings fluctuate between 12.5 % and 32.68 %. The average value equals to 18.69 %, once again being very similar to average results of the 119 and 316/318 series. The difference between all the three average results is less than 2 %. Taking into account an acceptable number of examples (total of 30 buildings) allows us to suggest that this kind of repair work make it possible to reduce the consumption of heat power by 20 % without any relation to the building type or series, at the same time being the only repair work performed in the building.

However, the above-mentioned suggestion needs to be approved by widening the range of the analysed houses, even possibly obtaining data on objects in other cities of Latvia, as well as taking into account the technology used to perform the insulation works, and to perform monitoring of the internal temperatures in different rooms of the buildings. The same specification of the research must be done for all calculations completed by the authors of this paper. This is the reason to continue the research because the steps for development are easily defined and are of interest to the society.

6. CONCLUSIONS

The overall renovation of the multi-apartment buildings allows preserving the object, as well as prolonging its lifespan. Single repair and maintenance works also allow reducing the amount of heat energy consumed and loss through the envelope.

It is highly important to develop an algorithm, which includes different renovation and preservation methods and scenarios for multi-apartment buildings. Such an algorithm can be proposed as the foundation for a program that would offer multiple variants of renovation, including costs, the forecast reduction in heat energy consumption, required documentation and types of agreement to be collected according to the funds collected by the community of apartment owners of a building, the type of the buildings, previously performed repairs and maintenance works.

REFERENCES

1. Energy Efficiency Law. Available at https://likumi.lv/ta/en/en/id/280932
2. Copenhagen Economics. (2012). *Multiple Benefits of Investing in Energy Efficient Renovation of Buildings. Impact on Public Finances.* Copenhagen.
3. Law on the Energy Performance of Buildings. Available at https://likumi.lv/ta/en/en/id/253635
4. Li, Z.R., Li, H.Z., & Yu, S. (2010). Development of Energy Efficiency Assessment Methods for Commercial Office Building in Shanghai. *ASHRAE TRANSACTIONS, 116* (2).
5. Lūce, I., Amoliņa, I., & Neibergs, M. (2021). Renovation of Multi-Apartment Residential Buildings in Latvia. *Rural Development*, 375–385. doi:10.15544/RD.2021.065
6. Chegut, A, Eichholtz, P, Holtermans, R, & Palacios, J. (2019). Energy Efficiency Information and Valuation Practices in Rental Housing. *Journal of Real Estate Finance and Economics,* 60 (1–2), 181–204, https://doi.org/10.1007/s11146-019-09720-0
7. United Nations Economic Commission for Europe. (2013). *Good practices for energy-efficient housing in the UNECE region.* New York and Geneva.
8. Čolić-Damjanović, V.M., & Šišović, G. (2021). Energy efficiency in social housing sector in Serbia: Problems and benefits. In *Proceedings of the 6th International Symposium on Environment-Friendly Energies and Applications (EFEA 2021*). 24–26 March 2021, Sofia, Bulgaria**.** doi: 10.1109/EFEA49713.2021.9406272
9. Cabinet Regulation No. 384 of the Republic of Latvia. (2021). *Construction Standard LBN 405-21.* Available at https://likumi.lv/ta/id/324221-buvju-tehniskas-apsekosanas-buvnormativs-lbn-405-21
10. Cabinet Regulation No. 907 of the Republic of Latvia. (2010). *Regulations Regarding the Survey, Technical Servicing, Current Repairs and Minimal Requirements for Energy Efficiency of the Residential House*. Available at https://likumi.lv/ta/en/en/id/218831
11. Ionescu, C.V., & Darie, G. (2020). Energy effectiveness-new energy performance indicator to optimize the industrial energy consumptions. In *2020 International Conference and Exposition on Electrical and Power Engineering (EPE)*. 22–23 October 2020, Iasi, Romania. doi: 10.1109/EPE50722.2020.9305663
12. AW Therm. (n.d.). *The Regulation of the heating System of an Office Building /* Регулирование системы отопления офисного здания. Available at https://aw-therm.com.ua/regulirovanie-sistemy-otopleniya-ofisnogo-zdaniya/

13. *Starppaneļu* šuvju *renovācijas tehnoloģija.* (n.d.). Available at https://site-343831.mozfiles.com/files/343831/Suvju_renovacijas_tehnologija.pdf

14. Building.lv. (n.d.). *Bēniņu siltināšana - nosiltini, nevis aizbāz ar zeķi!* Available at https://building.lv/raksts/B%C4%92NI%C5%85U-SILTIN%C4%80%C5%A0ANA-%E2%80%93-nosiltini,-nevis-aizb%C4%81z-ar-ze%C4%B7i

sciendo

LATVIAN JOURNAL OF PHYSICS
AND TECHNICAL SCIENCES
2023, N 5

DOI: 10.2478/lpts-2023-0032

THE DESIGN AND PERFORMANCE OF INTERNALLY COOLED CUTTING TOOLS FOR TURNING: A LITERATURE REVIEW

A. Korenkovs*, E. Gerins, A. Kromanis

Faculty of Mechanical Engineering, Transport and Aeronautics,
Riga Technical University,
6B Ķīpsalas Str., Riga, LATVIA
*e-mail: arturs.korenkovs@edu.rtu.lv

Near–dry machining and dry machining lead to increased temperature of the cutting tools. To reduce tool wear and extend the tool lifetime, and, eventually, to keep the accuracy of manufactured parts within acceptable limits as long as possible, a sustainable cooling technique is required. The technology of internal cooling of the cutting tool appears to be the most promising, because it allows eliminating the presence of the coolant on the manufacturing part and delivers the heat–transferring fluid to the very cutting area of the tool. This paper provides a literature review on the closed–loop internally cooled cutting tools (CLICCT) for turning. The current level of knowledge and experimental machining with prototypes has proven that CLICCT can utilize the benefits of dry cooling, having a longer tool life.

Keywords: *Closed–loop internal cooling, dry machining, internally cooled cutting tool, near–dry machining, turning.*

1. INTRODUCTION

Dry cutting due to the non-use of coolants is environmentally friendly and has become an important feature in today's green manufacturing [1]. The removal of metal working fluids (MWF) from the machining processes is of benefit to the machine operator, swarf recycling, and ultimately the environment [2]; it also reduces coolant–related costs [3].

Based on the environmental impact and health care, dry cutting is the best method of cutting, but it has some limitations, especially with the hard-to-cut material, where a large amount of heat is generated [4].

Dry machining (DM) leads to increased cutting temperatures and higher wear rates resulting in shorter tool life; this is particularly evident in the cutting of high-strength

materials [5]. In the machining of special materials such as rocket solid fuel, the cutting temperature must be strictly controlled; otherwise, it would explode and result in an accident [6]; also machining sensitive materials for optics or bio-medical applications or when machining harmful materials such as radioactive materials [7]. The internal coolant is sufficient to reduce the cutting temperature and avoid critical cutting temperatures [8].

Dry machining technology can be classified as near-dry cutting (NDC) and dry cutting [9].

Several cooling techniques are used for near–dry machining and dry machining (DM), such as minimum quantity lubrication (MQL) [10]; high-pressure cooling [10]; compressed air/vapor/gas cooling [9]; cryogenic cooling (liquid nitrogen) [11]–[14]; cryogenic MQL [15], [16]; internal cooling (heat sinks [5], heat exchangers [5], vortex tubes [5], heat pipes [5], pulsating heat pipes [17]–[19]; open circuit internal cooling [20].

The combination of cooling methods is also used: heat pipe and internal cooling [21], closed circuit internal cooling and spray cooling [22]–[26], closed circuit internal cooling and external MQL [27], and micro-texture self-lubricating tool with pulsating heat pipes [17].

Closed-loop internally cooled cutting tool (CLICCT) utilizes the benefits of internal cooling more fully because there is no contact between the cooling fluid and machined part, coolant might be reused, and it has no influence on the operator.

The aim of this paper is the literature review of the scientific articles dedicated to the development and research of internally cooled cutting tools (ICCT) for dry machining (DM), with the particular scope of research – closed-loop internally cooled cutting tools (CLICCT) for turning.

2. LITERATURE SYSTEMATIZATION CRITERION

The research of the literature consists of reviewing publicly available scientific publications, using abstract and citation online database Scopus.

The search for English language publications corresponding to the tag "internal cooling cutting tool" resulted in a list of 199 final publications, which was reduced to 68 articles by applying keyword filters ("cutting tools", "internal cooling", "turning") (see Fig. 1). Similarly, the search for "internally cooled cutting tool" resulted in the list of 43 publications, and was reduced to 10 (filter keywords: turning, internally cooled cutting tools); the search for "indirect cooling cutting tool" resulted in the list of 14 articles; the search for "cryogenic internal cooling" resulted in the list of 369 publications, and was reduced to 4 articles (filter keywords: cutting tools, turning); and the search for "dry turning internal cooling" resulted in the list of 34 articles, and was reduced to 12 (filter keywords: cutting tools).

The search for "internal cooling cutting tool" (with corresponding keyword filters applied) results in 68 articles – the most full list of scientific publications defined as a part of this review. This list states that there were 4 articles published before 1990, 2 articles in the period of 1990–2000 (0.2 articles per year on average), 3 articles in 2000–2010 (0.3), 42 articles in 2010–2020 (4.2), and 11 articles in 2020–2022 (5.5). That indicates an increase in the average number of publications per year about internally cooled cutting tools (ICCT), particularly since 2000.

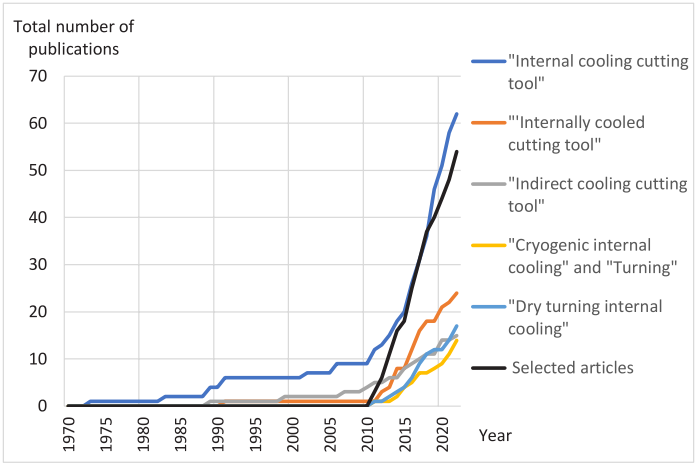

Fig. 1. Total number of publications by year based on searched keywords and applied filters.

Due to keyword matching, some articles appeared in more than one search. Leaving only publicly accessible articles, whose scope of research fits the definition of ICCT for turning, the total number of selected articles is equal to 54.

25 articles [1], [2], [5]–[7], [12], [22], [23], [28]–[46] out of the 54 selected articles cover different designs of CLICCT, 5 articles [6], [29], [36], [38], [43] cover only the FE and CDF simulations of CLICCT and 18 articles describe experimental turning with CLICCT prototypes [1], [2], [5], [7], [12], [28], [30], [32]–[34], [35], [37], [39], [41], [42], [44]–[46] (see Fig. 2).

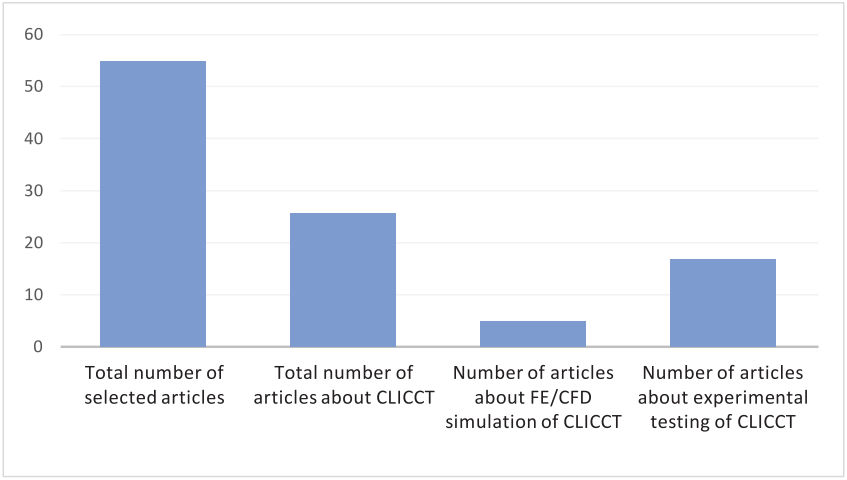

Fig. 2. Arrangement of selected publications by field of research.

In 6 articles [6], [30], [35], [37], [41], [44] the CLICCT design was defined as "novel" and in 1 article [42] as "innovative".

3. MAJOR TRENDS OF DESIGN OF THE CLOSED-LOOP INTERNALLY COOLED CUTTING TOOLS FOR TURNING

The design of CLICCT consists of CT itself and the coolant supply and circulation system. A schematic view of CLICCT proposed by Zakaria et al. [44] is shown in Fig. 3 and represents the main components of the cooling circuit: coolant tank, pump and hoses (tubes or pipes), and flow meter.

The purpose of the ICCT, apart from forming the cutting edge of the tool, is to deliver the coolant and remove the heat from the tool–chip contact area of the tool.

The internal cooling can be provided by different geometric patterns such as providing tiny grooves beneath the toolholder, providing the chamber under the shim of the toolholder, and designing profiles by utilizing the maximum area of cross-section [8].

The design of ICCT proposed by Shu et al. [31] is shown in Fig. 4 and represents the ICCT for turning with a cooling chamber (formed between standard cutting insert and support seat), where the coolant is supplied to support seat through the micro holes in the toolholder.

One of the main drawbacks of internally cooled tools with closed circuit flow is their complicated manufacturing [48].

Ghani et al. [50] in their research consider that the issue in improving the design of the internally cooled cutting tool is that the internally cooled cutting tool cannot be manufactured by using a conventional machine due to the complex shape of the cooling channel. In the research [50], [51] the use of additive manufacturing technologies in the manufacturing of ICCT was studied, concluding that: the selective laser melting (SLM) process provided higher precision and had a better surface roughness than the direct metal laser sintering (DMLS) process, but, the DMLS process performed better in dimensional accuracy than SLM [50]; and that the SLM could produce ICCT with high relative density (99 %) and low surface roughness (4.61 μm), showing minimum microstructure defects that encouraged the internal channel design [51].

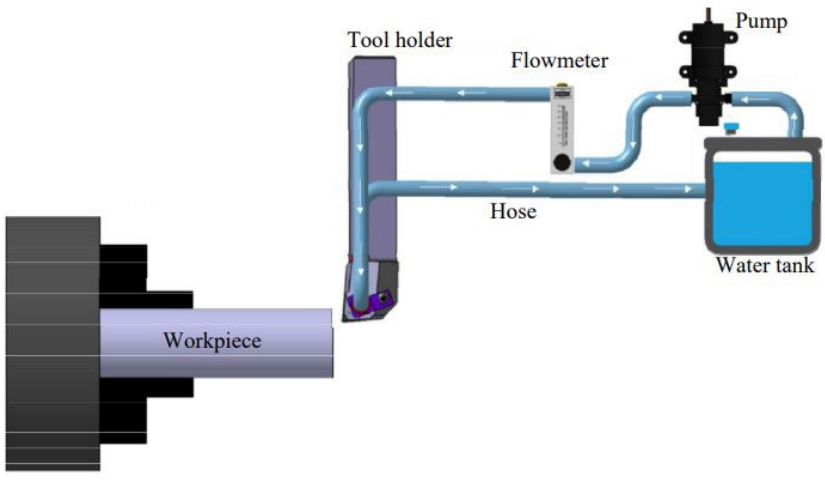

Fig. 3. Schematic view of the closed loop internally cooled cutting tool for turning [44].

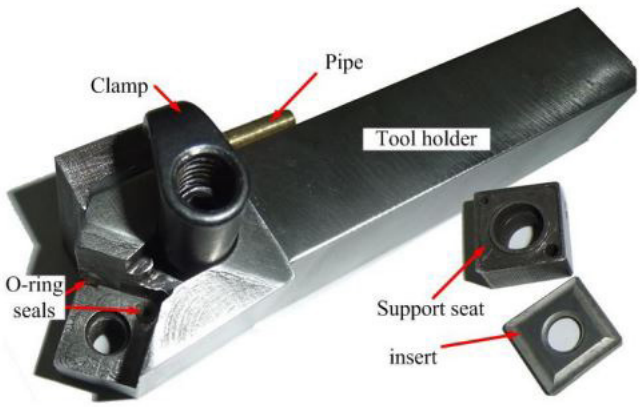

Fig. 4. Schematic view of the smart cutting tool [31].

The availability of modern machining and manufacturing technologies, accurate measuring instruments, precise computing and simulating software allows reaching the designed accuracy of the CT, establishing a tool condition monitoring system for adjustment of the operating parameters in real time, and development of smart cutting tools.

The temperature-based smart cutting tool focuses on the development of the internally cooled cutting tool, reducing the cutting temperature around the cutting edge, in order to extend tool life and produce a better surface finish at the workpiece [53]. The cutting tool can be also used as a smart tool by sensoring the cutting tip temperature in real time by continuously measuring the cooling inlet and outlet temperatures, and correlating them through a smart algorithm [47]. Artificial Neural Networks can be used to predict the underlying non-linear trends in tool temperature data obtained over a range of machining conditions [49].

The concept of an internally cooled smart cutting tool (ICSCT) for turning with closed-loop cooling circuit was proposed in [6] and realized in [30]. The authors of the research [41] proposed to use thermocouples for real-time measurement of coolant inlet and outlet temperatures, and coolant flow rate control system, for developing adaptive control machining, where abnormal temperature rising of the cutting tool and thus tool wear could be avoided and adaptively controlled.

The performance of the different designs of CLICCT can be predicted with the help of FE and CFD simulation software.

4. MAJOR TRENDS IN FE DESIGNS AND CFD SIMULATIONS FOR ICCT FOR TURNING

Turning tools with closed internal cooling systems must meet a different set of requirements compared to conventional tools. In particular, they must ensure the mechanical stability of the deployed cooling medium [52]. The research [54] on the profile configuration of the internal cooling channels in cutting insert concludes: the provision of internal cooling channel increases the cooling effect by decreasing the temperature; the variation

of the profile structure leads to temperature difference; the heat transfer rate of the fluid depends upon the profile structure [54].

Computational fluid dynamics (CFD) software allows simulating the flow of cooling fluid inside the internal channels of the tool and predicting the performance of the tool, i.e. the temperature of the tool–chip contact area, and eventually developing a tool design that meets the set of specific requirements for CLICCT.

In the scope of selected scientific articles, the researchers used different approaches for the IC simulation of CT.

Shu et al. [6] conducted a simulation test of the smart cutting tool with closed–loop internal cooling. The simulation imitates machining with and without internal cooling (see Fig. 5). The authors concluded that the proposed micro internal structure could substantially decrease the tool temperature of the cutting process (from 381.62 ˚C to 273.9 ˚C) and that the temperature of the tool tip might be estimated by measuring the coolant inlet and outlet temperature; as well as the simulations showed that a wall thickness of 1 mm towards the rake face and a minimum wall thickness of 0.7 mm towards the flank face were sufficient to withstand the mechanical loads [6].

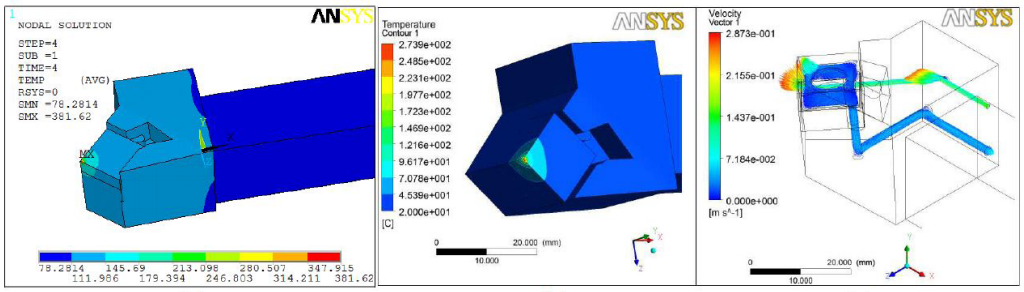

(a) (b) (c)

Fig. 5. Examples of tool temperature contours and velocity vector (a) without internal cooling, (b) with internal cooling, (c) velocity of cooling liquid [6].

Saiful et al. [29] simulated a water jet impingement cooling of a commercially available CI with a designed internal microchannel varying three parameters (space between the channel and internal wall of the insert, channel diameter, and fluid temperature). Researchers concluded that internal cooling could reduce the cutting temperature by more than 50 ˚C (compared to DM), the minimum cutting temperature was achieved when the cooling fluid temperature was low, and the space between the channel and the internal wall of the insert was high [29].

Zakaria et al. [36] carried out a FEM simulation test to define the effect of cutting load exerted on the modified tool holder (made of alloy steel, cubic boron nitride, and cemented carbide) with internal cooling channels (with diameters of 1.6, 4.2, and 5.0 mm) during the turning process of titanium alloy and aluminium. The researchers concluded that the application of the integrated cooling inside the tool holder led to the weakening of tool holder strength consequent of porosity forming; displacement of the tool holder was proportionally increased with incremental of hole diameter size, and maximum stress occurred at the fix mounted end, whose value of stress should not exceed the Young Modulus value [36].

Li et al. [38] used a thermal topologi-

cal optimization model of the insert plane to evaluate the mechanical properties and heat transfer of CT, simulating DM and machining with two different types of ICCT. Among other things, the authors concluded that the proposed optimization model was suitable for ICCT design to determine the layout of the flow channel and that the topological configuration design performed well both in the mechanical and thermal analysis (maximal stress of the topologically designed tool was 7.6 % higher, and maximum displacement was 6.5 % higher, but the maximum temperature was 6.2 ˚C lower, compared to traditional configured ICCT; and 180.4 ˚C compared to DM with non-cooled CT) [38].

Uhlmann and Meier [43] performed a numerical investigation of the heat flow with consideration of the thermomechanical load of the ICCT (with tool thickness of 1.58 mm and 4.76 mm) and flow characteristics of the cooling liquids (water and water–glycol at various temperatures and flow rates). They concluded that the process behavior showed a dependence of the flow rate (the inlet coolant temperature became less important with increased flow rate) and tool thickness (which shall be minimized under simultaneous consideration of the mechanical tool load) in terms of tool temperature reduction (reaching maximum simulated tool temperature reduction value equal to 193 ˚K, at –10 ˚C water/glycol inlet temperature and 10 l/min flow rate) [43].

More publications consist of computational simulation of IC and actual experimental machining.

5. THE PERFORMANCE AND THE RESULTS OF THE EXPERIMENTAL MACHINING WITH CLICCT

The conditions of the experiments to the fullest extent possible are described in the reviewed publications. In this paper, only the main aspects of published experiments are mentioned.

Vicentin et al. [28] machined SAE J775 XEV-F steel with the experimental CLICCT (cooled with R-123 refrigerant) with a cemented carbide CI (with triple layer coating) and compared the results of IC machining with DM and machining with external cutting fluid cooling (three cutting tools were used for each cooling method). The research among other things resulted in conclusions that internal cooling offered clear economic gains mainly in the increase of tool life (compared to DM), and was competitive once the costs involved with cutting fluids was a significant part of the piece total costs (compared to external cutting fluid cooling) and that the proposed IC system produced surface roughness values noticeably lower than with dry machining [28].

Uhlmann et al. [45] studied the influence of the coolant fluid temperature on the flank wear, performing the experiment of machining aluminium alloy AlSi7Mg0.3 with CLICCT (with customized 1.0 mm thick cemented carbide CI) for turning, applying different temperature coolant (20 ˚C and –10 ˚C) for dry and wet machining conditions. The research resulted in the conclusion that a decrease in flank wear of 10 % could be achieved by internal cooling (if wet machining was considered a reference), and the wear could be reduced by 32 % with coolant temperatures at 20 ˚C and by 20 % with coolant temperatures at –10 ˚C (if DM was used as a reference level); that IC increased quality by reducing surface roughness; and that

the ICCT had advantages for the machining AlSi7Mg0.3 [45].

Minton et al. [5] experimented with the machining of titanium 2 CP with CLICCT under conditions of dry-machining and inserted jet impingement cooling with ethylene glycol (directed through micro milling machined steel cooling block with a fluid reservoir, inlet, and outlet channels), with uncoated and diamond–coated (8 μm medium thickness, crystalline, diamond coating deposited via hot filament CVD) tungsten carbide CI (with reduced thickness to 1 mm). Researchers concluded that the introduction of an internally cooled cutting tool with enhanced thermal conductivity showed an increased tool life over conventional tools in DM of titanium (by approximately 41 % from 15 to 24 minutes of the cutting process, depending on machining conditions) and that the combination of the heat-spreading layer and indirect cooling provided an effective method of controlling thermally induced wear [5].

Shu et al. [30] carried out numerical modelling to optimize the design of CI (simulating different mechanical load conditions) and to evaluate the maximum temperature of the tool, and performed experimental machining aluminium alloy 6061-T6 (under different cutting conditions) with the designed closed–loop ICSCT (cooled with purified water; and consists of a toolholder with microholes, support seat with an annular groove, reduced to 1.8 mm thick tungsten carbide CI and thermocouples). Researchers concluded that the proposed average cutting temperature prediction model (which evaluated the maximum temperature of the tool equal to 442.28 ˚C for DM and equal to 359.6 ˚C for IC) possessed good accuracy and that there was a time lag in the smart cutting tool system (because the outlet temperature took time to reach steady) [30]. The authors also suggested that it was worthwhile to apply the smart cutting tool for adaptive control machining, where abnormal temperature rising of the cutting tool and thus tool wear could be avoided and adaptively controlled [30].

Ferri et al. [7], as a part of the experiment, machined AA6082–T6 aluminium alloy (see Fig. 6) with purpose-built ICCT (cooled by water with corrosion inhibitor) with tungsten carbide CI (modified to achieve squared bottle-cup shape). The statistical analyses showed that the measured chip temperature appeared to depend significantly only on the depth of cut but not on the feed rate or the cutting speed [7].

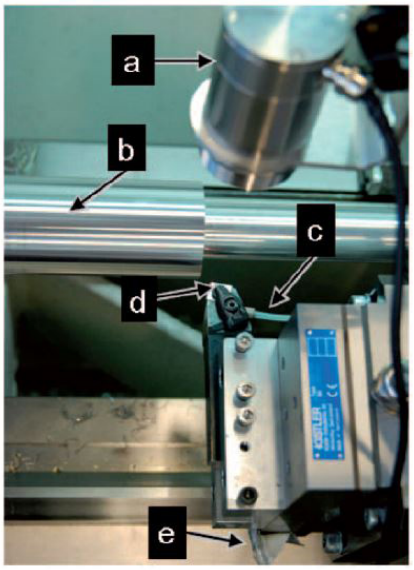

Fig. 6. Experimental set-up of the internally cooled tool on the CNC lathe: (a) pyrometer, (b) workpiece, (c) coolant outlet, (d) cutting tool, (e) coolant inlet [7].

Ferri et al. [2] machined aluminium 6082-T6 with CLICCT with tungsten carbide CI (modified with microfluidic structures), measuring coolant (ethylene glycol and water solution) inlet and outlet temperatures, together with the cutting and the thrust forces. The data analysis resulted in the conclusion that the specific efficiency

once log-transformed was found linearly increasing with the depth of cut and feed rate, and the maximum expected efficiency was equal to 10.96 % (at 0.10 mm/rev feed rate and 250 m/min cutting speed) [2].

Neto et al. [46] carried out experimental machining of stainless steel SAE XEV-F under internally cooled, externally cooled (flooded) and dry cutting conditions with designed CLICCT, with coated cemented carbide CI, connected to a silver interface in the annular channel of the tilted vaporization chamber (for phase-changing coolant Dupont R141b). Among other things, the authors concluded that the internal cooling method, compared to dry cutting, was less damaging to the cutting tool and provided a greater tool life, but the effectiveness of that method, compared to the method with applied cutting fluid, was not satisfactory (due to no lubricating action and lesser cooling capacity) [46].

Neto et al. [32] performed a thermal simulation for heat conduction analysis of the cutting tool temperature profile (for DM and IC conditions) and tested a CLICCT with phase-change coolant (Dupont R141b), and uncoated cemented carbide CI (contacting silver interface), machining AISI 1045 steel, to compare the performance with dry cutting and flood cutting conditions, during continuous and interrupted turning. The authors concluded that the IC was able to extend the cutting tool lives by 5 8% and 13 % in relation to the cutting fluid application and dry cutting, respectively; and the IC method was able to extend the cutting tool lives by 7 % and by 45 % in relation to the cutting fluid application and cutting, respectively; the temperatures recorded and the results of the simulation demonstrated a reduction of 10 % [32].

Isik [33] in his manuscript describes a session of experiments of machining of nickel-based superalloy Waspaloy AMS5708 with a designed CLICCT (with CVD-coated carbide CI), which is cooled by 18 ˚C purified water, at different experimental conditions (different cutting speeds). Isik [33], among other things, concludes that compared with dry machining IC decreases maximum tool–chip temperature by 9 %, reaches an extension of tool life by 12 %, achieves up to 13 % better surface quality (the lowest surface roughness value was Ra=0.699 μm at a cutting speed of 95 m/min, an inlet velocity rate of 1.6 m/s, and a depth of cut of 0.5 mm).

Sanchez et al. [34] developed a heat conduction model and carried out simulations (to estimate the temperature and heat flux at any point of the cutting tool), which followed by experimental machining of SAE J775 XEV-F steel with designed CLICCT (cooling fluid – refrigerant R22) with a CI. The authors concluded that the condition of steady state was reached in a shorter time when using the internal cooling and temperatures in the cutting region were lower; the effectiveness of the toolholder with internal cooling was only noticeable in machining processes that exceeded the time required to reach a steady state; and that in relation to dry machining, the proposed system offered clear economic gains mainly in the increase of tool life (due to the smaller rate of tool wear) [34].

Isik et al. [35] carried out finite element analysis (to develop a temperature simulation model) and testing of designed CLICCT (water cooled) with CVD-coated carbine CI, machining DIN 1.2379 cold work die steel (50 HRC). Within the limits of the experimental setup, the authors concluded that internal cooling of CT decreased the maximum temperature at the tool–chip interface from 607 ˚C to 545 ˚C, provided up to 12 % better surface quality (than DM), extended tool life up to 15 % [35]. It was also concluded that the temperature

of the differences between the inlet and outlet decreased with the increase in the flow rate and that the tool temperature could be reduced by up to 11 % [35].

Yao et al. [37] carried out a numerical analysis of the thermal performance of the designed water-cooled ICCT (to evaluate tool temperature at various machining conditions) and experimental machining of carbon steel 1045 with the tool prototype (consisting of the toolholder with a V-shaped cooling channel and carbide CI) under IC and dry cutting conditions. They, among other things, concluded that temperature data measured during experimental machining was highly consistent with those of numerical simulations and that the internal cooling decreased the maximal temperature at the measured point by almost 30 % (compared with dry cutting) [37].

Reiter et al. [39] performed FEM simulations of water-cooled ICCT (for defining the size and the position of an internal cooling channel) and carried out experimental machining of iron-carbon alloy (EN–GJS–600–3) with a designed tool, with PCD-coated (poly-crystalline diamond) cemented tungsten carbide CI, which was modified with the internal cooling channel. The researchers came up with the design of a modified CI with 1.25 mm minimal distance to the main cutting edge, and after experimental machining concluded that the temperature in the cutting area at the cutting edge decreased considerably below 700 ˚C (the critical temperature for PCD) with the use of internal cooling [39].

Continuing their previous research [38], Li et al. [40] performed numerical analysis (for mechanical and thermal optimization of the topological channel), carried out experimental machining of steel AISI 1045 with the designed water-cooled ICCT (consists of toolholder, modified CI, and adaptor), and compared three different types of CI (with the topological IC channels, with conventional IC channels [38], and without IC channels), measuring cooling liquid inlet and outlet line temperatures with two thermocouples. The researchers concluded that, compared to conventional IC channels, the topological channel had better heat transfer ability (under the same fluid volume) and smaller maximum temperature (topological CI was 16.32 ˚C cooler under the same cutting conditions) could improve mechanical properties (deformation in the main cutting force direction was 0.03–0.0207 mm smaller) and was more effective for the reduction of tool wear [40].

Ravi et al. [1] performed experimental machining of sandblasted air-quenched high chrome white cast iron (HCWCI) bars using CLICCT of their design, which was cooled with pure water and had cubic boron nitride (CBN) CI. Researchers concluded that internal cooling resulted in a reduction in the machining force (up to 23 %), flank wear (up to 19 %), and crater wear (up to 18 %), and that an internal cooling system enhanced tool life and brought a lot of scopes for hard turning process [1].

Wu et al. [41] carried out a numerical analysis of the tool thermal performance and tested (by heating with the temperature-controlled soldering iron and by experimental machining) the designed CLICCT, which consisted of the toolholder, modified CI, adaptor module, thermocouples (for real-time measurement of coolant inlet and outlet temperatures), and coolant (purified water) flow rate control system. Among other things, researchers concluded that the inlet velocity of the coolant should be matched with the amount of heat generated (excessive cooling would only bring energy waste and increase the cost) [41].

Ozturk et al. [42] manufactured self-designed closed–loop ICSCT with the cooling–control system, able to adjust the

cooling water flow referring to the CI tip temperature, for testing the machining process of 1040 steel. As a result, ICSCT with the cooling–control system and self-calibration based software could estimate the CI tip temperature and control the coolant flow rate and inlet temperature; under the same boundary conditions, the CI tip temperature could be decreased by as much as 107 ˚C in the internally cooled condition compared to the dry condition and made significant improvement on the surface of quality compared to dry turning in experiments [42]. The data presented in the research allowed calculating that the average surface roughness value of ICSCT machined specimen was 163 % smaller (compared to DM).

Zakaria et al. [44] performed experimental machining of AZ31 magnesium alloy with the CLICCT of their design, consisting of a toolholder with uncoated carbide CI and modified with the cooling module, which was installed on the top of the CI and delivered coolant (20 ˚C water) on the top rake face. The researchers concluded that internal cooling (what authors defined as "submerged convective cooling") reduced the cutting temperature up to 15 %, with 6 % cutting force and 12 % feed force reduction, compared to dry machining [44].

The results of the reviewed 18 articles, describing experiments with tool prototypes, and covering different aspects of machining with the CLICCT, are evaluated in the discussion section of this paper.

6. DISCUSSION AND CONCLUDING REMARKS

There are several aspects of the 25 overviewed publications that have distinct approaches (numerical simulations, cooling systems, the design and material of CT, the conditions and setups of experimental machining, and the main direction of research) that shall be addressed for the sake of comparison.

6.1 Numerical Simulations

In the scope of 25 selected publications, 5 articles [6], [29], [36], [38], [43] cover only the FE and CDF simulations of CLICCT and in 9 articles [30], [32], [34], [35], [37], [39]–[42] simulations are only a part of ICCT research.

The numerical simulations were used for two main purposes: prediction of temperature distribution and mechanical load simulations. The goal of temperature distribution simulations is for the estimation of the maximal temperature in tool–chip contact area of ICCT [6, 37] and the comparison of estimations of maximal temperature in tool–chip contact area in cases of DM and IC machining ([29], [30], [32], [34], [35], [38], [41]–[43]). The aim of mechanical load simulations is to define the wall thickness between the cutting edge and internal cooling channel [6], [30], [36], [39], to define maximal stress and displacement values of the tool (at various boundary conditions) [38], and to optimize the design of the internal topological channel [40].

6.2 The Design of Cooling Systems of Proposed CLICCT Prototypes

There are several parameters that define closed–loop cooling systems: the type of coolant, coolant inlet temperature, coolant flow rate and velocity, and coolant flow direction in CT. The data available in the selected publications are presented in Table 1.

Table 1. CLICCT Cooling System Parameters

	Coolant	Temperature, ˚C	Flow rate, l/min	Velocity, m/s	Coolant flow direction, inlet / outlet
[28]	R123	28			CE side / shank
[45]		-10 / 20			shank / shank
[5]	ethylene glycol based coolant	26	0.3		cooling block / cooling block
[30]	water	21.3	0.01	0.2	CE side / CE side
[7]	water with corrosion inhibitor		0.3		CE side / shank
[2]	25/75 ethylene glycol and water solution		0.3		CE side / shank
[46]	R141b	32	1.78		CE side / shank
[32]	R141b	32	1.78		CE side / shank
[33]	water with corrosion inhibitor	18	8.3 – 33.3	0.8 – 1.6	CE side / CE side
[34]	R22	24			CE side / shank
[35]	water	18		0.8 – 1.6	CE side / CE side
[37]	water		0.08		CE side / CE side
[39]	water		1.2		CE side / CE side
[40]	water	11		0.001	adaptor module / adaptor module
[1]	water	15			Not clear
[41]	water	12		0.001	adaptor module / adaptor module
[42]	water	22		0.7 – 1.57	CE side / CE side
[44]	water	20	0.4		cooling module / cooling module

In Table 1, “CE side” corresponds to the front part of the CT (closest to the cutting edge), but “shank” corresponds to the far–end (to cutting edge) part of toolholder; and for all refrigerant (phase–changing coolants) cooled systems [28], [32], [34], [46], the temperature of the coolant corresponds to its boiling temperature at atmospheric pressure.

Different fluids were proposed by researchers for IC of CT in selected articles: in 11 articles water (pure, distilled, mixted with additives) [1], [7], [30], [33], [35], [37], [39], [41], [42], [44] was proposed as a cooling fluid, in 4 articles – phase changing coolants [28], [32], [34], [46], and in 2 articles – ethylene glycol solutions [2], [5].

Most researchers chose water as a coolant for CLICCT systems (in 11 articles out of 18 selected publications describing experimental machining with ICCT). That choice can be explained: as the variation of coolant can have a significant impact on heat transfer efficiency and water was preferred as a coolant due to its beneficial thermal properties [43].

The cooling performance of ICCT with the coolant temperatures below 0 ˚C was studied only in one publication [45]; however, the type of the coolant was not clearly stated in the publication. Publication [45] is the only one, where a comparison of the cooling performance of ICCT, with different coolant temperatures, at the same machining condition, was carried out.

The comparison of the cooling efficiency at changing coolant velocity (and unchanging machining conditions) was studied in three articles [33], [35], [42], and the comparison of the cooling efficiency at changing flow rate of the coolant (and unchanging machining conditions) was

studied in one article [33].

No comparison of the cooling performance of the different types of coolants (under the same machining conditions) with the same design ICCT was found, and no comparison of the influence of the coolant flow direction was carried out.

All 18 selected articles [2], [5], [7], [28], [30], [32]–[35], [37], [39], [40]–[42], [44]–[46] resulted in a conclusion that IC reduced the temperature of CT and that internal cooling had lower temperatures in tool–chip contact area, compared with DM. However, due to differences in cooling parameters (type of coolant, coolant inlet temperature, coolant flow rate and velocity, and coolant flow direction), the direct comparison of numerical values is considered irrelevant.

The cooling efficiency is not solely based on fluid parameters, but cutting and workpiece material, tool coatings and engagement conditions, respectively, process parameters, which can have a relevant thermal influence [43].

6.3 The Design of Prototypes of Proposed CLICCT

The design of proposed CLICCT of selected articles is based on the modification of standard CT for turning.

Cooling channels are located in the plane of contact of CI and the toolholder [1], [33], [35], [37], [39], [45], in the plane of contact of CI and the intermediate piece [2], [5], [7], [30], [40]–[42], [44], or there is a cooling chamber [28], [32], [34], [46], which is separated from the CI with the intermediate piece.

The design data of proposed CLICCT prototypes (type of CI, modification of CI, description of the intermediate piece, and its manufacturing technology) from selected articles are presented in Table 2.

The cutting edge of the proposed CLICCT prototypes is formed by the standard CI in 8 articles [1], [28], [32], [33], [35], [37], [39], [46] and by the modified indexable CI in 9 articles [1], [2], [5], [7], [30], [39]–[41], [45]. In [34], the type of CI (and if any modifications were done) is not stated.

Table 2. The Design of Prototypes of Proposed CLICCTs

Reference	Standard indexable cutting insert (CI)	CI Modification	Intermediate piece (IM)	IM manufacturing technology
[28]	TNMA 160408 IC9015 (cemented carbide; TiN, Al_2O_3 and TiCN triple layer coating)	NO	cooper board	
[45]	SPUN 12XX08 (cemented carbide)	thickness reduced to 1 mm	NO	-
[5]	2x SNGN 120708 (tungsten carbide wiith 6 % cobalt; uncoated and 8 μm nano-crystalline diamond coated)	thickness reduced to 1 mm; diamond coating by hot filament CVD	steel cooling block	machining with a micro mill
[30]	YD201 SNMG120408 (tungsten carbide)	electrical discharge wire cutting (EDWC), to reduce thickness to 1.8 mm	support seat with	
[7]	SNUN 120408 (6 % cobalt; tungsten carbide)	electrical discharge machining (EDM), to fabricate a squared bottle–cap shape (1 mm wall thickness)	cooling adaptor	microchannel machining with a 5 axis micro mill

Reference	Standard indexable cutting insert (CI)	CI Modification	Intermediate piece (IM)	IM manufacturing technology
[2]	SNUN 120408 (6 % cobalt; tungsten carbide)	EDM to create a hollow with a 1 mm wall thickness	mild steel cooling adaptor	
[46]	TPUN 160308 IC 9054 (cemented carbide; coated with TiN, TiCN, Al_2O_3)	NO	silver interfacing part	
[32]	TPUN 160308 IC 20 (uncoated cemented carbide)	NO	silver interfacing part	
[33]	CNMG 190604–IC907 (CVD–coated carbide)	NO	NO	-
[34]	Not specified		cooper base	
[35]	CNMG 190608 IC907 (carbide; CVD-coated)	NO	NO	-
[37]	YT14 31303C (carbide)	NO	NO	-
[39]	TCMW 16T312 (cemented tungsten carbide; poly-crystalline diamond PVC–coated)	EDM to create a cooling channel	NO	-
[40]	GY3X (3 % cobalt; cemented carbide)	CI modified; modification type not specified	carbon steel adaptor module (coated with nickel)	
[1]	cubic boron nitride (CBN) CI	EDM drilling	NO	-
[41]	DNMA 150404	CI modified; modification type not specified	adaptor module	
[42]	CNMG 190608 (CVD–coated)	NO	stainless steel seat	
[44]	CNMA 120408 (carbide)	NO	cooling module	

6.4 The Conditions of Experimental Machining with CLICCT

The conditions of experimental machining of selected publications are presented in Table 3.

Regardless of the grades, steel machining with CLICCT is researched in 7 articles [28], [32], [34], [35], [37], [40], [42], aluminium – in 2 articles [2], [7], aluminium alloys – in 2 articles [30], [45]; and 1 article for each: titanium [5], stainless steel [46], nickel-based superalloy [33], iron–carbon alloy [39], high chrome white cast iron [1], magnesium alloy [44]. In 5 articles [5], [28], [30], [33], [46] the machined materials were defined as difficult-to-machine. In one article [41] material is not specified.

The machined material chemical composition is presented in 9 publications [1], [2], [5], [7], [28], [32], [33], [35], [44] and machined material mechanical properties are presented in 4 publications [1], [28], [32], [46]. The machining setup data are available in all selected articles (Table 4).

The main directions of the research are: tool wear research, machined surface roughness (surface quality) research, and tool temperature research. The tool wear research is in the focus of the study in 12 articles [1], [5], [28], [32]–[35], [39], [40], [44]–[46], surface roughness research – in 6 articles [28], [32], [33], [35], [42], [45], and tool temperature research – in 13 articles [5], [7], [30], [32]–[35], [37], [40]–[42], [44], [46].

Table 3. The Conditions of Experimental Machining with CLICCT

Reference	Machined material	Difficult-to-machine material	Material chemical composition present	Material properties present	Machining setup data	Tool wear research	Surface roughness research	Tool temperature research	Compression with DRY machining	Compression with WET machining
[28]	steel SAE J775 XEV-F	X	X	X	X	X	X		X	X
[45]	aluminium alloy AlSi7Mg0.3				X	X	X		X	X
[5]	Titanium 2 CP	X	X		X	X		X	X	
[30]	aluminium alloy 6061-T6	X			X			X	X	
[7]	aluminium AA6082-T6		X		X			X	X	
[2]	aluminium 6082-T6		X		X					
[46]	stainless steel SAE XEV-F	X		X	X	X		X	X	X
[32]	steel AISI 1045		X	X	X	X	X	X	X	X
[33]	nickel–based superalloy Waspaloy AMS5708	X	X		X	X	X	X	X	
[34]	steel SAE J775 XEV-F				X	X		X	X	
[35]	steel AISI D2 (DIN 1.2379		X		X	X	X	X	X	
[37]	steel AISI 1045 (0.45% carbon				X			X	X	
[39]	iron-carbon alloy (EN–GJS–600–3				X	X			X	X
[40]	steel AISI 1045				X	X		X	X	
[1]	high chrome white cast iron (HCWCI)		X	X	X	X			X	
[41]					X			X	X	
[42]	steel AISI 1040				X		X	X	X	
[44]	magnesium alloy AZ31		X		X	X		X	X	

Three articles [32], [33], [35] cover three directions of research, 8 articles [5], [28], [34], [40], [42], [44]–[46] cover two directions of research, and 6 articles cover one direction of research [1], [7], [30], [37], [39], [41]. In article [2], the research is aiming to identify and quantify the effect of the cutting parameters on the effectiveness of the internal cooling system.

In 17 articles [1], [5], [7], [28], [30], [32]–[35], [37], [39]–[42], [44]–[46], the performance of ICCT is compared with DM (at the same machining setup). In 5 articles [28], [32], [39], [45], [46], in addition to DM comparison, the performance of ICCT is compared with conventional wet or flood cooling.

Because 17 selected research [1], [5], [7], [28], [30], [32]–[35], [37], [39]–[42], [44]–[46] have results for machining with IC and DM, and comparison of those results, there is enough experimentally achieved data to evaluate tool wear, surface roughness, and cooling effectiveness (tool

temperature reduction) for both machining conditions.

The comparison of the numerical values of the results (the tool wear values, specimen surface roughness values, the values of temperature reduction in the tool–chip contact area due to IC), due to differences in the machining conditions (machining material, machining setup) and the directions of research, as well as insufficient or not presented information (machined material composition and properties), is considered irrelevant.

Table 4. The Setups of Experimental Machining with CLICCT

	Cutting speed V_C, m/min	Feed rate f, mm/rev	Depth of cut a_P, mm	Specimen diameter D, mm	Specimen length L, mm
[28]	140	0.43	0.50	50	300
[45]	1000	0.15	0.30		
[5]	80	0.20	1.00	60	150
[7]	250 / 300 / 350	0.10 / 0.15 / 0.20	0.20 / 0.35 / 0.50	65	450
[2]	250 / 300 / 350	0.10 / 0.15 / 0.20	0.20 / 0.35 / 0.50	65	450
[46]	80 / 100	0.20 / 0.40	0.50		
[32]	80 / 100	0.20 / 0.40	1.0	50	250
[33]	45 / 65 / 95	0.10	0.50	38	300
[34]	100 / 130 / 170	0.10	1.0	50	155
[35]	80 / 113 / 170	0.08	0.50	45	300
[39]	180	0.07	1.2		
[1]	55 / 88 / 136	0.096 / 0.124 / 0.179	0.1 / 0.2 / 0.3		
[41]		0.16	1.0		
[44]	120 / 180 / 240	0.20	1.0	30	100
	Cutting speed V_C, rpm	Feed rate f, mm/rev	Depth of cut a_P, mm	Specimen diameter D, mm	Specimen length L, mm
[37]	410	0.10	1.0	60	
[40]	320	0.16	1.0	100	
[42]	500 / 710 / 1000	0.08 / 0.11 / 0.14	1.0 / 2.0 / 3.0	30	30
	Cutting speed V_C, rpm	Feed rate f, mm/min	Depth of cut a_P, mm	Specimen diameter D, mm	Specimen length L, mm
[30]	220 / 430 / 670 / 1525	45	1.00	50	500

6.5 The Main Directions of the Research and Results

The tool wear of ICCT and its comparison with the wear of dry-machining CT, in the scope of selected articles, consist of flank wear [1], [5], [28], [32]–[35], [39]–

[40], [44]–[46], nose wear [28], crater wear [1], [32], [40], [46], built-up edge [44], [45], built-up layer and tool chipping wear [44].

In 12 studies [1], [5], [28], [32]–[35], [39]–[40], [44]–[46] authors concluded that IC reduced flank wear of ICCT (compared with DM). The nose wear of an ICCT is smaller than the nose wear of dry-machining CT at the same machining setup [28]. The build-up edge [44] and build-up layer [44] rates are also lower, compared with dry-machining CT at the same machining setup.

The results of crater wear evaluation for ICCT and dry-machining CT, in the scope of selected articles, are divided: ICCT crater wear is smaller compared to DM [1], [40], and ICCT crater wear, depending on machining setup, is smaller, approximately equal or bigger, compared to DM [32], [46]. The difference in the crater wear related results might be explained by the difference in machined material and machining setup.

The authors of 4 articles [5], [28], [33], [46] refer to ISO 3685-1993 standard (Tool–life testing with single–point turning tools), for the guidance for verifiable tool wear evaluation method.

The surface roughness research was presented in 6 articles: the authors of 5 articles [5], [28], [33], [42], [45] concluded that the surface roughness of the machined with ICCT specimen is smaller (surface quality is better), compared with the dry-machined specimen; and the authors of article [32] concluded that the surface roughness of the machined with ICCT specimen, depending on machining setup, was smaller, approximately equal or bigger, compared to DM.

The authors of 13 publications [5], [7], [30], [32]–[35], [37], [40]–[42], [44], [46], where tool temperature research was carried out, concluded that the temperature in tool–chip contact area of ICCT during machining with IC was lower that the temperature in tool–chip contact area of CT during DM.

7. CONCLUSIONS

The number of scientific articles focusing on internally cooled cutting tools increased from 6 in 2000 to 62 in 2022.

Experimental turning with prototypes of closed-loop internally cooled cutting tools proved that:

1. closed-loop internally cooled cutting tools can be used for turning various materials including difficult-to-machine materials: steel and stainless steel, aluminium and aluminium alloys, iron–carbon alloy, high chrome white cast iron, titanium, nickel-based superalloy, magnesium alloy;
2. closed-loop internally cooled cutting tools for turning have smaller tool wear and a longer lifetime, due to lower temperature in tool–chip contact area, compared to dry-machining;
3. closed-loop internally cooled cutting tools for turning provide a better surface quality (smaller surface roughness) of the machined parts, compared to dry-machining;
4. turning with closed-loop internally cooled cutting tools shares the same advantages as dry turning: no coolant contamination, no coolant consumption, it is environmentally friendly, and has fewer health hazards.

More specific research on a design for the development of a sustainable CLICCT is still a field for future research.

REFERENCES

1. Ravi, A.M., & Murigendrappa, S.M. (2018). Experimental study on internal cooling system in hard turning of HCWCI using CBN tools. In 1st International Conference of Design, Materials and Manufacture (ICDEM 2018), 29–31 January 2018. Karnataka: AIP Publishing. doi:10.1063/1.5029629.
2. Ferri, C., Minton, T., Ghani, S.B.C., & Cheng, K. (2014). Efficiency in Contamination-Free Machining using Microfluidic Structures. *CIRP Journal of Manufacturing Science and Technology*, 7 (2), 97–105. doi:10.1016/j.cirpj.2013.12.001.
3. Rahim, W.M.F.W.A., Shahrizad, A.F.M., Khor, C.Y., Rosli, M.U., Jahidi, H., Ishak, M.I., … & Nik-Ghazali, N. (2018). Turbulent coolant inside cutting tool to control heat transfer during cutting process. In 4th International Conference on Green Design and Manufacture (IConGDM 2018), 29–30 April 2018. Ho Chi Minh: AIP Publishing. doi:10.1063/1.5066771.
4. Abdelrazek, A.H., Choudhury, I.A., Nukman, Y., & Kazi, S.N. (2020). Metal Cutting Lubricants and Cutting Tools: A Review on the Performance Improvement and Sustainability Assessment. *International Journal of Advanced Manufacturing Technology*, *106* (9–10), 4221–4245. doi:10.1007/s00170-019-04890-w.
5. Minton, T., Ghani, S., Sammler, F., Bateman, R., Fürstmann, P., & Roeder, M. (2013). Temperature of Internally-Cooled Diamond-Coated Tools for Dry-Cutting Titanium. *International Journal of Machine Tools and Manufacture*, *75*, 27–35. doi:10.1016/j.ijmachtools.2013.08.006.
6. Shu, S., Ding, H., Chen, S., & Cheng, K. (2012). Fem-Based Design and Analysis of a Smart Cutting Tool with Internal Cooling for Cutting Temperature Measurement and Control. *Applied Mechanics and Materials*, 217–219, 1874–1879. doi:10.4028/www.scientific.net/AMM.217-219.1874.
7. Ferri, C., Minton, T., Ghani, S.B.C., & Cheng, K. (2014). Internally cooled tools and cutting temperature in contamination-free machining. *Proceedings of the Institution of Mechanical Engineers, Part C: Journal of Mechanical Engineering Science*, *228* (1), 135–145. doi:10.1177/0954406213480312.
8. Sowgandhi, B., & Pavani, P. N. L. (2019). Recent Studies in the Application of Internal Cooling System in Conventional Machining Process. *International Journal of Scientific and Technology Research*, *8* (8), 441–444.
9. Wu, Z., Yang, Y., Su, C., Cai, X., & Luo, C. (2017). Development and Prospect of Cooling Technology for Dry Cutting Tools. *International Journal of Advanced Manufacturing Technology*, *88* (5–8), 1567–1577. doi:10.1007/s00170-016-8842-7.
10. Anton, S., Andreas, S., & Friedrich, B. (2014). Heat dissipation in turning operations by means of internal cooling. In *25 DAAAM International Symposium on Intelligent Manufacturing and Automation (DAAAM 2014)*, 26–29 November 2014 (pp. 1116–1123). Vienna: Procedia Engineering. doi:10.1016/j.proeng.2015.01.474.
11. Rozzi, J. C., Sanders, J. K., & Chen, W. (2011). The Experimental and Theoretical Evaluation of an Indirect Cooling System for Machining. *Journal of Heat Transfer*, *133* (3). doi:10.1115/1.4002446.
12. Bogajo, I.R., Tangpronprasert, P., Virulsri, C., Keeratihattayakorn, S., & Arrazola, P.J. (2020). A Novel Indirect Cryogenic Cooling System for Improving Surface Finish and Reducing Cutting Forces when Turning ASTM F-1537 Cobalt-Chromium Alloys. *International Journal of Advanced Manufacturing Technology*, 111 (7–8), 1971–1989. doi:10.1007/s00170-020-06193-x.

13. Narayanan, D., & Jagadeesha, T. (2019). Process capability improvement using internally cooled cutting tool insert in cryogenic machining of super duplex stainless steel 2507. In *1st International Conference on Innovative Product Design and Intelligent Manufacturing System (ICIPDIMS 2019)*, 17–18 May 2019 (pp. 323–330). Rourkela: Lecture Notes in Mechanical Engineering. doi:10.1007/978-981-15-2696-1_31.
14. Ortiz-De-Zarate, G., Soriano, D., Madariaga, A., Garay, A., Rodriguez, I., & Arrazola, P.J. (2021). Experimental and FEM analysis of dry and cryogenic turning of hardened steel 100Cr6 using CBN wiper tools. In *18th CIRP Conference on Modeling of Machining Operations (CMMO 2021)*, 15–17 June 2021 (pp. 7–12). Ljubljana: Procedia CIRP. doi:10.1016/j.procir.2021.09.002.
15. He, A., Ye, B., & Wang, Z. (2014). Experimental Effect of Cryogenic MQL Cutting 304 Stainless Steel. *Key Engineering Materials*, *621*, 3–8. doi:10.4028/www.scientific.net/KEM.621.3.
16. Lin, H., Wang, C., Yuan, Y., Chen, Z., Wang, Q., & Xiong, W. (2015). Tool Wear in Ti-6Al-4V Alloy Turning Under Oils on Water Cooling Comparing with Cryogenic Air Mixed with Minimal Quantity Lubrication. *International Journal of Advanced Manufacturing Technology*, *81* (1–4), 87–101.doi:10.1007/s00170-015-7062-x.
17. Wu, Z., Deng, J., Su, C., Luo, C., & Xia, D. (2014). Performance of the Micro-Texture Self-Lubricating and Pulsating Heat Pipe Self-Cooling Tools in Dry Cutting Process. *International Journal of Refractory Metals and Hard Materials*, *45*, 238–248. doi:10.1016/j.ijrmhm.2014.02.004.
18. Wu, Z., Yang, Y., & Luo, C. (2016). Design, Fabrication and Dry Cutting Performance of Pulsating Heat Pipe Self-Cooling Tools. *Journal of Cleaner Production*, *124*, 276–282. doi:10.1016/j.jclepro.2016.02.129.
19. Wu, Z., Bao, H., Xing, Y., & Liu, L. (2022). Dry Cutting Performance and Heat Transfer Simulation of Pulsating Heat Pipe Self-Cooling Tool Holder. *Journal of Manufacturing Processes*, *83*, 129–142. doi:10.1016/j.jmapro.2022.08.055.
20. Peng, R., Jiang, H., Tang, X., Huang, X., Xu, Y., & Hu, Y. (2019). Design and Performance of an Internal-Cooling Turning Tool with Micro-Channel Structures. *Journal of Manufacturing Processes*, *45*, 690–701. doi:10.1016/j.jmapro.2019.08.011.
21. Shu, S., Chen, S., & Cheng, K. (2011). Investigation of a novel green internal cooling in turning application. In *2011 International Conference on Electronic and Mechanical Engineering and Information Technology (EMEIT 2011)*, 12–14 August 2011 (pp. 1156–1159). doi:10.1109/EMEIT.2011.6023299.
22. Bleicher, F., Pollak, C., Brier, J., & Siller, A. (2016). Reduction of Built-Up Edge Formation in Machining Al- and Cast Iron Hybrid Components by Internal Cooling of Cutting Inserts. *CIRP Annals – Manufacturing Technology*, *65* (1), 97–100. doi:10.1016/j.cirp.2016.04.090.
23. Bleicher, F., Brier, J., & Siller, A. (2016). Simultaneous machining of a material combination with an internally and externally cooled cutting insert. In *7th CIRP Conference on High Performance Cutting (HPC 2016)*, 31 May – 2 June 2016 (pp. 15–18). Chemnitz: Procedia CIRP. doi:10.1016/j.procir.2016.03.196.
24. Bleicher, F., & Reiter, M. (2017). Wear reduction on cutting inserts by additional internal cooling of the cutting edge. In *15th Global Conference on Sustainable Manufacturing (GCSM 2017)*, 25–27 September 2017 (pp. 518–524). Haifa: Procedia Manufacturing. doi:10.1016/j.promfg.2018.02.152.
25. Shu, S., Zhang, Y., Xiao, C., Qi, X., & Liu, L. (2019). Cooling performance improvement of circulating internal cooling turning tool by built-in additional spray cooling nozzle. In *2019 7th International Conference on Mechanical Engineering, Material Science and Civil Engineering (ICMEMSCE 2019)*, 17–18 December 2019. Sanya: IOP Conference Series: Material Science and Engineering. doi:10.1088/1757-899X/758/1/012062.

26. Shu, S., Zhang, Y., He, Y., & Zhang, H. (2021). Design of a Novel Turning Tool Cooled by Combining Circulating Internal Cooling with Spray Cooling for Green Cutting. *Journal of Advanced Mechanical Design, Systems and Manufacturing*, *15* (1). doi:10.1299/JAMDSM.2021JAMDSM0003.

27. Gupta, S., Venkatesan, K., Devendiran, S., & Mathew, A.T. (2019). Experimental Investigation of IN725 Under Different Cooling Environments using New Tool Holder. *Materials and Manufacturing Processes*, *34* (6), 637–647. doi:10.1080/10426914.2018.1532583.

28. Vicentin, G.C., Sanchez, L.E.A., Scalon, V.L., & Abreu, G.G.C. (2011). A Sustainable Alternative for Cooling the Machining Processes using a Refrigerant Fluid in Recirculation Inside the Toolholder. *Clean Technologies and Environmental Policy*, *13* (6), 831–840. doi:10.1007/s10098-011-0359-z.

29. Saiful, C.-G., Cheng, K., Sun, X., & Bateman, R. (2011). Optimizing heat transfer rate in an internally cooled cutting tool: FE-based design analysis and experimental study. In *6th International Congress of Precision Machining (ICPM2011)*, 13–15 September 2011. doi:10.4028/www.scientific.net/KEM.496.188.

30. Shu, S., Cheng, K., Ding, H., & Chen, S. (2013). An Innovative Method to Measure the Cutting Temperature in Process by using an Internally Cooled Smart Cutting Tool. *Journal of Manufacturing Science and Engineering*, *135* (6). doi:10.1115/1.4025742.

31. Shu, S.R., Ding, H., Chen, S.J., & Cheng, K. (2013). Thermal design and analysis of an internally cooled smart cutting tool and its implementation perspectives. In *15th International Manufacturing Conference in China (IMCC 2013)*, 16–18 October 2013 (pp. 120–125). Material Science Forum. doi:10.4028/www.scientific.net/MSF.770.120.

32. Neto, R.R.I., Scalon, V.L., Fiocchi, A.A., & Sanchez, L.E.A. (2016). Indirect Cooling of the Cutting Tool with a Pumped Two-Phase System in Turning of AISI 1045 Steel. *International Journal of Advanced Manufacturing Technology*, *87* (9–12), 2485–2495. doi:10.1007/s00170-016-8620-6.

33. Isik, Y. (2016). Using Internally Cooled Cutting Tools in the Machining of Difficult-to-Cut Materials Based on Waspaloy. *Advances in Mechanical Engineering*, *8* (5), 1–8. doi:10.1177/1687814016647888.

34. Sanchez, L.E.D.A., Neto, R.R.I., Fragelli, R.L., Junior, C.E.D.S., & Scalon ,V.L. (2015). Machining with internally cooled toolholder using a phase change fluid. In *48th CIRP International Conference on Manufacturing Systems (CIRP CMS 2015)*, 24–26 June 2015 (pp. 847–851). Ischia: Procedia CIRP. doi:10.1016/j.procir.2015.12.007.

35. Isik, Y., Kus, A., Coskun, S., Ozdemir, K., & Cakir, M.C. (2017). A Novel Approach to use Internally Cooled Cutting Tools in Dry Metal Cutting. *Indian Journal of Engineering and Materials Sciences*, *24* (3), 239–246.

36. Zakaria, M.S., Nordin, F., Jamalludin, M.R., Rosli, M.U., Rahim, W.M.F.W.A., Ishak, M.I., & Khor, C.Y. (2017). Finite element study on the integrity of tool holder with integrated internal cooling channel. In *3rd Electronic and Green Materials International Conference 2017 (EGM 2017)*, 29–30 April 2017. Aonang Krabi: AIP Conference Proceeding. doi:10.1063/1.5002254.

37. Yao, B., Sun, W., Chen, B., Yu, X., He, Y., Feng, W., & Wang, S. (2017). An Independent Internal Cooling System for Promoting Heat Dissipation during Dry Cutting with Numerical and Experimental Verification. *Applied Sciences (Switzerland)*, *7* (4). doi:10.3390/app7040332.

38. Li, T., Wu, T., Ding, X., Chen, H., & Wang, L. (2017). Design of an Internally Cooled Turning Tool Based on Topology Optimization and CFD Simulation. *International Journal of Advanced Manufacturing Technology*, *91* (1–4), 1327–1337. doi:10.1007/s00170-016-9804-9.

39. Reiter, M., Brier, J., & Bleicher, F. (2018). Machining of Iron-Carbon Alloys by the use of Poly-Crystalline Diamond Cutting Inserts with Internal Cooling. *Journal of Manufacturing and Materials Processing*, *2* (3). doi:10.3390/jmmp2030057.

40. Li, T., Wu, T., Ding, X., Chen, H., & Wang, L. (2018). Experimental Study on the Performance of an Internal Cooled Turning Tool with Topological Channel. *International Journal of Advanced Manufacturing Technology*, *98* (1–4), 479–485. doi:10.1007/s00170-018-2278-1.

41. Wu, T., Li, T., Ding, X., Chen, H., & Wang, L. (2018). Design of a Modular Green Closed Internal Cooling Turning Tool for Applications. *International Journal of Precision Engineering and Manufacturing – Green Technology*, *5* (2), 211–217. doi:10.1007/s40684-018-0021-x.

42. Ozturk, E., Yildizli, K., & Saglam, F. (2021). Investigation on an Innovative Internally Cooled Smart Cutting Tool with the Built-in Cooling-Control System. *Arabian Journal for Science and Engineering*, 46 (3), 2397–2411. doi:10.1007/s13369-020-05002-7.

43. Uhlmann, E., & Meier, P. (2021). Numerical investigation on the process behavior of a closed-loop internal cooling system for turning operations. In *18th CIRP Conference on Modeling of Machining Operations (CMMO 2021)*, 15–17 June 2021 (pp. 73–78). Ljubljana: Procedia CIRP. doi:10.1016/j.procir.2021.09.013.

44. Zakaria, M.S., Mustapha, M., Azmi, A.I., Ahmad, A., Danish, M., & Rubaiee, S. (2022). Machinability Investigations of AZ31 Magnesium Alloy Via Submerged Convective Cooling in Turning Process. *Journal of Materials Research and Technology*, *19*, 3685–3698. doi:10.1016/j.jmrt.2022.06.127.

45. Uhlmann, E., Furstmann, P., Roeder, M., Richarz, S., & Sammler, F. (2012). Tool wear behaviour of internally cooled tools at different cooling liquid temperatures. In *10th Global Conference on Sustainable Manufacturing*. Istanbul.

46. Neto, R.R.I., Fragelli, R.L., Fiocchi, A.A., Scalon, V.L., & Sanchez, L.E.A. (2015). Toolholder Internally Cooled by a Phase Change Fluid in Turning of SAE XEV-F. *Applied Mechanics and Materials*, *798*, 486–490. doi:10.4028/www.scientific.net/AMM.798.486.

47. Sun, X., Bateman, R., Cheng, K., & Ghani, S.C. (2012). Design and Analysis of an Internally Cooled Smart Cutting Tool for Dry Cutting. *Proceedings of the Institution of Mechanical Engineers, Part B: Journal of Engineering Manufacture*, *226* (4), 585–591. doi:10.1177/0954405411424670.

48. Kromanis, A. Pikurs, G. Muiznieks, G. Kravalis, K. & Gutakovskis, V. (2014). Design of internally cooled tools for DRY cutting. In *9th International Conference of DAAAM Baltic: Industrial Engineering (DAAAM-Baltic 2014)*, 24–26 April 2014 (pp. 109–114). Tallinn: Proceedings of the International Conference of DAAAM Baltic "Industrial Engineering".

49. Wardle, F., Minton, T., Ghani, S.B.C., Furstmann, P., Roeder, M., Richarz, S., & Sammler, F. (2013). Artificial Neural Networks for Controlling the Temperature of Internally Cooled Turning Tools. *Modern Mechanical Engineering, 3* (2A), 1–10. doi:10.4236/mme.2013.32A001.

50. Ghani, S.A.C., Zakaria, M.H., Harun, W.S.W., & Zaulkafilai, Z. (2016). Dimensional accuracy of internal cooling channel made by selective laser melting (SLM) and direct metal laser sintering (DMLS) processes in fabrication of internally cooled cutting tools. In *2nd International Conference on Automotive Innovation and Green Vehicle (AiGEV 2016)*, 2–3 August 2016. Cyberjaya, Selangor: MATEC Web of Conferences. doi:10.1051/matecconf/20179001058.

51. Zakaria, M.H., Ghani, S.A.C., Harun, W.S.W., Zaulkafilai, Z., & Mohamed, S.R. (2017). Fabrication of Aluminium Internally Cooled Cutting Tool by Means of Selective Laser Melting (SLM). *Journal of Mechanical Engineering*, *SI 3* (1), 185–198.

52. Uhlmann, E., Peukert, B., Thom, S., Prasol, L., Fürstmann, P., Sammler, F., & Richarz, S. (2017). Solutions for Sustainable Machining. *Journal of Manufacturing Science and Engineering, Transactions of the ASME*, *139* (5). doi:10.1115/1.4034850.

53. Cheng, K., Niu, Z.-C., Wang, R.C., Rakowski, R., & Bateman, R. (2017). Smart Cutting Tools and Smart Machining: Development Approaches, and their Implementation and Application Perspectives. *Chinese Journal of Mechanical Engineering (English Edition)*, *30* (5), 1162–1176. doi:10.1007/s10033-017-0183-4.

54. Singh, R., & Sharma, V. (2022). CFD Based Study of Fluid Flow and Heat Transfer Effect for Novel Turning Tool Configured with Internal Cooling Channel. *Journal of Manufacturing Processes*, *73*, 164–176. doi:10.1016/j.jmapro.2021.10.063.